THE FREQUENCY OF TROPOPAUSE-LEVEL THICK AND THIN CIRRUS CLOUDS AS OBSERVED BY CALIPSO AND THE RELATIONSHIP TO RELATIVE HUMIDITY AND OUTGOING LONGWAVE RADIATION

A Thesis

by

ALLISON L. CARDONA

Submitted to the Office of Graduate Studies of
Texas A&M University
in partial fulfillment of the requirements for the degree of

MASTER OF SCIENCE

August 2008

Major Subject: Atmospheric Sciences

THE FREQUENCY OF TROPOPAUSE-LEVEL THICK AND THIN CIRRUS CLOUDS AS OBSERVED BY CALIPSO AND THE RELATIONSHIP TO RELATIVE HUMIDITY AND OUTGOING LONGWAVE RADIATION

A Thesis

by

ALLISON L. CARDONA

Submitted to the Office of Graduate Studies of
Texas A&M University
in partial fulfillment of the requirements for the degree of

MASTER OF SCIENCE

Approved by:

Chair of Committee,   Andrew Dessler
Committee Members,   Ping Yang
                                     Steven Quiring
Head of Department,   Kenneth Bowman

August 2008

Major Subject: Atmospheric Sciences

ABSTRACT

The Frequency of Tropopause-level Thick and Thin Cirrus Clouds as Observed by
CALIPSO and the Relationship to Relative Humidity and Outgoing Longwave
Radiation. (August 2008)

Allison L. Cardona, B.S., Millersville University

Chair of Advisory Committee: Dr. Andrew Dessler

Thin cirrus clouds play an important radiative role in the earth's atmosphere and climate system, yet are one of the least understood components of the climate system. With the use of data from Cloud-Aerosol Lidar and Infrared Pathfinder Satellite Observations (CALIPSO), thin cirrus and thick cloud distributions in the tropics are analyzed at 121, 100, and 82 hPa. Observations obtained between December 2006 and November 2007 show that thin cirrus between 30°N and 30°S occur in close proximity to regions of intense convection and are positively correlated with low values of outgoing longwave radiation (OLR).

In conjunction with the CALIPSO data, water vapor data from the Earth Observing System (EOS) Microwave Limb Sounder (MLS), OLR data provided by the NOAA/OAR/ESRL PSD, Boulder, Colorado, USA, from their Web site at http://www.cdc.noaa.gov/, and linearly interpolated NCEP reanalysis temperature data were used. These data were used to examine how thick and thin cirrus cloud fractions at 121-hPa and 100-hPa are related to relative humidity with respect to ice (RHI),

temperature, and OLR. Our observations show that both RHI and convection play important roles in the development and maintenance of thick and thin cirrus clouds at the pressure levels of interest. The highest fractions of clouds are almost always seen within OLR values representative of convection and at relatively high values of RHI. However, when peaks in cloud fraction are found above the convective threshold, higher RHI values are needed than are needed when convection is responsible for the formation and maintenance of these clouds.

DEDICATION

I dedicate this manuscript first and foremost to my family who has supported me throughout the years, as well as my friends who have been my family away from home and provided me with the support needed to complete my degree and this manuscript.

ACKNOWLEDGEMENTS

I would like to thank my advisor, Dr. Andrew Dessler for the guidance and support that he has provided me in my time spent at Texas A&M University and for the wonderful opportunity he has provided me to continue my education. I would also like to thank the other members of my committee, Dr. Ping Yang and Dr. Steven Quiring for their time and help in editing this manuscript.

I would also like to thank Sun Wong for all the time he took out of his schedule to help me with any research issues I was having, as well as always being there to help me understand anything that I was having trouble understanding. Without his help, this thesis would have taken considerably longer to complete.

Last, but certainly not least, I would like to thank my family and friends. If it wasn't for my family and all the support they have given me, I wouldn't be where I am today. I want to thank them for always being there for me and believing in me, no matter what. And to my friends, thank you for being my family away from home and always being there for me whether it was to help me with my research or just to listen when things got hard and never letting me give up. I couldn't have done any of this without you.

TABLE OF CONTENTS

LIST OF FIGURES

LIST OF TABLES

1. INTRODUCTION

Clouds play an important role in the earth's atmosphere and climate, yet are one of the least understood components of the climate system. Recently, much attention has been given to thin, near tropopause cirrus (TNTC) [*Dessler et al.,* 2006a; *Wang et al.,* 1996; *Prabhakara et al.,* 1993; *Jensen et al.*, 1996a; *Jensen et al.,* 1996b; *Jensen et al.*, 1999]. TNTC are primarily found in the tropical atmosphere, within about one kilometer of the tropical tropopause and have optical depths of much less than one [*Dessler et al.,* 2006a]. It is believed that TNTC play a significant role in earth's radiation budget, and may also be important in helping to dehydrate air entering the stratosphere [*Jensen et al.*, 1996b].

According to Jensen et al. [1999], subvisible (optical depth < 0.03) thin cirrus may lead to a reduction of outgoing longwave radiation (OLR) of up to a few W-m^{-2}. Though they have been detected by satellites, space shuttle-borne lidars [*Winker and Trepte,* 1998], as well as ground-based lidar [*Nee et al.*, 1998], many uncertainties remain about these clouds due to difficulties in measuring them.

TNTC can form from: (i) outflow from the cirrus anvils of cumulonimbus clouds or (ii) in situ nucleation and growth of ice crystals near the tropical tropopause [*Jensen et al., 1996a; Massie et al.,* 2002]. TNTC form from the outflow from the cirrus anvils of cumulonimbus clouds as these clouds are thinned by advection and diffusion

_____
This thesis follows the style of *Journal of Geophysical Research*.

[*Prabhakara et al.,* 1993]. The in situ nucleation is believed to be driven by slow vertical motion or turbulent mixing. This uplift can be initiated via flow over continental-scale bulges in the troposphere, flow over large-scale convective systems, or lifting above the stratiform regions of mesoscale convective systems (MCS) [Churchill and Houze, 1990]. These mechanisms explain why thin cirrus are primarily a tropical cloud. Not only is convective activity a maximum in the tropics, but the fact that the tropical tropopause is higher leads to lower tropopause temperatures. It has been observed that at these lower temperatures ice nucleation occurs at relatively low ice supersaturations, leading to the generation of high numbers of ice crystals and thin cirrus that are persistent. Thin cirrus are found in the midlatitudes, but the lower tropopause height leads to warmer tropopause temperatures and thin cirrus that persist on a time scale of hours instead of days, which is often seen in the tropics [*Jensen et al.,*1996a].

TNTC are observed around the tropical tropopause layer (TTL) approximately 50% of the time in warm pool regions [*Prabhakara et al.,* 1993] and this is believed to be due to the fact that convection dominates in these areas. Dessler et al. [2006a] found that there is a negative correlation between thin cirrus and OLR and that maxima in thin cirrus are found over regions of intense convective activity.

TNTC may also be an important factor in the dehydration of air entering the stratosphere [*Jensen et al*., 1996b; *Holton and Gettelman*, 2001]. The dryness of the lower stratosphere is believed to be caused by the "freeze-drying" of air as it crosses the TTL region and then enters the lower stratosphere [*Sherwood and Dessler*, 2000]. How this process occurs is still somewhat unclear.

One theory is that TNTC that are formed via vertical motions on longer time-scales tend to be composed of fewer crystals and have more time for crystal sedimentation. This leads to reductions in water vapor at the tropical tropopause as large as 1 part per million by volume (ppmv). Gradual lifting near the tropical tropopause, along with these water vapor reductions may lead to the dehydration of air entering the stratosphere [*Jensen et al.*, 1996b].

Another theory that was proposed by Hartmann et al. [2001] is that TNTC accompanied by lower-level clouds produce net radiative cooling in the tropopause regions. As the region becomes colder, the saturation vapor pressure decreases, and growth of ice particles, and subsequent dehydration, can result. So air parcels that cross through this region into the lower stratosphere are drier, leading to the relatively low mixing ratios that are found in the region.

Another component of interest is the upper-tropospheric relative humidity. This is a quantity that is not well understood due to the limitations of radiosondes at the cold tropopause temperatures. However, the use of satellites has aided in understanding the role that relative humidity plays at high altitudes. Sandor et al. [2000] found that there is a strong correlation between the frequency of thin cirrus at 147-hPa and tropical water vapor. That is, as water vapor increases, so does the thin cirrus frequency. High upper-tropospheric humidities are not only a proxy for thin cirrus occurrence, but also play an important radiative role. According to Jensen et al. [1999], a nearly saturated upper-troposphere can lead to OLR reductions of 1-2 $W\text{-}m^{-2}$. So the combination of high RHI values along with the presence of TNTC can lead to reductions in OLR of more than a

few W-m^{-2}. These reductions in OLR may have important implications not only in terms of climate and radiation models, but also in the basic understanding of the role that thin cirrus play in earth's radiation budget.

This thesis looks to validate previous findings with new data from the Cloud-Aerosol Lidar and Infrared Pathfinder Satellite Observations (CALIPSO) and the Earth Observing System (EOS) Microwave Limb Sounder (MLS). CALIPSO is able to detect thin cirrus at optical depths smaller than previous satellites and may provide insight and better understanding into the distribution of thin cirrus in the tropics, as well as the role that humidity plays in the development and distribution of thick, as well as thin cirrus in the tropical tropopause.

This study has two goals. First, we want to create a climatology of thick and thin cirrus clouds in the tropical tropopause using CALIPSO data. Second, we want to examine the types of environments in which these clouds tend to form in the TTL. Sandor et al. [2000] believed that by knowing the RHI distribution, one would know the fractional occurrence of thin cirrus since the fraction of these clouds would increase as the RHI increased. We don't believe this to be the case. We hypothesize that while RHI plays a role in the thin cirrus and thick cloud fractions in the TTL region, we don't believe that RHI is the only variable responsible. We believe that convection plays an important role in the distribution of thick and thin cirrus clouds in this region and that the two quantities both play an important role in the distribution of thick and thin cirrus clouds in the TTL region.

Information on the data used and discussion of the methodology in the present study will be presented in Section 2. Section 3 will discuss the thick and thin cirrus distributions as seen by CALIPSO and discuss how this compares to previous studies. An investigation of the relationship between cloud fraction and relative humidity and OLR will be presented in Section 4. And finally, in Section 5, the conclusions will be summarized and discussed.

2. ANALYSIS METHODS

2.1 Data

The period for the study is December 2006 to November 2007. The data is broken into seasonal averages: December-February (DJF), March-May (MAM), June-August (JJA), September-November (SON). However, data were not available past 11 November 2007, so SON plots only contain data up to this date. We will use data from the Cloud-Aerosol Lidar and Infrared Pathfinder Satellite Observations (CALIPSO) and the Earth Observing System (EOS) Microwave Limb Sounder (MLS). CALIPSO is a nadir-viewing, sun-synchronous satellite, which was launched on 28 April 2006 and is a joint effort between the National Aeronautic Space Administration (NASA) and the Centre National d'Etudes Spatials (CNES). The aim of the CALIPSO project is to study the impact of clouds and aerosols on the radiation budget and climate of the earth [*Winker et al.,* 2003].

The payload of CALIPSO consists of three parts: (i) Cloud-Aerosol Lidar with Orthogonal Polarization (CALIOP), (ii) the imaging infrared radiometer (IIR), and (iii) the wide field camera (WFC). CALIOP measures at wavelengths of 532 nm and 1064 nm and has a vertical resolution of 30-60 m and a horizontal resolution of 333 m [*Winker et al.,* 2003].

The present study uses the five-kilometer CALIPSO data. In this data product, there is a cloud detection horizontal resolution of five kilometers and a vertical range between approximately 20.2 km above sea level and -0.5 km below sea level. Between

-0.5 and 8.2 km, the vertical resolution is 30 m and between 8.2 and 20.2 km, the vertical resolution is 60 m [*Winker et al.,* 2003].

The EOS MLS began observations on 13 August 2004 and is on the NASA EOS Aura Mission. The EOS MLS is a sun-synchronous satellite and is in a near-polar 705 km altitude orbit, making 13 orbits per day [*Waters et al.,* 2006].

The EOS MLS observes thermal microwave emissions from earth's "limb". It measures thermal emissions from broad spectral bands that are centered at 118, 190, 240, 640, and 2250 GHz and measures atmospheric composition, temperature, humidity, and cloud ice. The EOS MLS is used primarily in this study for water vapor measurements and these are obtained using the 190 GHz radiometer [*Waters et al*., 2006].

2.2 Methods

Cloud data were obtained from measurements made by the Cloud-aerosol Lidar and Infrared Pathfinder Satellite (CALIPSO). In this thesis, we use version 1 of the CALIPSO level-2 5-km cloud layer data. We will use nighttime data exclusively for cloud frequency plots in Section 3 because the detection of layers is more reliable at night. During the day, high noise levels due to solar background signals reduces the ability of the instrument to detect the thinnest clouds [*Winker et al.,* 2003]. For thin cirrus occurrence tables in Section 3, as well as all figures in Section 4, we use both day and night data. We will also use the 532-nm data because of its superior ability to detect thin cirrus.

Optical depth data is unavailable in the version 1 data we are using, so we use integrated attenuated backscatter to separate thin from thick clouds. Backscatter is simply the reflection of light back to the direction it came from. The integrated attenuated backscatter is just the backscatter that is measured by CALIPSO integrated over the depth of the cloud [*Platt*, 1979]. Fig. 1 shows a scatter plot of optical depth vs. integrated attenuated backscatter in one month of version 2 CALIPSO level-2 5-km data. Based on Fig. 1, we define thin clouds as those having an integrated attenuated backscatter of less than 0.011, which corresponds to an optical depth of about 0.3. We also require thin cirrus to be less than 2-km thick. Thick clouds are defined as any cloud having an integrated attenuated backscatter greater than 0.011. We believe the scatter of the data around an optical depth of 0.2 to be due to the geometric thickness of the cloud. In Fig. 1, we used a geometric thickness of less than 2-km. However when examining the data in this region as we decreased the geometric thickness of the clouds, this scatter disappeared.

CALIPSO measures the geometric altitude of the clouds. National Centers for Environmental Predication (NCEP) reanalysis data [*Kalnay et al.,* 1996] was used in order to calculate the large-scale parameters of interest. These variables include cloud-top and cloud-base temperatures, cloud-top and cloud-base pressures, as well as the temperatures at each of the pressure levels of interest.

To do the interpolation, we assume that geometric height measured by CALIPSO, and geopotential height, which is reported in the meteorological data sets, are

equivalent. We then use linear interpolation to find the log(pressure) and temperature of the cloud boundaries.

Water vapor fields are intimately connected to cloud fields. To test this, we will also analyze water vapor measurements made by the Microwave Limb Sounder, onboard NASA's Aura spacecraft. In this study, we will use MLS version 2.21 water vapor mixing ratio retrieved at 121, 100, and 82 hPa. The precision of these measurements at 100-hPa is 15%. The accuracy, however, has yet to be determined [*Read et al.,* 2007]. Relative humidity with respect to ice (RHI) is calculated from MLS mixing ratio measurements and temperatures from the NCEP reanalysis data. NCEP data is linearly interpolated to the latitude, longitude, and log(pressure) of the MLS measurements.

CALIPSO and MLS both fly on the "A-train". CALIPSO has an equatorial crossing time of approximately 1:31pm local time, while Aura has an equatorial crossing time of 1:38pm local time. The track of CALIPSO is generally 1.8° east of that of MLS [*Waters et al.,* 2006].

For a particular CALIPSO profile, we find two MLS profiles located closest to it in location and time. We then linearly interpolate the MLS water vapor mixing ratio with respect latitude to the CALIPSO profile's latitude and take the interpolated MLS water vapor profile as that corresponding to the CALIPSO profile. The interpolated profile should be offset longitudinally by about 1.8° from the CALIPSO profile. Since our analysis is averaged for large-scale structure (10° longitude), this offset will not affect our conclusions.

Daily interpolated OLR data were provided by the NOAA/OAR/ESRL PSD, Boulder, Colorado, USA, from their Web site at http://www.cdc.noaa.gov/. This data is used in order to construct plots of 3-month averages of OLR, as well as in any plots relating cloud fraction and OLR. The resolution of these data are 2.5° latitude by 2.5° longitude [*Liebmann and Smith,* 1996].

3. ANALYSIS: THICK CLOUD AND THIN CIRRUS DISTRIBUTIONS

We will focus on the region between 30°N and 30°S, which includes the seasonal range of the Intertropical Convergence Zone (ITCZ) and the important Northern Hemisphere monsoon circulations.

In calculating the thick and thin cirrus frequencies, bins of 5° latitude by 10° longitude were used. The frequency is defined as the number of observations of clouds with tops above and bottoms below the pressure level of interest in each bin divided by the total number of observations in that bin. For frequency plots, the pressure levels of interest include 146, 121, 100, and 82 hPa. These pressure levels correspond to geometric altitudes of 13.7-14.6, 14.9-15.8,16.1-16.9, and 17.3-18.0 km. The 100-hPa level is closest to the WMO-defined and cold-point tropopauses, and 121-hPa and 82-hPa are levels found close to the tropopause. Levels with less than one hundred total cloud observations are not analyzed.

3.1 Regions Where Tropical Convection Is Found

Since thin cirrus are intimately connected with convection [*Prabhakara et al.,* 1993; Dessler et al., 2006a], it is important to know the areas in the tropics where convection is typically found. When looking at the seasonal averages of cloud frequency, there are three "semi-permanent" areas of convection [*Hastenrath*, 1989]. These areas are found in the Western Pacific, the Congo basin, and South America.

Hastenrath [1989] postulated that the convective centers may be caused by the ascending portions of the zonal overturning circulation cells that are found in the tropics.

These zonal circulation cells are due to longitudinal circulations, which are driven by temperature differences in different portions of the oceanic regions. There is a cold-water belt that is often found near the equator. When this belt is well developed, the air above it is cold and, as a result, it is too heavy to rise in the ascending portion of the Hadley cell. Instead, the Hadley circulations from the two hemispheres cause the air to flow westward, where it encounters warmer waters. These warmer waters heat and provide more moisture to the air, which allows the air to take part in the large-scale, moist-adiabatic ascent, which then leads to the development of convection in these areas [*Bjerknes,* 1969].

Generally, there are disagreements about the number and locations of these zonal circulation cells, but most agree that these circulations are found in the Atlantic, Indian, and Pacific Oceans. The most pronounced of these cells is the Pacific cell, also known as the Walker Circulation. The thermal circulations and convection that are found in the other oceans basins are relatively weak compared to that of the Walker Circulation, but continuous convection occurs throughout the year [*Bjerknes*, 1969].

There are two other features that play a role in the development and enhancement of convection in the tropics. These are the Intertropical Convergence Zone (ITCZ) and the South Pacific Convergence Zone (SPCZ).

The ITCZ is an area of low pressure that is found around the globe near the equator. It is the region in which the trade winds from each hemisphere converge. This convergence leads to rising motion and the development of convection [*Ahrens*, 2003].

The position of the ITCZ varies throughout the year. Over land, the migration of the ITCZ is more pronounced because the migration follows the sun's zenith angle. Migration is much more subtle over the ocean. This is because in order for convection to occur and be maintained, ocean temperatures needs to be above approximately 27.5°C [*Graham and Barnett*, 1987], which does not allow for as pronounced of a migration. In general, the ITCZ has a mean position of 15°N in boreal summer and 5°S in boreal winter [Ahrens, 2003].

The SPCZ is one of the largest and most persistent regions of convection, after the ITCZ. Its mean annual position stretches from New Guinea east-southeastward to 30°S, 120°W. The SPCZ has two sections, a more diagonally oriented section, and a more zonally oriented northwest sector that merges with the ITCZ. The SPCZ is found in a region of low-level moisture convergence between the northwesterly flow that is found to the west of the eastern Pacific subtropical high and the southeasterly flow that comes from higher latitudes [*Vincent*, 1993].

Though the exact cause of the SPCZ is still unclear, there are some ideas of what leads to the SPCZ phenomenon. These theories include: (i) sea surface temperature (SST) gradients, (ii) land-sea distribution, (iii) tropical/mid-latitude interaction, and (iv) equatorial/mid-latitude wave dynamics [*Vincent*, 1993]. Fig. 2 shows a schematic of the SPCZ and the ITCZ in the Pacific Ocean and their interaction.

3.2 OLR and Convection

In Figs. 3-6, which are three-month seasonal averages of OLR, the regions of convection previously discussed are visible as the areas of low OLR. Hastenrath's three "semi-permanent" areas of convection are visible in all seasons, though their locations vary from season to season. The ITCZ is visible in all months as the area of low OLR that is found around the equatorial regions. However, it is more defined in some seasons compared to others. Also visible is the SPCZ as the region of low OLR extending from New Guinea diagonally southeastward. Its strength also varies seasonally.

It is interesting to note in Fig. 5 is that the area of deep convection that was most prominent over the Western Pacific Ocean is no longer found in that region, but is now located near India and Southeast Asia. This convection is due to the Indian monsoon. The Indian monsoon is caused by the seasonal reversal of winds. These wind changes are due to land-ocean temperature differences. During the winter months, the land is cooler than the ocean, so the winds blow from the northeast, from land toward ocean. During the summer months as the land heats up, these winds change direction and blow from the southeast. These southeasterly winds bring with them moisture which leads to the strong convection that is seen in Fig. 5 over India and Southeast Asia and play a role in the high thick cloud and thin cirrus frequencies that are observed over the region in JJA [*Hartmann,* 1994; *Ahrens*, 2003].

There is also a monsoon over Western Africa that leads to strong convection in different seasons. The African monsoon has two distinct seasons, one in which convection develops in the late spring, the other in which convection develops in late

July and lasts through the remainder of the summer. The monsoon is a result of the seasonal shifts in the ITCZ and the temperature differences between the Sahara Desert and the Atlantic Ocean. During these seasons, the northeasterly trade winds are affected by the ITCZ and as a result shift to southerly winds, which bring precipitation to the West African region [*Ahrens,* 2003].

3.3 Seasonal Thick and Thin Cirrus Cloud Frequencies

Though studies looking at thin cirrus frequencies in the tropics have been done, CALIPSO offers a chance to compile a more accurate thin cirrus, as well as thick cloud, climatology in the tropics. CALIPSO can see clouds with optical depths as low as 0.01, which is what makes it useful in helping to identify thin cirrus. In Figs. 7-14, plots of thin cirrus and thick cloud frequencies have been constructed.

We can compare the results in Fig. 13, the CALIPSO SON thin cirrus frequencies, to the nighttime observations made by Dessler et al. [2006a] using the Geostationary Laser Altimeter System (GLAS). When comparing results obtained by CALIPSO and GLAS, a few assumptions must be made because the GLAS study looked at thin cirrus frequencies on a variety of theta surfaces, while the present study examines thin cirrus frequencies on different pressure levels. The 360-K theta surface is comparable to the 121-hPa pressure level in the present study, 377.5-K is comparable to 100-hPa, and 400-K comparable to 82-hPa. At 121-hPa, the CALIPSO thin cirrus frequencies are quite similar to what was observed by GLAS. Thin cirrus frequency maxima are found in the same areas in both studies. For the maximum over South

America, the CALIPSO data shows a maximum frequency of approximately 25%, while GLAS data shows a maximum frequency of approximately 20%, so CALIPSO is showing higher frequencies than the GLAS data in this region. However, over Africa and the Western Pacific, maxima in thin cirrus frequencies are the same in both studies.

When comparing the 100-hPa level, over South America and Africa the distributions appear quite similar with maximum values of thin cirrus frequency about equal. In the South America case, the maximum thin cirrus frequency is approximately 14% and in the Africa case, approximately 16%. Over Indonesia, though the values of thin cirrus frequency are similar, approximately 12%, the distribution is shifted to the east. On the 82-hPa pressure level, the distributions appear quite different and the frequencies are substantially larger in the GLAS study, with maximum frequencies over Africa approximately 4% and over South America and the Western Pacific on the order of 2%. In the CALIPSO case at 82-hPa, thin cirrus frequencies above 1.2% are not observed.

Some of the differences that appear between the two studies occur because the study periods differ. The GLAS study was completed using data from 29 September and 17 November 2003 [*Dessler et al.,* 2006a]. These data were compared with the data from the SON season of 2007 which could account for some of the observed differences.

3.4 Thin Cirrus Occurrence

Tables 1-4 show the seasonal thin cirrus occurrence integrated over each pressure level. The percentages are simply a ratio of the number of thin cirrus found at or above

146, 121, 100, and 82 hPa and the total number of thin cirrus for each of the seasons. The numbers represent the fraction of thin cirrus occurring at or above each of the pressure levels of interest. Tables 1-4 use both day and night data in order to compare to previous studies.

The highest percentages of thin cirrus occur in DJF at all pressure levels, yet the lowest percentages of thin cirrus occur at different levels in different seasons. When the pressure level is at an altitude higher than the 100-hPa level, the lowest thin cirrus percentages are seen in SON. However, in the 146-hPa and 121-hPa cases, the lowest thin cirrus percentages occur in JJA.

As is expected, a diurnal cycle is clearly evident in all seasons, with the fraction of thin cirrus in the evening exceeding what is seen during the day time hours. Though it is known that a diurnal cycle in deep convection exists over land, it is difficult to separate out the contribution from the superior signal-to-noise ratio during the night [*Dessler et al.,* 2006b; *Winker et al*., 2003].

A study was conducted by Wylie and Woolf [2002] using data from the International Satellite Cloud Climatology Project (ISCCP) and Geostationary Operational Environmental Satellite Visible Infrared Spin Scan Radiometer Atmospheric Sounder (GOES-VAS). This study found that the largest diurnal cycles for high clouds, which they classified as clouds with tops above 440-hPa, occurs in the summer months of JJA. CALIPSO data shows, however, that at all levels, except 82-hPa, JJA has the smallest diurnal variations. The largest diurnal variations appear to occur in SON and DJF. This difference may be due to the fact that the features that are looked at are

slightly different in the present study than in the Wylie and Woolf study. The fact that the present study is only looking at clouds above 146-hPa that have optical depths less than 0.3 and thicknesses less than two kilometers may lead to the differences in diurnal variations than when looking at clouds with tops above 440-hPa.

Table 5 shows the thin cirrus occurrence integrated over the pressure levels for the entire study period. Dessler et al. [2006b] did a similar study using Geostationary Laser Altimeter System (GLAS) data. Instead of looking at the thin cirrus occurrence integrated over the pressure levels, they looked at the integration over geometric altitude. In their study, the z > 14.5 km data is similar to that of the P ≤121-hPa data and the z >16.5 km data is similar to that of the P ≤100-hPa data in the present study.

When comparing the results obtained by GLAS to that of CALIPSO, CALIPSO is seeing higher percentages of clouds at the GLAS altitudes comparable to the pressure levels used in this study. Table 6 is a reproduction of the data from the Dessler et al. study. In the current study, total thin cirrus percentages are on the order of 60% at 121-hPa, but are only on the order of 25% at the same level in the GLAS study. Similarly, at 100-hPa CALIPSO total thin cirrus percentages are on the order of 25% while the GLAS percentages are on the order of 5%. The same trend is seen when separating these percentages into thin cirrus observed in the daytime and nighttime.

3.5 Thin Cirrus-Convection Relationship

As was stated previously, low values of OLR are a proxy for convection. Deep, convective systems have a cloud top at high altitudes. Because the cloud-tops are at such

high altitudes they are very cold and the colder an object is, the less radiation it will emit. In each of the figures in this section, the seasonal thin cirrus frequencies are plotted in the colored contours with OLR values of 230 W-m^{-2} and less in black contours. In Fig. 15, thin cirrus frequency distributions were combined with the average OLR for DJF in order to see where thin cirrus are found in relation to convection. It is seen that high values of thin cirrus frequency are found in close proximity to areas of deep convection. However, these areas are not perfectly collocated. That is, the maximum thin cirrus frequencies are slightly offset from the centers of convection. The reason for this displacement will be discussed in section 4.3. There is no general direction in which the thin cirrus is offset from the center of convection. At 121-hPa (Fig. 15a) the maximum thin cirrus frequencies over Africa are displaced to the southeast of the deep convection, while over the Western Pacific, maxima in thin cirrus are displaced to the north and in South America slightly to the northwest of the strong convection.

The DJF 100-hPa thin cirrus frequency distribution (Fig. 15b) is somewhat different than the distribution at 121-hPa. First, the maximum thin cirrus frequencies over Africa are not at all displaced from the convection. Instead, the thin cirrus frequency maximum is collocated with the center of convection in that region. Over the Western Pacific Ocean, the highest thin cirrus frequencies are still displaced from the convection, but are now more displaced to the east. The direction of displacement for the high thin cirrus frequencies does not change at 100-hPa, but the distance from the center of convection does become larger.

The direction and distance of displacement of high thin cirrus frequencies at 82-hPa (Fig. 15c) from the deep convection remains the same over the Western Pacific and South America from what is observed at 100-hPa. Over Africa, however, the largest frequencies of thin cirrus are now found to the west of the deep convection, located more towards the coast of western Africa.

The strongest convection in MAM (Fig. 16) is found in approximately the same areas as seen in DJF and the locations of the maximum thin cirrus frequencies with respect to convection have not changed drastically. At 121-hPa (Fig. 16a) over the Western Pacific, the maximum in thin cirrus frequency is again shifted to the east of the center of convection. Over Africa, maxima in thin cirrus frequency are displaced to the east of the deep convection. However, over South America, the maximum in thin cirrus frequency is not displaced, but is found to be collocated with the deep convection in that region.

Patterns at 100-hPa (Fig. 16b) differ slightly that what was observed at 121-hPa. The largest thin cirrus frequencies over South America are still collocated with the deep convection there. Over the Western Pacific region, the maximum thin cirrus frequencies are still displaced somewhat to the east, but by much less. And over Africa, the highest thin cirrus frequencies are collocated with the strongest convection, but extending such that high frequencies of thin cirrus are also found somewhat to the east of this deep convection.

However, things are a little less clear in Fig. 16c. There are clear maxima in thin cirrus frequency seen over South America and Africa. These maxima are, for the most

part, collocated with the deep convection found in these areas, though the thin cirrus maximum in Africa is displaced slightly to the east. Over the Indian Ocean and into the Western Pacific, however, no clear pattern can be seen with regard to the occurrence of thin cirrus and convection. This is believed to be due to the fact that in the MAM season, there are not very many thin cirrus found at the 82-hPa level, so it is hard to identify any patterns.

In Fig. 17, the areas of strongest convection have migrated from their MAM location. With the onset of the monsoon around the India/Southeast Asia region, the axis of convection in that region has made a substantial migration from its Western Pacific position in MAM. However, at 121-hPa (Fig. 17a), the maximum thin cirrus frequencies are still found over Indonesia and into the Western Pacific Ocean, well to the southeast of the monsoon convection. The area of convection in Africa, along with the South American convection, has moved somewhat to the north. So, too, have the areas of maximum thin cirrus frequencies. Over Africa, maximum thin cirrus frequencies are displaced slightly to the north of the convection and over South/Central America, the largest thin cirrus frequencies are displaced to the northwest of the convection in that region.

The highest thin cirrus frequencies are occurring primarily over the region affected by the monsoon at 100-hPa (Fig. 17b). This area of high frequency is collocated with the areas of strongest monsoon convection. The maxima in thin cirrus frequency over South/Central America and Africa, as noted earlier, are much smaller than the thin cirrus frequencies occurring in the monsoon region. The highest thin cirrus frequencies

associated with the convection found in South/Central America are displaced to the southeast. And the thin cirrus maximum over Africa is displaced slightly to the southwest of the deep convection in that region.

However, at 82-hPa (Fig. 17c) the thin cirrus are found only around the monsoon convection, not in any other convective areas. The maximum thin cirrus frequency found over the monsoon region at this level is collocated with the deep convection in that area.

In Fig. 18 the locations of the centers of convection over South America and Africa, for the most part, have not changed from their position in the previous season. The only change is that the convection begins to migrate southward. Over the India/Southeast Asia region, the convection associated with the summer monsoon begins to move southwestward, back toward the Indonesian region. At 121-hPa (Fig. 18a), the thin cirrus frequencies associated with the Indian Ocean convection are displaced a large distance from the deep convection over the Indian Ocean and are found closer to the Western Pacific region. Over Africa, the highest thin cirrus frequencies are collocated with the strongest convection, but are once again more spread out around it. Over South America, the highest thin cirrus frequencies are found to the south of the deep convection in that region.

The displacements of maximum thin cirrus frequencies at 100-hPa (Fig. 18b) relative to the convective centers are not very large. The maximum thin cirrus frequencies over South America are found slightly to the south of the convection and near Indonesia, the maxima appear to be collocated with the deep convection. Over

Africa, the maximum thin cirrus frequencies are found slightly displaced to the west of the convection.

There is a small area of thin cirrus found in South America which is displaced well to the south of the main convection at 82-hPa (Fig. 18c). Over Africa, the maximum thin cirrus frequency is located slightly to the southwest of the convection. There are two maxima in thin cirrus frequency around the Indonesia region. One of which is found slightly to the north of the main convective area. There is another maximum in thin cirrus found in an area not at all related to convection over Northern Australia. This is evident because the average OLR values are very high in this region. In this case, convection is not related to the thin cirrus maximum seen.

From these plots, one is able to conclude that maxima in thin cirrus are generally found in close proximity to convection. This is in agreement with Dessler et al. [2006a] who found that maxima in thin cirrus tend to occur over regions of very intense convection, which is seen mainly over Africa, South America, and into the Western Pacific. While the CALIPSO results agree that maxima in thin cirrus are found near areas of intense convection, it is only in a few cases in which these maxima are actually collocated with the intense convection. This may be due to one of the primary formation mechanisms of thin cirrus clouds. The fact that thin cirrus may be formed from ice crystals that moved away from the convection via advection and diffusion would cause the maxima in thin cirrus frequency to be found not at the center of the intense convective activity, but somewhat downstream of it.

4. ANALYSIS: RELATIVE HUMIDITY, OLR, AND CLOUD FRACTION

4.1 Relative Humidity in the TTL and OLR

The second portion of this study examines how both RHI and OLR are related to tropopause-level cloud fractions. With the help of the MLS on board the Aura satellite, we can gain insight into what controls the cirrus cloud distribution. There are some theories on the factors that are believed to control tropopause-level thin cloud occurrence in the upper troposphere and lower stratosphere. First, RHI is believed to play a role in the distribution of TNTC. A strong correlation between RHI in the TTL region and thin cirrus frequency of occurrence has been observed, such that thin cirrus frequency increases as RHI increases [*Sandor et al.*, 2000].

As was discussed in the previous section, thin cirrus are often formed from convection and found within convective regions. By using OLR data, one can estimate the proximity to convection. From this information, we hypothesize that the fraction of tropopause-level clouds in the tropics will increase as the RHI increases and, as a result, higher fractions of clouds will be observed at colder temperatures. However, we believe that these clouds are not caused by RHI changes alone, but that convection plays a role in the formation and development of these clouds, and thus high fractions of clouds will be observed at low OLR values. For this portion of the analysis, we look at only 121-hPa and 100-hPa. There are too few observations at 82-hPa to draw any conclusions.

With the use of water vapor data from the Aura MLS and OLR data from NOAA/OAR/ESRL PSD, Boulder, Colorado, we can test our hypothesis to determine

the role that both RHI and OLR play in determining cloud fraction near the tropopause.

Through this examination, we will see the types of environments in which these clouds

tend to form, as well as the mechanisms that tend to generate these clouds.

4.2 Cloud Fraction and RHI

In Figs. 19-34, we examine the relationship between RHI and number of clouds,

RHI and number of observations, and RHI and cloud fraction for each of the seasons at

121-hPa and 100-hPa. In general, for each season at 121-hPa, the peak in number of

clouds, as well as number of observations is found very close to a RHI value of 50%. At

100-hPa, however, these distributions are shifted towards higher values of RHI. The

peaks, in general, are found closer to 100% RHI. For completeness, in this and following

sections, figures for each season and for both thick and thin cirrus cases will be included.

However, due to the fact that many of these plots are very similar, an in-depth analysis

of each figure is not included, only a few cases will be discussed.

Figs. 35-38 are the same distributions that are plotted in Figs. 19-34, except that

all of the seasons are plotted together for ease of comparing any differences between the

seasons. When examining the distribution of cloud fraction as a function of RHI at 121-

hPa, there is a clear trend in which cloud fraction increases as the RHI increases,

however at approximately 50% RHI in the thick cloud case (Fig. 35) and 75% RHI in

the thin cirrus case (Fig. 36), the cloud fraction remains constant as RHI increases,

before finally decreasing. The trend of cloud fraction increasing as RHI increases is also

visible at 100-hPa for both the thick (Fig. 37) and thin cirrus (Fig. 38) cases for each

season. The only difference between these two pressure levels is that while at 100-hPa the cloud fraction continues to increase as the RHI increases, at 121-hPa there is a point in which the distribution stops increasing and becomes constant before finally decreasing.

We also examined cloud fraction as a function of RHI and optical depth at 121-hPa and 100-hPa for each of the seasons in Figs. 39-46. Each bin within the region enclosed by the dashed line contains at least 50 observations. The first thing that one notices is that in each season, this line is at much higher RHI values at 100-hPa than at 121-hPa. This shows us that clouds are generally found at higher RHI values at 100-hPa. These plots also reveal that at 121-hPa, clouds are generally thicker and found at lower RHI values than is observed at 100-hPa. This can be seen by looking at any of the seasons. For example, when comparing the MAM season at 121-hPa (Fig. 41) and 100-hPa (Fig. 42), the cloud fraction distribution is found at much higher RHI values in Fig. 42. Also in Fig. 42, cloud fractions of 0.25 and above are all found below an optical depth value of 0.5, while at 121-hPa cloud fractions of 0.25 can be found as high as an optical depth of 1.0.

One interesting aspect of these plots is the observations of clouds at RHI values less than 100%. While it is possible that these clouds were observed in the process of evaporating, it seems more likely that this is a result of the differing field of views of the instruments. CALIPSO observes clouds in a volume that is 30-m high, 5-km wide, and 5-km long, while MLS measures water vapor in a volume that is ~3-km high, 10-km wide, and 200-km long. If the cloud fills only a small portion of the MLS volume, then it

is possible that the air around the cloud is saturated while the average water vapor in the MLS volume is subsaturated [*Waters et al*., 2006; *Winker et al.,* 2006; *Clark et al*., 2003].

Separating the observations by season and optical depth shows that both the season and the thickness of the cloud play a role in the cloud fraction distribution as a function of RHI. In the thick cloud case at both 121-hPa and 100-hPa, the cloud fraction appears to be much smaller than what is observed in the thin cirrus cases at these pressure levels. While, on average the cloud fractions appear to increase as the RHI increases, there are changes in the distributions from season to season. For example, in the thick cloud case at 100-hPa, the MAM peak in thick cloud fraction occurs close to 180% RHI, while in DJF the largest peak occurs close to 110% RHI. These differences are likely due to the differences in the RHI distribution from season to season.

4.3 Cloud Fraction and OLR

One important aspect of this study is to determine the relationship of tropopause-level thick and thin cirrus clouds to convection. It is clear that RHI plays an important role in the generation and maintenance of these clouds, so the question is whether convection plays a role beyond the role it plays in regulating RHI. For example, convection might produce small-scale temperature fluctuations that are not resolved by the large-scale reanalysis fields we are using to calculate RHI.

In Section 3, we examined the frequency of thin cirrus in relation to average OLR (Figs. 15-18) in order to observe where thin cirrus occur in relation to convection.

It was observed that, in most cases, thin cirrus were found near areas of intense convection, but that the maxima in thin cirrus frequency were generally displaced some distance from the center of the intense convection. In a few cases it was found that thin cirrus frequency peaks were collocated with intense convection.

In Figs. 47-50, we examine the frequency of thick clouds at 121-hPa and 100-hPa in relation to seasonal averages of OLR in order to see what differences exist between thick and thin cirrus cloud distributions with respect to convection. It was found that thick clouds at these pressure levels are almost always perfectly collocated with areas of low OLR. The only cases where this does not occur are in Fig. 47a over the Western Pacific Ocean and Fig. 50 over Indonesia. However, the peaks in cloud frequency in these cases are only slightly displaced from the centers of convection in their respective regions.

In section 3.5 it was mentioned that the displacement of thin cirrus frequency maxima from the center of intense convection may be due to the fact that thin cirrus may be formed from ice crystals that moved away from the convection via advection and diffusion. Figs. 51-54 are a reproduction of Figs. 15-18 at 100-hPa with the thin cirrus frequencies in colored contours and OLR values of 230 $W\text{-}m^{-2}$ and less in black contours. Wind data for each season is plotted from NCEP reanalysis data to determine if the displacement of thin cirrus frequency maxima is in fact due to advection. In general, from these plots we conclude that the winds can, for the most part, explain the separations of the thin cirrus frequency maxima from the centers of intense convection over Africa and South America, but not over the Western Pacific. In order to more

definitively determine whether convection is, in fact, responsible for the formation of thin cirrus around centers of convection trajectory analysis of the air parcels that make up the thin cirrus may be performed. It is, however, beyond the scope of this study. Trajectory analysis performed in a study by Spang et al. [2002] found that in many cases the displacement of thin cirrus frequency maxima can be explained by advection and that 70-80% of all clouds found in the tropopause region have convective history, while 20-30% are more likely formed from in situ processes.

Figs. 55-58 show cloud fraction as a function of OLR at 121-hPa and 100-hPa. For each season we look at a variety of RHI ranges. At 121-hPa we look at clouds that are found in RHI ranges of 20-40%, 40-60%, and 60-80% and at 100-hPa we look at clouds found in RHI ranges of 70-90%, 90-110%, and 110-130% to see how the distribution of the fraction of clouds as a function of OLR changes with respect to changes in RHI. In addition to this, we also investigated if there is any correlation between OLR and RHI within the small bins of RHI that we use in Figs. 55-58. In doing so, we determined that there is no correlation (not shown) between these two quantities whether examining them at 121-hPa or 100-hPa.

In all cases, the largest peaks occur at very low values of OLR, within the convective threshold, which is defined as OLR values below 220 W-m^{-2} [*Guojun and Zhang*, 2002]. For example, in Fig. 55, which is the thick cloud case at 121-hPa for each of the seasons, there is only one peak and it occurs at very low values of OLR. This makes sense because these thicker clouds are going to prevent the escape of OLR, so we would expect to see low OLR values with thicker clouds.

In the thin cirrus case, peaks once again primarily occur within the convective threshold. However, in the thin cirrus cases at 121-hPa (Fig. 56) and 100-hPa (Fig. 58), substantial fractions of thin cirrus are occurring at OLR values above the convective threshold. So while convection is the dominant formation and maintenance mechanism for thin cirrus (since the largest peaks are found at convective values), in situ processes do play an important role in the generation and maintenance of these clouds, as well, since we still see substantial fractions of thin cirrus above convective OLR values.

What is interesting to note in each of these cases is how the cloud fraction distributions change for the different RHI ranges in each season. For example, for the thick cloud case at 100-hPa in DJF (Fig. 57a), the highest cloud fractions are seen at RHI values between 70-90%, with cloud fractions in the RHI ranges of 90-110% and 110-130% substantially lower. However, at the same pressure level in JJA (Fig. 57c), the largest cloud fractions are now seen at 110-130% RHI, with the peak in cloud fraction between RHI values of 70-90% almost the same as the 110-130% peak. This shows that there are seasonal changes that affect the cloud fraction distribution, as well.

Figs. 59-74 show the cloud fraction distribution for thick and thin cirrus clouds as a function of OLR and RHI. Each bin within the region enclosed by the dashed line contains at least 50 observations, while outside of this region there are fewer than 50 observations.

Generally, the same patterns that were observed when examining cloud fraction as a function of OLR (Figs. 55-58) are observed when examining cloud fraction as a function of OLR and RHI. Just as was seen in Figs. 55-58, the thick clouds are found

primarily in the convective region at 121-hPa and 100-hPa. Just as was observed in Fig. 55b, the largest peak in thick cloud fraction in MAM at 121-hPa (Fig. 63) is found within the convective threshold and at RHI values between 40-80%. Also, just as was seen in Fig. 57a, the peak in thick cloud fraction in DJF at 100-hPa (Fig. 61) occurs at very low OLR values.

The thin cirrus distributions are a little different than their thick cloud counterparts, however. As observed in Figs. 55-58, the thin cirrus distribution is much more spread out between the OLR values than was seen in the thick cloud cases. For example, in the thin cirrus case in JJA at 121-hPa (Fig. 68), high fractions of thin cirrus are found at OLR values within the convective threshold, but are also found outside of the convective region. This supports the idea that while convection is important in the formation and maintenance of these clouds, that in situ processes are also important.

What one does tend to notice is that peaks in thin cirrus fraction at high OLR values tend to occur at higher RHI values than thin cirrus fraction peaks that occur within the convective threshold. This can be seen in any of the figures in which there are substantial cloud fractions at both low and high OLR values. A good example of this phenomenon can be seen in the SON 121-hPa thin cirrus case (Fig. 72). In this case, the thin cirrus distribution has a small positive slope. The cloud fractions occurring within the convective threshold have RHI values closer to 50%, while thin cirrus fractions found at higher OLR values, above the convective threshold, have RHI values closer to 100%. What this suggests is that both RHI and convection play a role in the development and maintenance of clouds at these pressure levels. We cannot simply

know what the cloud fraction distribution will look like by knowing only the RHI distribution, as was suggested by Sandor et al. [2000] and Clark et al. [2003]. Instead, cloud fraction distributions are determined by a combination of both the OLR and RHI distributions. However, when high cloud fractions are found above the convective threshold, higher values of RHI are needed than when these clouds are formed and maintained via convective methods.

5. SUMMARY AND CONCLUSIONS

In this paper, we have analyzed the distribution of near tropopause-level thin cirrus and thick clouds using Cloud-Aerosol Lidar and Infrared Pathfinder Satellite Observations (CALIPSO) data obtained between December 2006 and November 2007. Though other studies have presented climatologies of thin cirrus [*Wang et al.,* 1996; *Dessler et al.,* 2006a], CALIPSO, with its ability to detect optical depths as low as 0.01, has provided an unprecedented look at the distribution of tropical TNTC, as well as thick clouds.

We have investigated the distribution of thick and thin cirrus clouds at 121, 100, and 82 hPa. In general, the CALIPSO distribution presented here tends to agree with the GLAS distribution presented by Dessler et al. [2006a], though CALIPSO tends to see higher percentages of thin cirrus clouds. Maxima in TNTC, as well as thick clouds, are observed in regions of intense convective activity over Africa, South America, and the Western Pacific Ocean.

Relative humidity with respect to ice (RHI), temperature, and outgoing longwave radiation (OLR) have been compared to thick and thin cirrus cloud fractions at 121-hPa and 100-hPa in order to observe what factors tend to influence the formation and maintenance of these clouds. We have determined that high fractions of TNTC and thick clouds occur as RHI increases and temperature decreases. We have also found that convection and RHI distributions are both important in determining thin cirrus and thick cloud frequencies. However, when high fractions of these clouds are found above the

convective threshold, higher values of RHI are needed than are needed when these clouds are generated and maintained via convection.

Our analysis has not only created a climatology of thin cirrus and thick clouds in the tropics, but has examined the environments where these clouds are typically found. It is a first step in beginning to understand these clouds that play such an important radiative role in earth's climate. As these clouds begin to be examined in greater frequency and better understood, not only will we have a better understanding of our atmosphere, but we can begin to make the improvements to radiative and climate models.

REFERENCES

Ahrens, C. D. (2003), Meteorology Today: An Introduction to Weather, Climate, and the Environment. Brooks & Cole, United States.

Bjerknes, J. (1969), Atmospheric teleconnections from the Equatorial Pacific, *Monthly Weather Review, 97,* 163-173.

Churchill, D. D., and R. A. Houze, Jr. (1990), Radiatively driven stratosphere-troposphere interactions near the tops of tropical cloud clusters. Preprints, *Seventh Conference on Atmospheric Radiation,* San Francisco, American Meteorological Society, J125- J128.

Clark, H. L., R. S. Harwood, A. Billingham, and H. C. Pumphrey (2003), Cirrus and water vapor in the tropical tropopause layer observed by Upper Atmosphere Research Satellite (UARS), *Journal of Geophysical Research, 108,* ACL4.1-ACL4.12.

Dessler, A. E., S. P. Palm, and J. D. Spinhirne (2006a), Tropical cloud-top height distributions revealed by the Ice, Cloud, and Land Elevation Satellite (ICESat)/ Geoscience Laser Altimeter System (GLAS), *Journal of Geophysical Research, 111,* D12215.1-D12215.11.

Dessler, A. E., S. P. Palm, W. D. Hart, and J. D. Spinhirne (2006b), Tropopause-level thin cirrus coverage revealed by ICESat/Geoscience Laser Altimeter System, *Journal of Geophysical Research, 111,* D08203.1-D08203.10.

Graham, N. E. and T. P. Barnett (1987), Sea surface temperature, surface wind divergence, and convection over tropical oceans, *Science, 238,*657-659.

Guojun, G. and C. Zhang (2002), Cloud components of the Intertropical Convergence Zone, *Journal of Geophysical Research, 107,* ACL4.1-ACL4.12.

Hartmann, D. L. (1994), *Global Physical Climatology.* Academic Press, San Diego, CA.

Hartmann, D. L., J. R. Holton, and Q. Fu (2001), The heat balance of the tropical tropopause, cirrus, and stratospheric dehydration, *Geophysical Research Letters, 28*, 1969-1972.

Hastenrath, S. (1989), The relationship of highly reflective clouds to tropical climate anomalies, *Journal of Climate, 3*, 353-365.

Holton, J. R. and A. Gettelman (2001) Horizontal transport and the dehydration of the stratosphere, *Geophysical Research Letters, 28,* 2799-2802.

Jensen, E. J., O. B. Toon, L. Pfister, and H. B. Selkirk (1996a), Dehydration of the upper troposphere and lower stratosphere by subvisible cirrus clouds near the tropical tropopause, *Geophysical Research Letters, 23,* 825-828.

Jensen, E. J., O. B. Toon, H. B. Selkirk, J. D. Spinhirne, and M. R. Schoeberl (1996b), On the formation and persistence of subvisible cirrus clouds near the tropical tropopause, *Journal of Geophysical Research, 101*, 21,361-21,375.

Jensen, E. J., W. G. Read, J. Mergenthaler, B. J. Sandor, L. Pfister, et al. (1999), High humidities and subvisible cirrus near the tropical tropopause, *Geophysical Research Letters, 26,* 2347-2350.

Kalnay, E., M. Kanamitsu, R. Kistler, W. Collins, D. Deaven, et al. (1996), The NCEP/NCAR 40-year reanalysis project, *Bulletin of the American Meteorological Society, 77,* 437-471.

Liebmann, B. and C. A. Smith (1996), Description of a complete (interpolated) outgoing longwave radiation dataset, *Bulletin of the American Meteorological Society, 77,* 1275-1277.

Massie, S., A. Gettelman, and W. Randel (2002), Distribution of tropical cirrus in relation to convection, *Journal of Geophysical Research, 107*, AAC19.1-AAC19.16.

Nee, J. B., C. N. Len, W. N. Chen, and C. I. Lin (1998), Lidar observation of the cirrus cloud in the tropopause at Chung-Li (25°N, 121°E), *Journal of Atmospheric Sciences, 55,* 2249-2257.

Platt, C. M. R. (1979), Remote sounding of high clouds: I. Calculation of visible and infrared optical properties from lidar and radiometer measurements, *Journal of Applied Meteorology, 18*, 1130-1143.

Prabhakara, C., D. P. Kratz, J. M. Yoo, G. Dalu, and A. Vernekar (1993), Optically thin cirrus clouds: radiative impact on the warm pool, *J. Quant. Spectrosc. Radiat. Transfer, 49*, 467-483.

Read, W. G., L. Froidevaux, R. S. Harwood, R. F. Jarnot, H. M. Pickett, et al. (2007), Aura Microwave Limb Sounder upper tropospheric and lower stratospheric H_2O and relative humidity with respect to ice validation, *Journal of Geophysical Research, 112,* D24S35.

Sandor, B. J., E. J. Jensen, E. M. Stone, W. G. Read, J. W. Waters, et al. (2000), Upper tropospheric humidity and thin cirrus, *Geophysical Research Letters, 27,* 2645-2648.

Sherwood, S. C. and A. E. Dessler (2000), On the control of stratospheric humidity, *Geophysical Research Letters, 27,* 2513-2516.

Spang, R., G. Eidmann, M. Riese, D. Offermann, and P. Preusse (2002), CRISTA observations of cirrus clouds around the tropopause, *Journal of Geophysical Research, 107,* CRI2.1-CRI2.18.

Vincent, D. G. (1993), The South Pacific Convergence Zone (SPCZ): A Review, *Monthly Weather Review, 122,* 1949-1970.

Wang, P. H., P. Minnis, M. P. McCormick, G. S. Kent, and K. M. Skeens (1996), A 6-year climatology of cloud occurrence frequency from stratospheric aerosol and gas experiment II observations (1985-1990), *Journal of Geophysical Research, 101,* 29,407-29,429.

Waters, J. W., L. Froidevaux, R. S. Harwood, R. F. Jarnot, H. M. Pickett, et al. (2006), The Earth Observing System Microwave Limb Sounder (EOS MLS) on the Aura Satellite, *IEEE Transactions on Geoscience and Remote Sensing, 44,* 1075-1092.

Winker, D. M. and C. R. Trepte (1998), Laminar cirrus observed near the tropical tropopause by LITE, *Geophysical Research Letters, 25,* 3351-3354.

Winker, D. M., J. Pelon, and M. P. McCormick (2003), The CALISPO mission: Spaceborne lidar for observation of aerosols and clouds, *SPIE, 4893,* 1-11.

Wylie, D. P. and H. M. Woolf (2002), The diurnal cycle of upper-tropospheric clouds measured by GOES-VAS and the ISCCP, *Monthly Weather Review, 130,* 171-179.

APPENDIX A

FIGURES AND TABLES
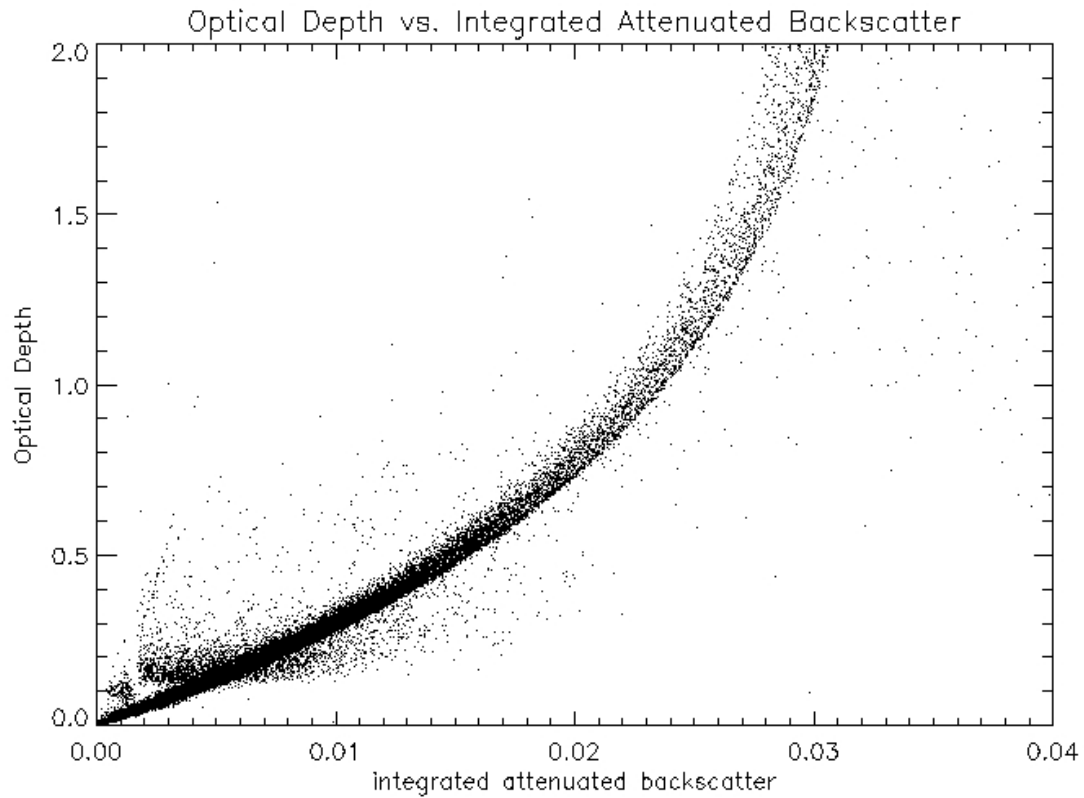
Figure 1: Optical depth vs. integrated attenuated backscatter for clouds between 30°N and 30°S with tops above 13 km and thicknesses less than 2-km for March 2007.
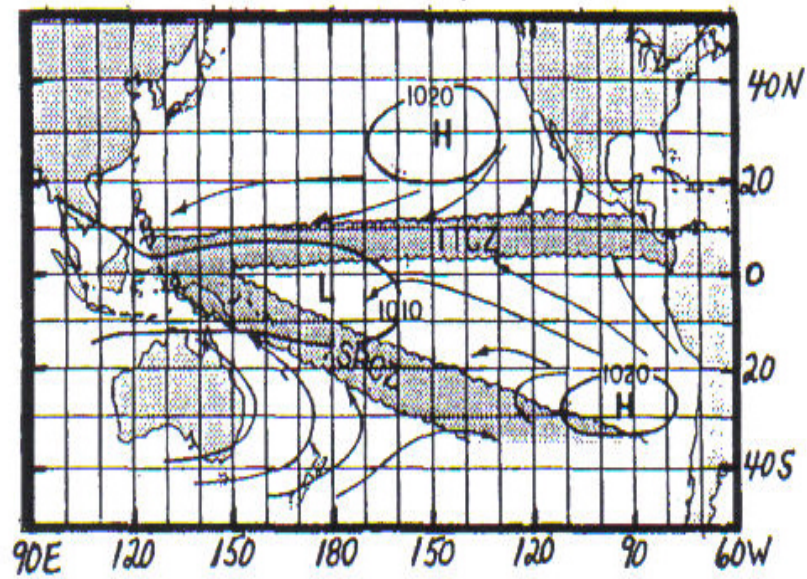
Figure 2: From Vincent [1993], a schematic of the location of the SPCZ and the ITCZ in the Pacific Ocean.
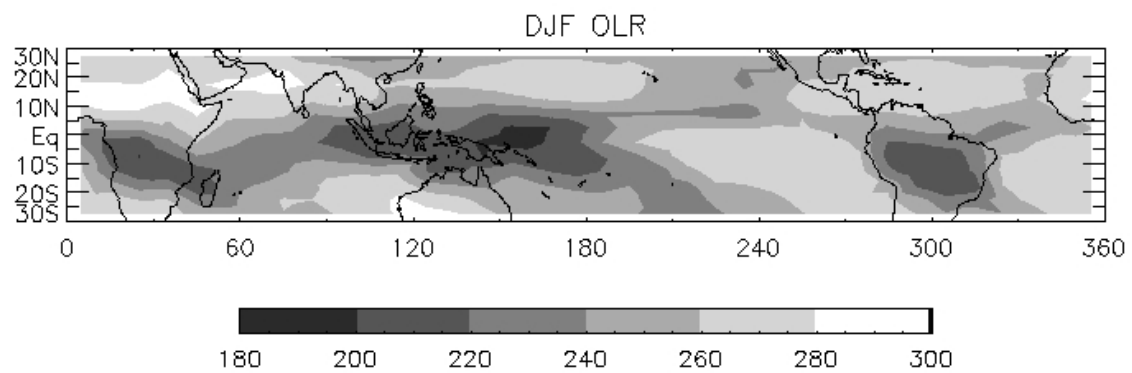
Figure 3: Three month average of outgoing longwave radiation (OLR) for DJF provided by the NOAA/OAR/ESRL PSD, Boulder, Colorado, USA. OLR has units of W-m^{-2}.
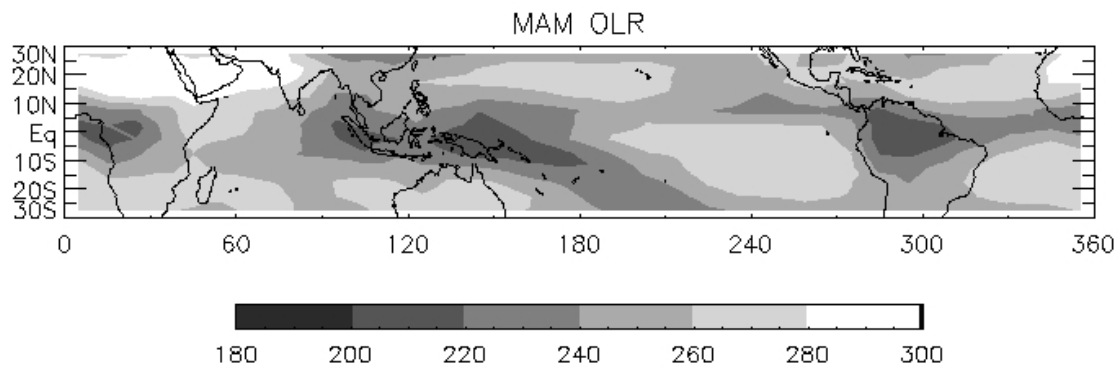
Figure 4: Three month average of outgoing longwave radiation (OLR) for MAM provided by the NOAA/OAR/ESRL PSD, Boulder, Colorado, USA. OLR has units of $W\text{-}m^{-2}$.
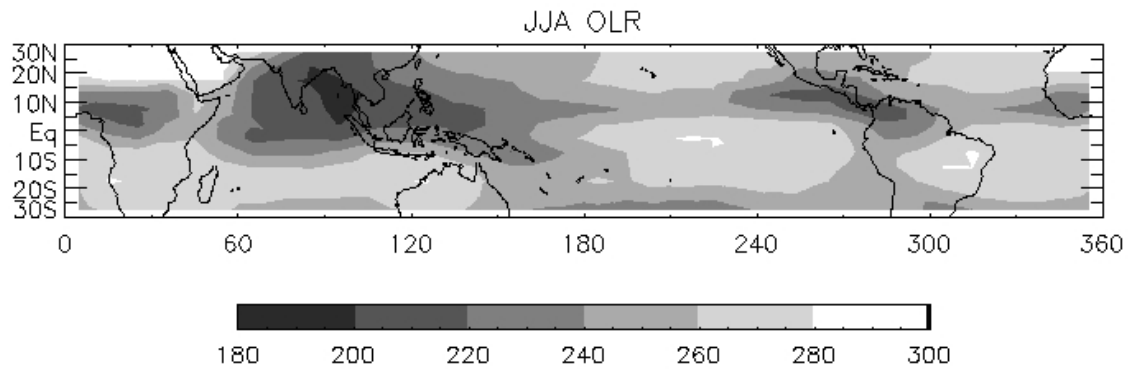
Figure 5: Three month average of outgoing longwave radiation (OLR) for JJA provided by the NOAA/OAR/ESRL PSD, Boulder, Colorado, USA. OLR has units of $W\text{-}m^{-2}$.
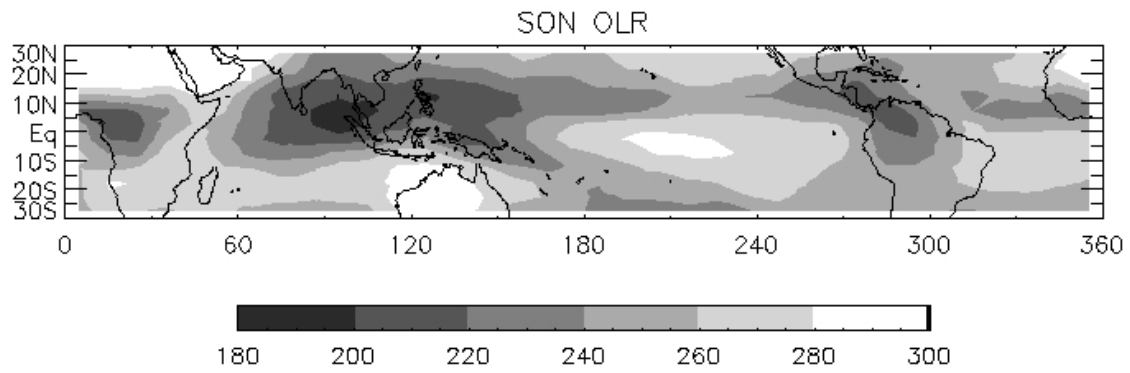
Figure 6: Three month average of outgoing longwave radiation (OLR) for SON provided by the NOAA/OAR/ESRL PSD, Boulder, Colorado, USA. OLR has units of W-m^{-2}.
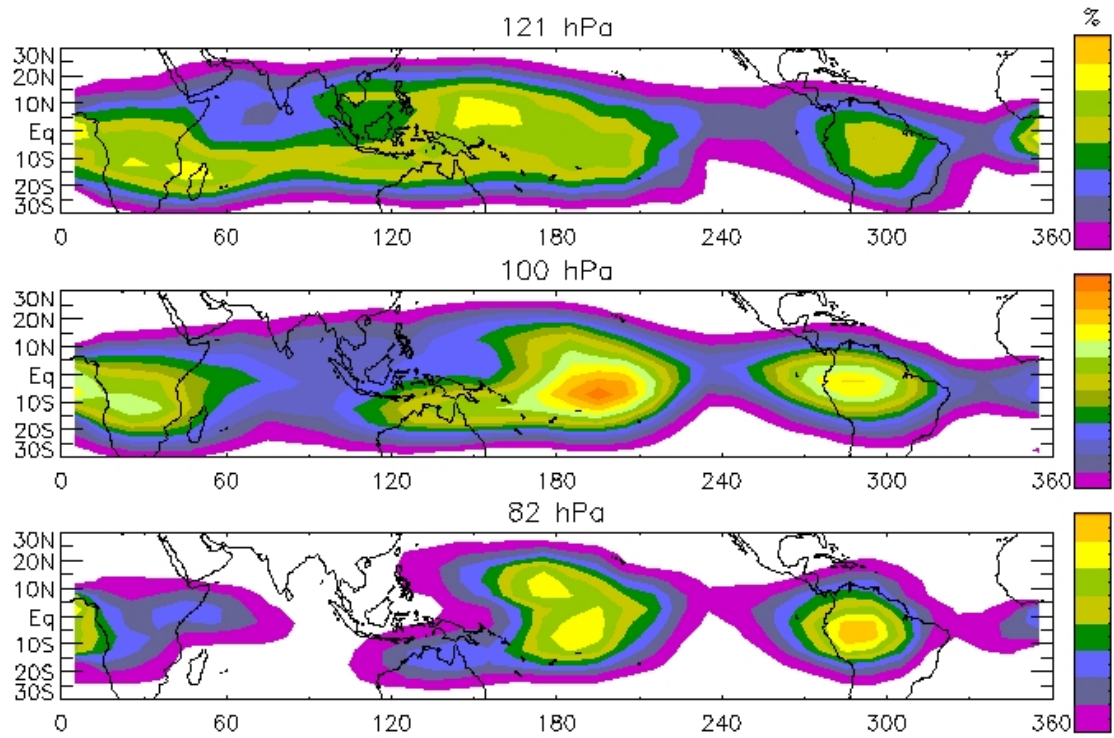
Figure 7: Thin cirrus frequencies, in percent, for DJF.
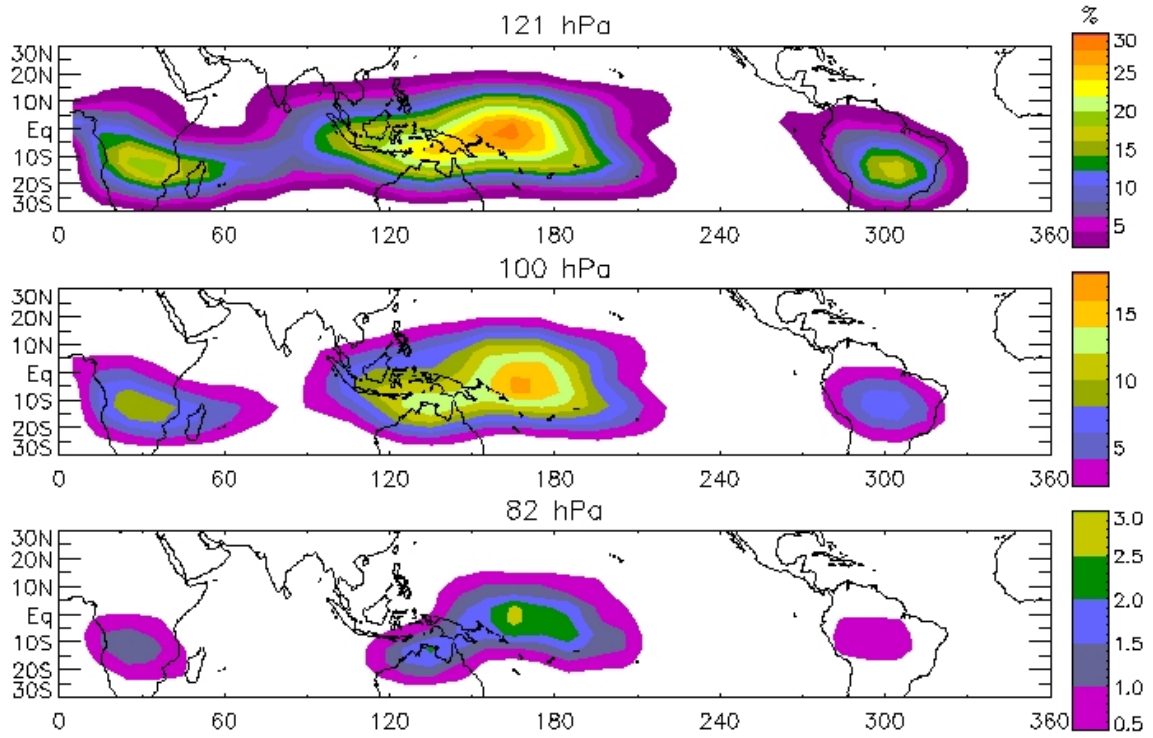
Figure 8: Thick cloud frequencies, in percent, for DJF.
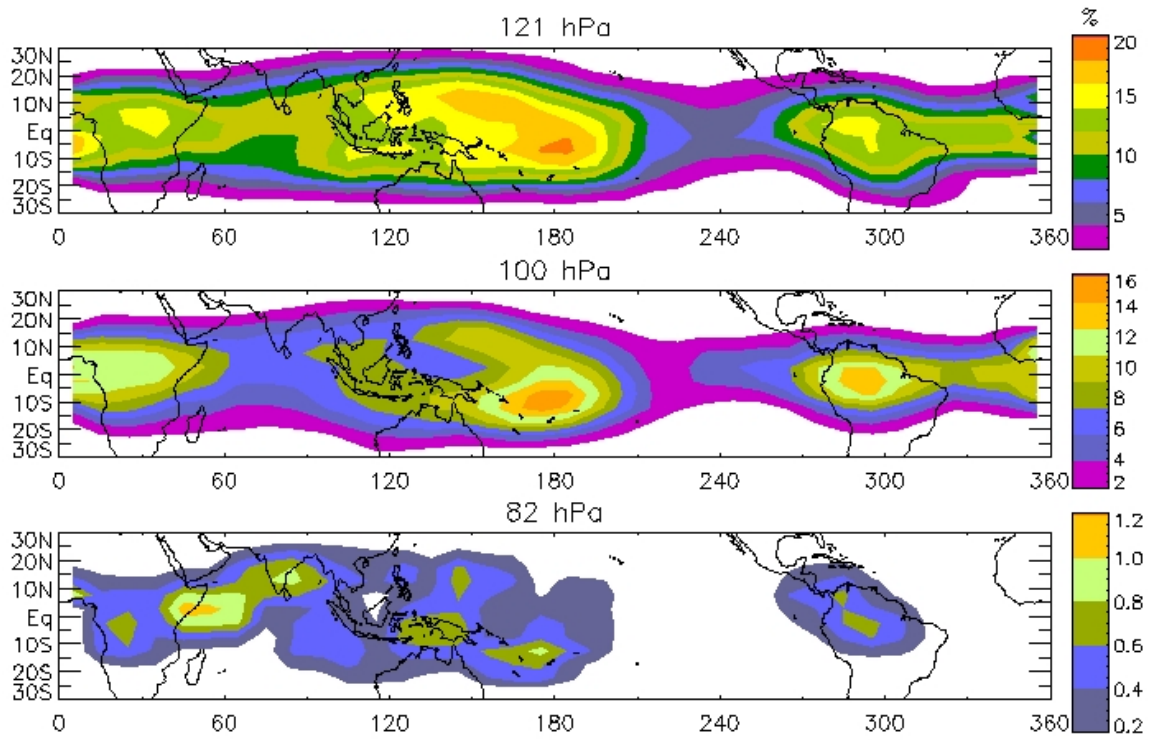
Figure 9: Thin cirrus frequencies, in percent, for MAM.
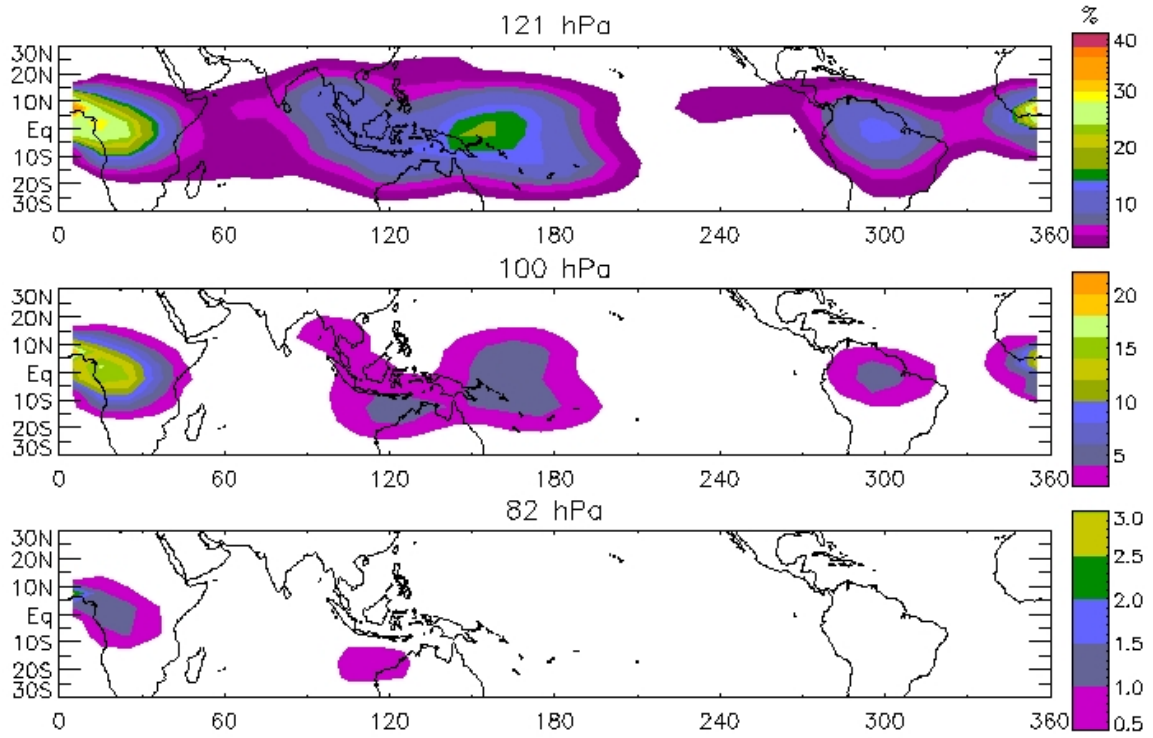
Figure 10: Thick cloud frequencies, in percent, for MAM.
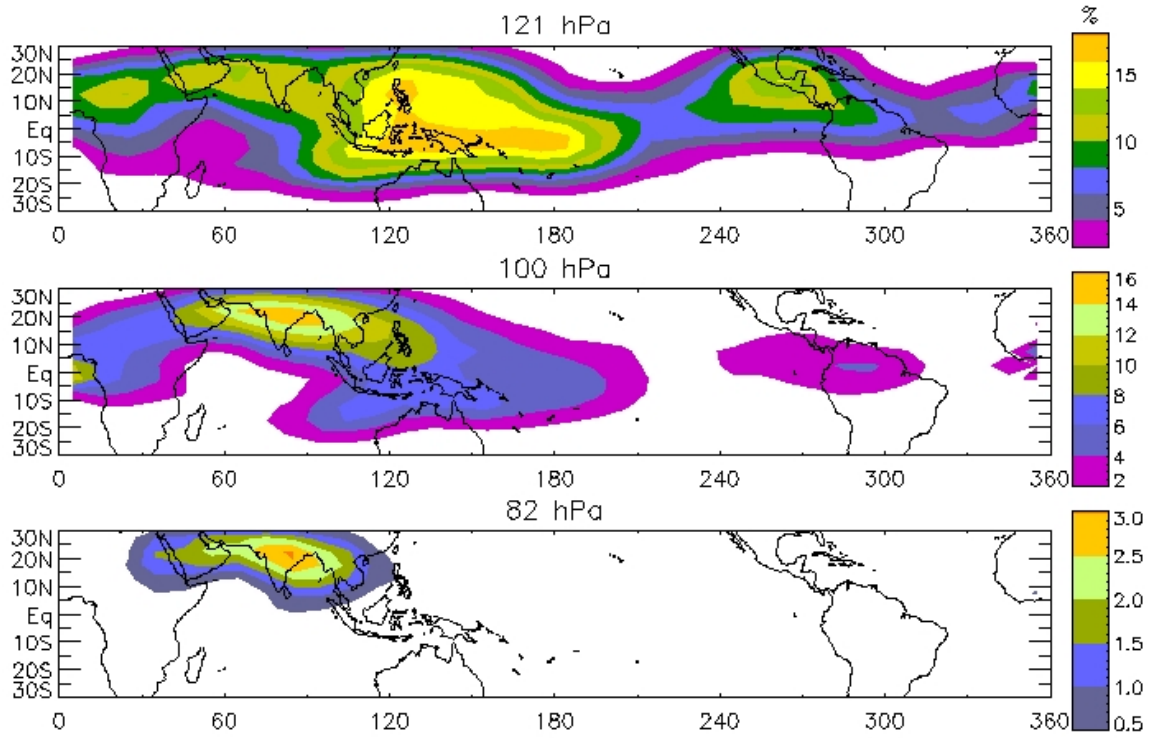
Figure 11: Thin cirrus frequencies, in percent, for JJA.
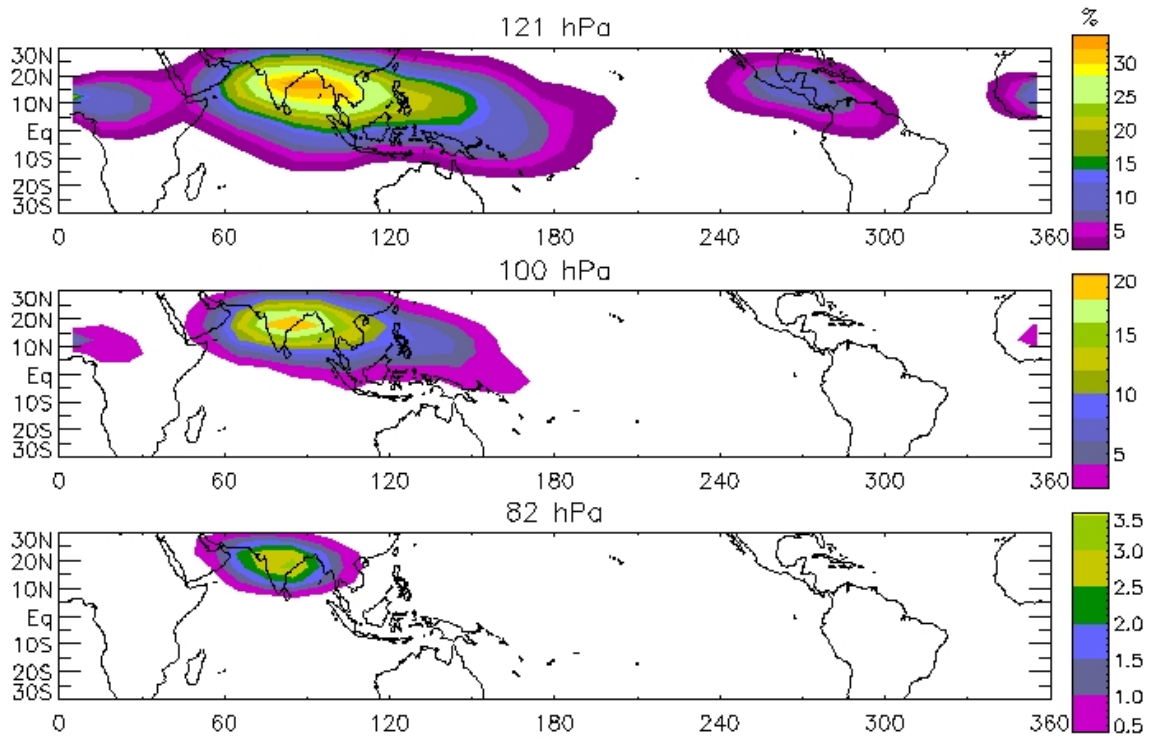
Figure 12: Thick cloud frequencies, in percent, for JJA.
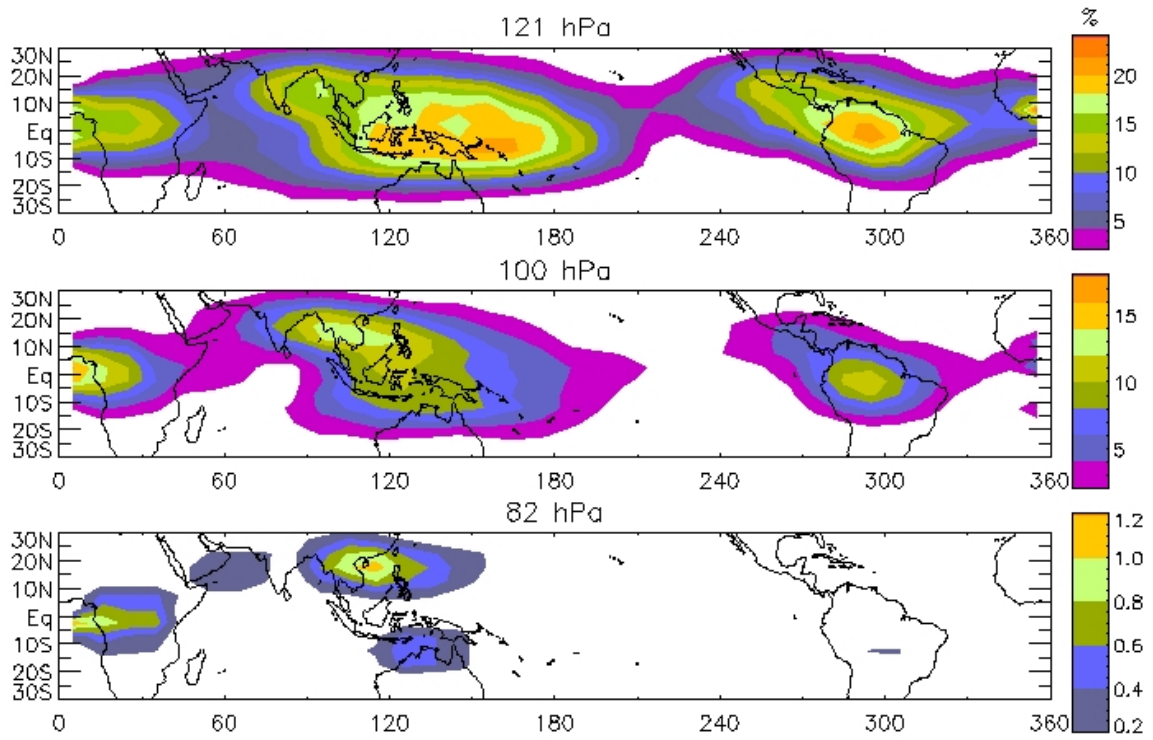
Figure 13: Thin cirrus frequencies, in percent, for SON.
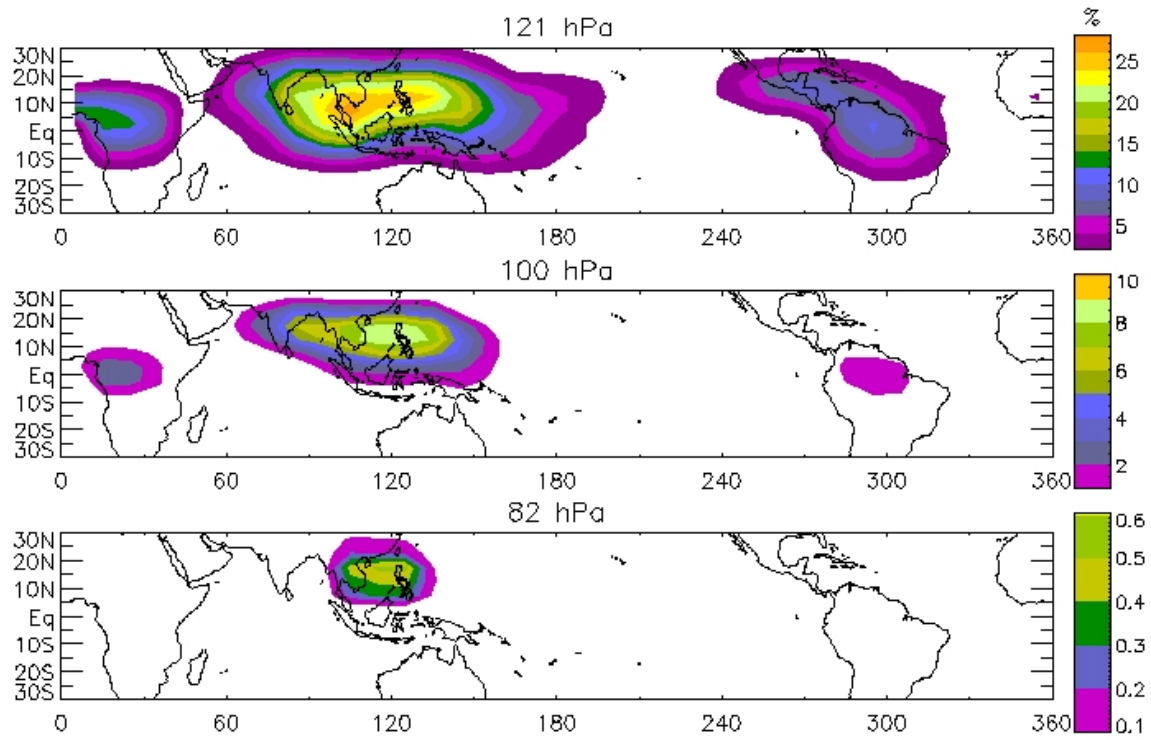
Figure 14: Thick cloud frequencies, in percent, for SON.
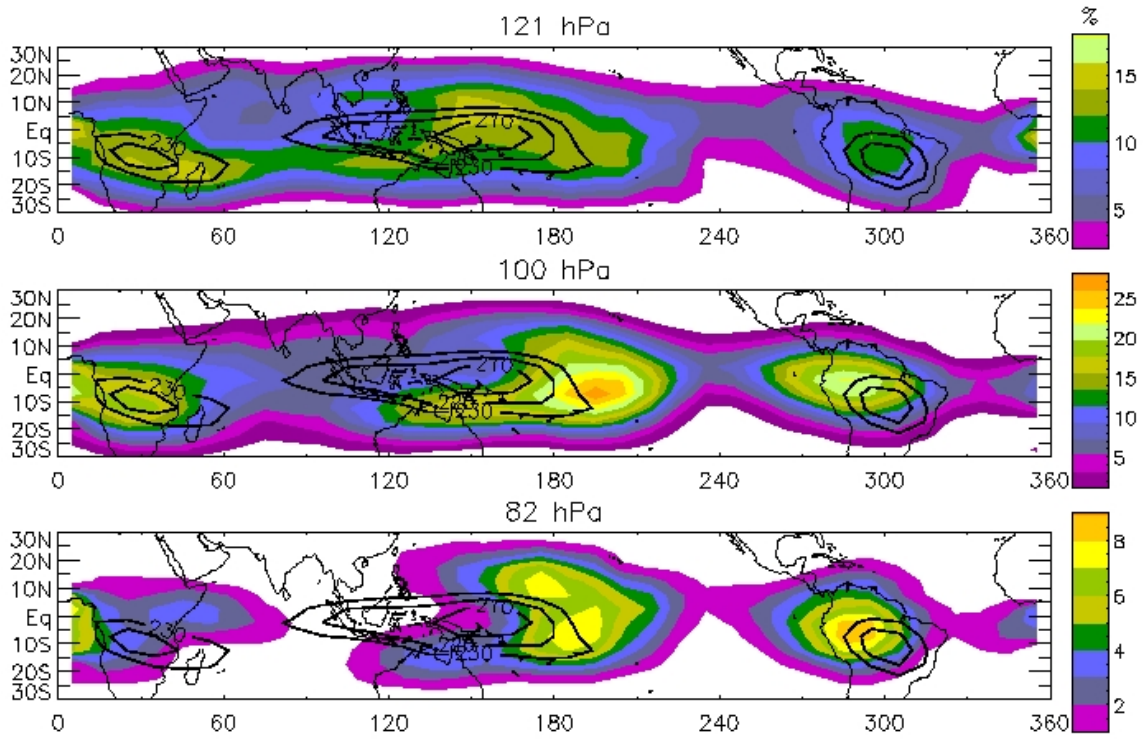
Figure 15: DJF thin cirrus frequencies in colored contours at a) 121-hPa, b) 100-hPa, and c) 82-hPa with OLR values of 230 W-m^{-2} in black contours.
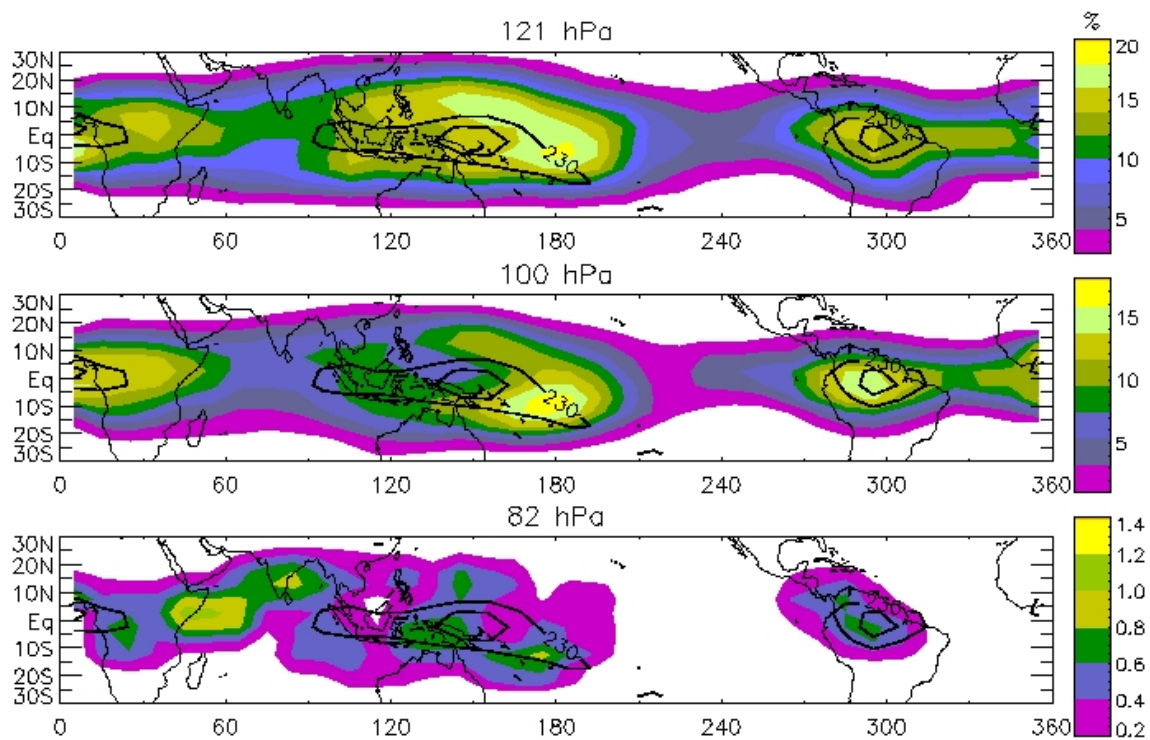
Figure 16: MAM thin cirrus frequencies in colored contours at a) 121-hPa, b) 100-hPa, and c) 82-hPa with OLR values of 230 W-m^{-2} in black contours.
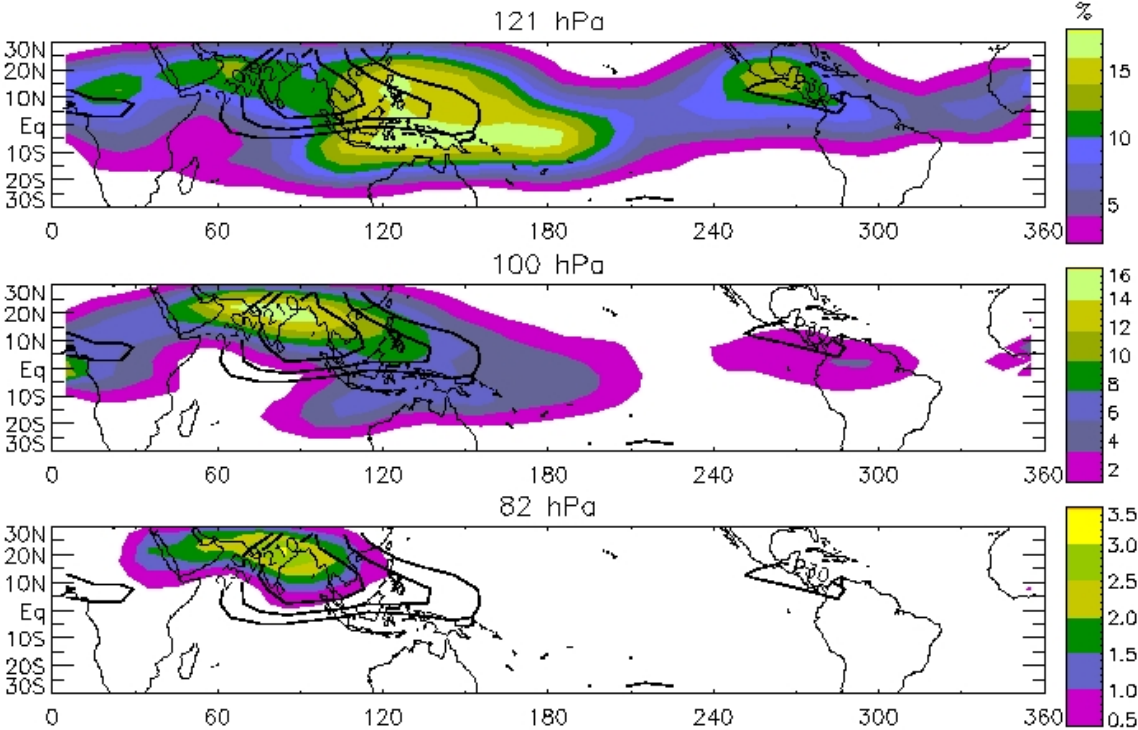
Figure 17: JJA thin cirrus frequencies in colored contours at a) 121-hPa, b) 100-hPa, and c) 82-hPa with OLR values of 230 W-m^{-2} in black contours.
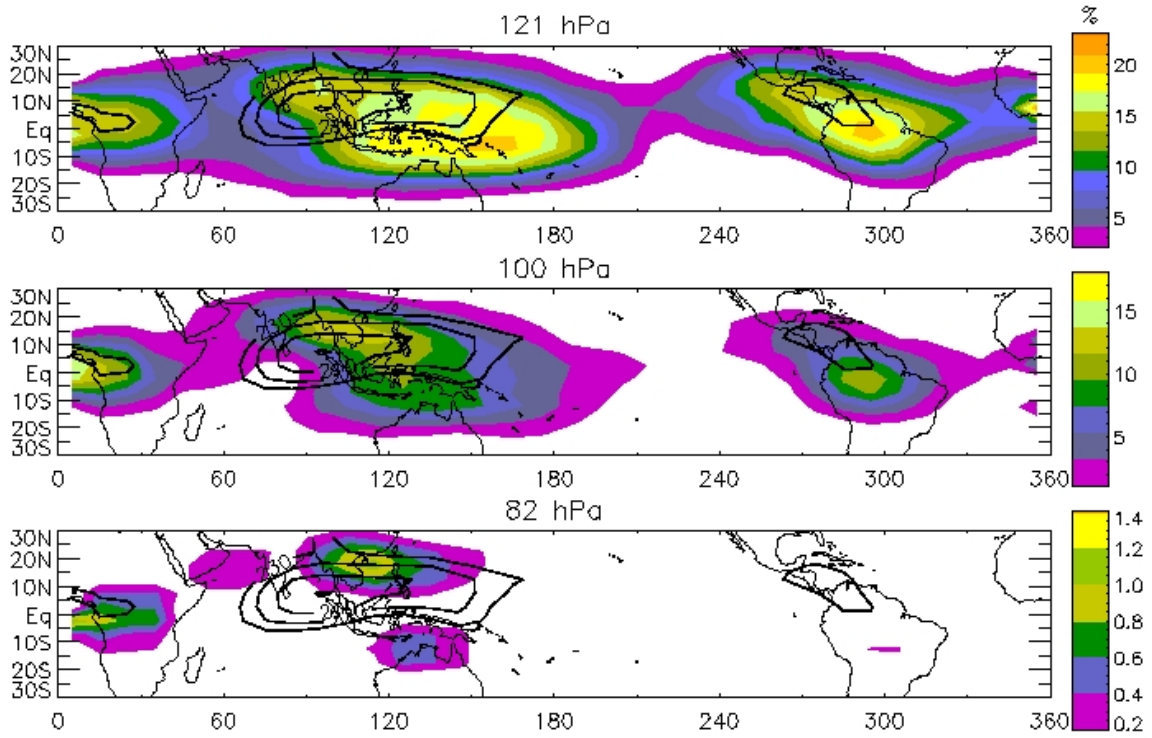
Figure 18: SON thin cirrus frequencies in colored contours at a) 121-hPa, b) 100-hPa, and c) 82-hPa with OLR values of 230 W-m^{-2} in black contours.
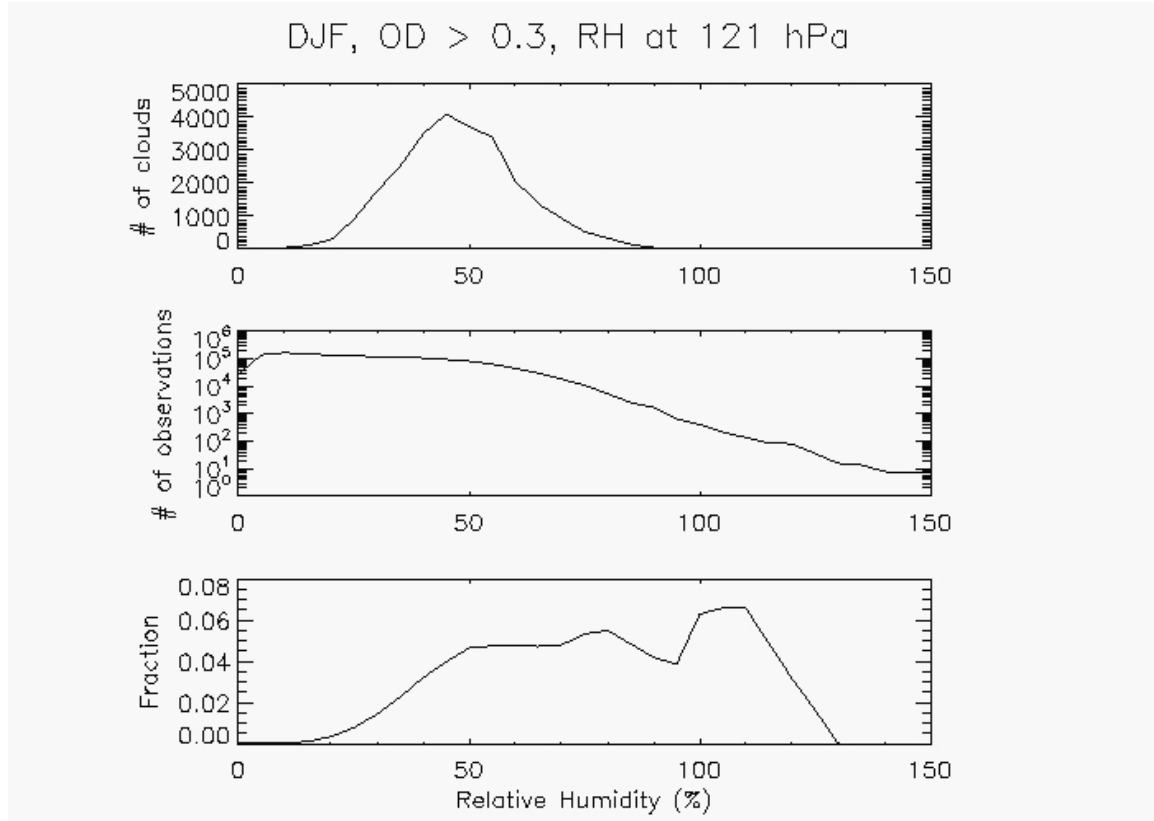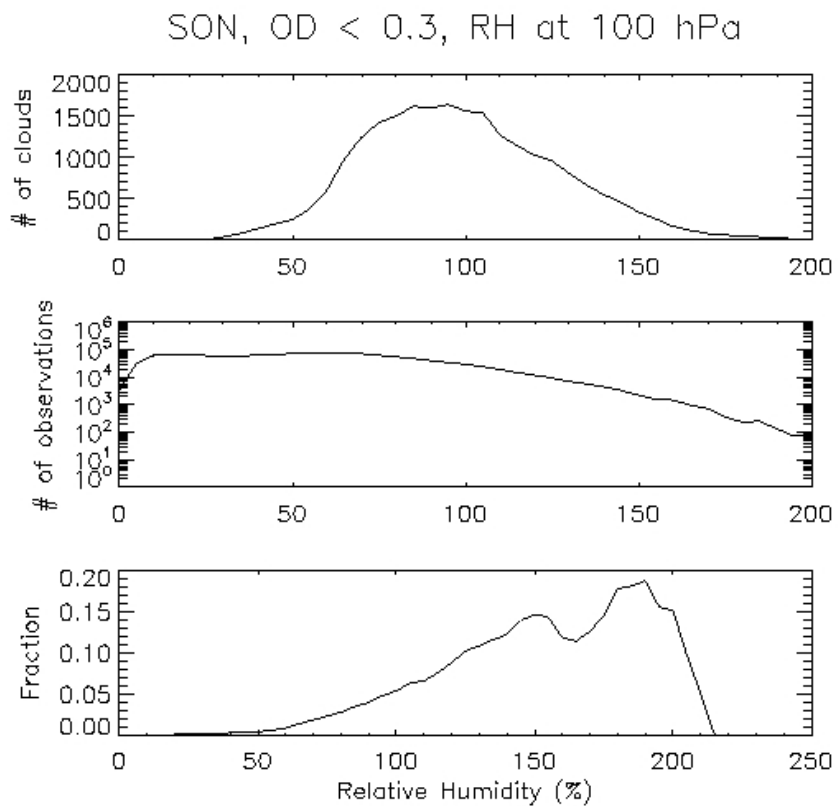
Figure 19: a) Number of thick clouds, b) number of observations, and c) thick cloud fraction as a function of RHI at 121 hPa for DJF. Bin size of 5% RHI is used.
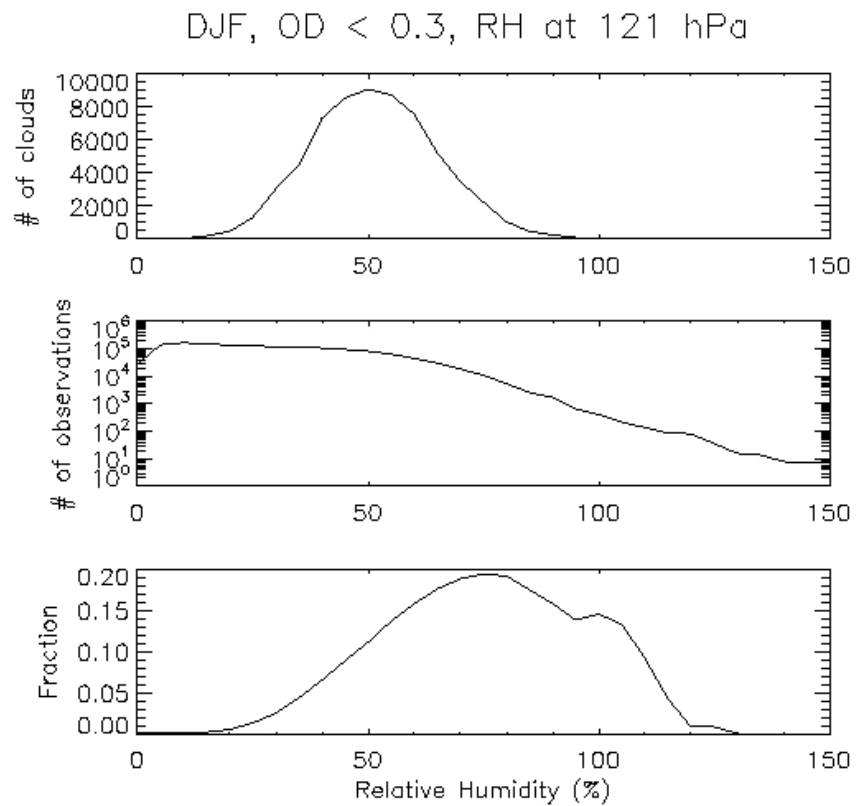
Figure 20: a) Number of thin clouds, b) number of observations, and c) cloud fraction as a function of RHI at 121 hPa for DJF. Bin size of 5% RHI is used.
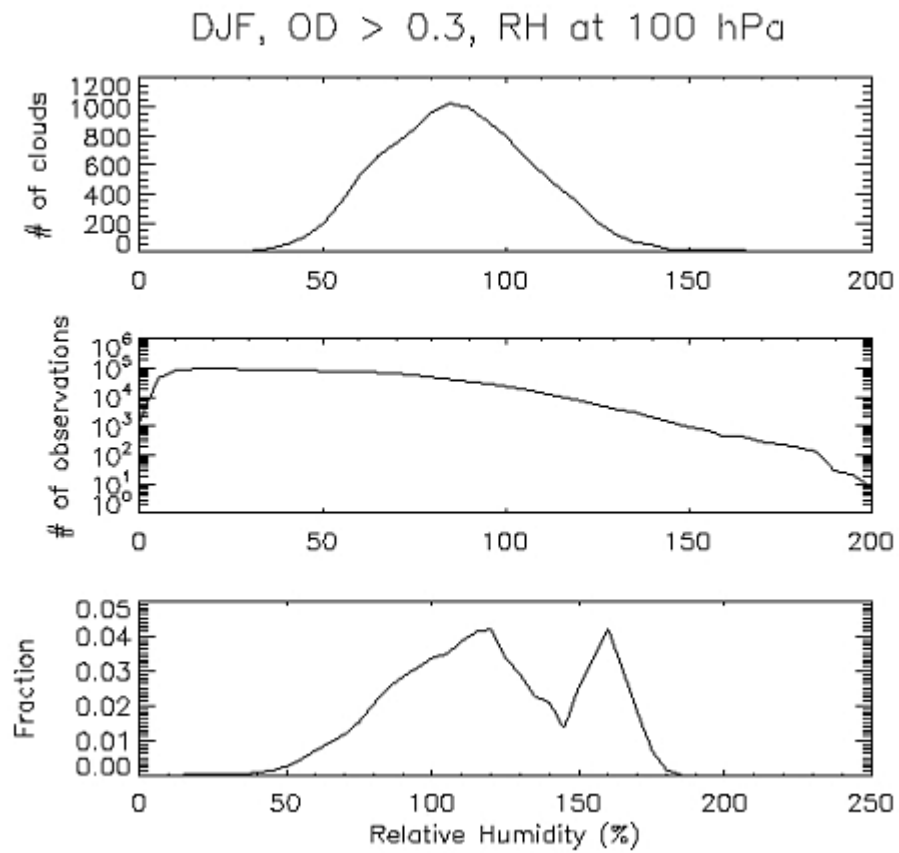
Figure 21: a) Number of thick clouds, b) number of observations, and c) cloud fraction as a function of RHI at 100 hPa for DJF. Bin size of 5% RHI is used.
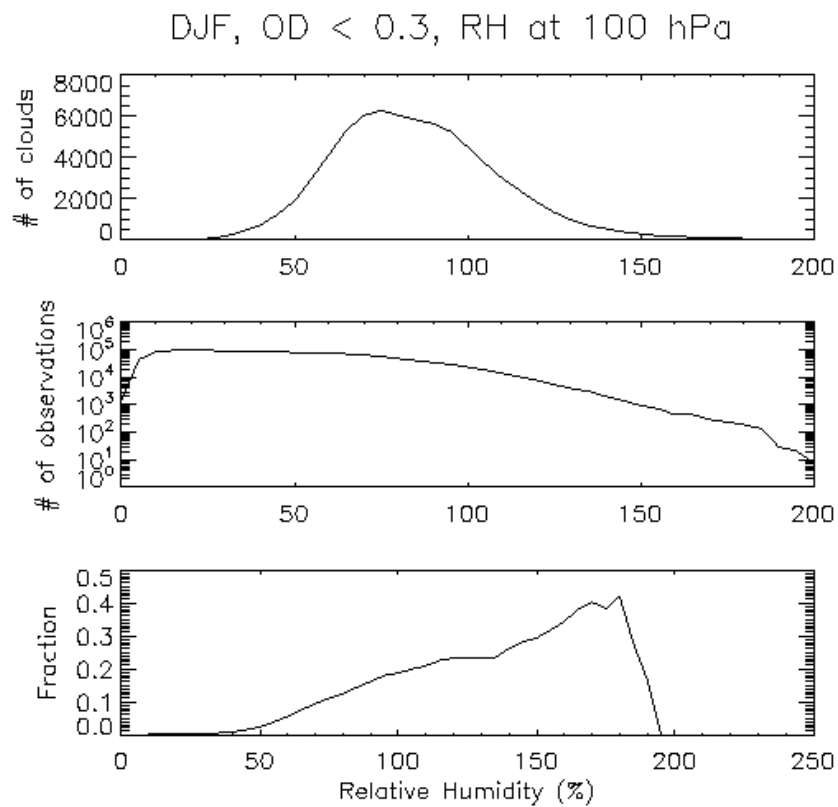
Figure 22: a) Number of thin clouds, b) number of observations, and c) cloud fraction as a function of RHI at 100 hPa for DJF. Bin size of 5% RHI is used.
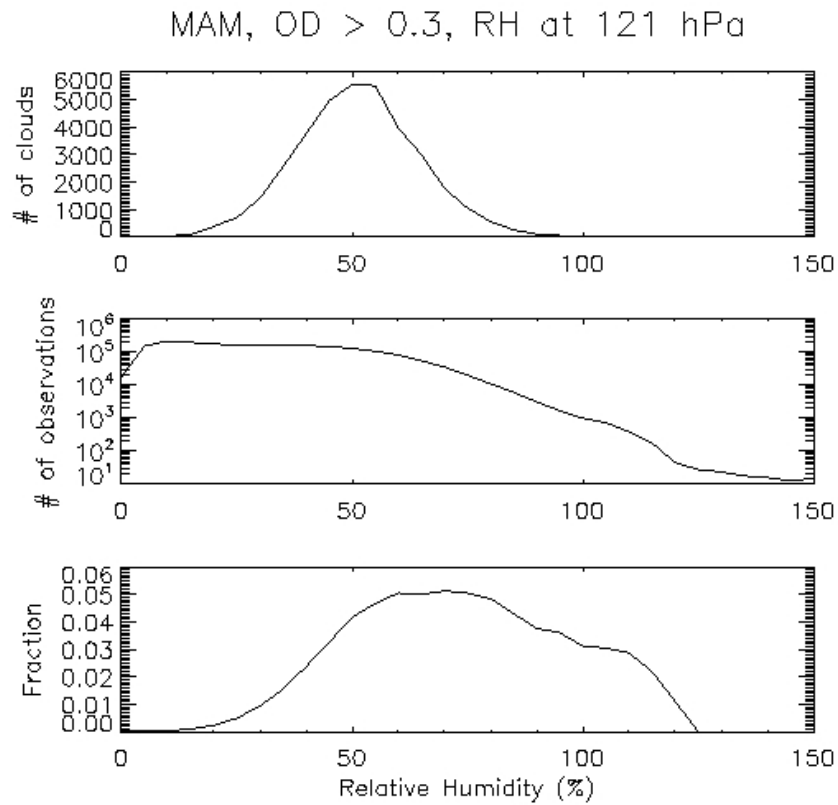
Figure 23: a) Number of thick clouds, b) number of observations, and c) cloud fraction as a function of RHI at 121-hPa for MAM. Bin size of 5% RHI is used.
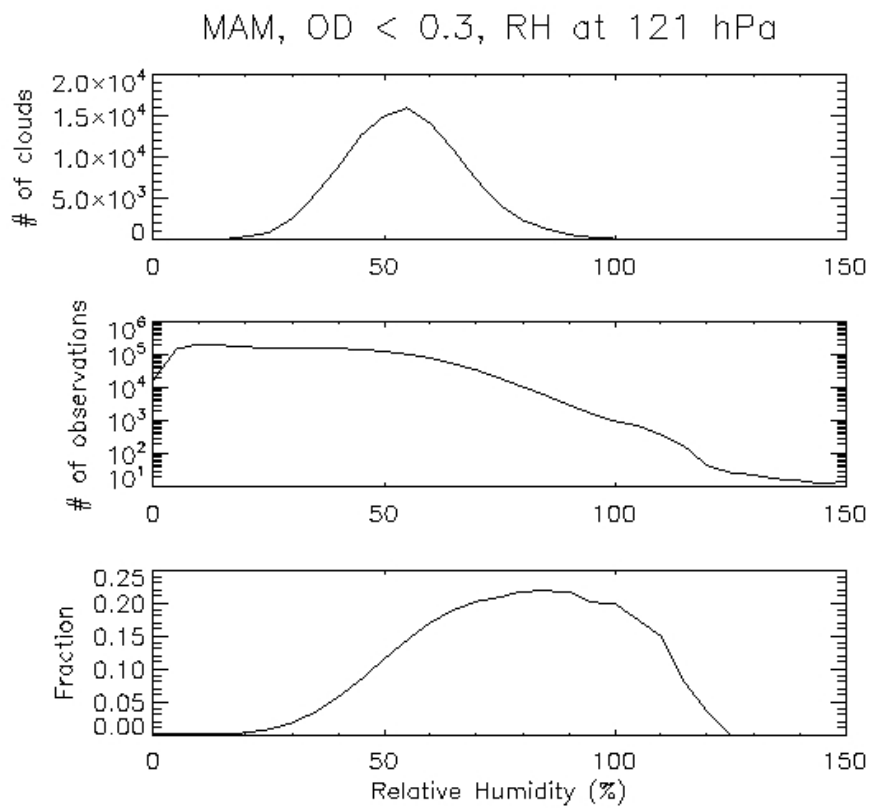
Figure 24: a) Number of thin clouds, b) number of observations, and c) cloud fraction as a function of RHI at 121-hPa for MAM. Bin size of 5% RHI is used.
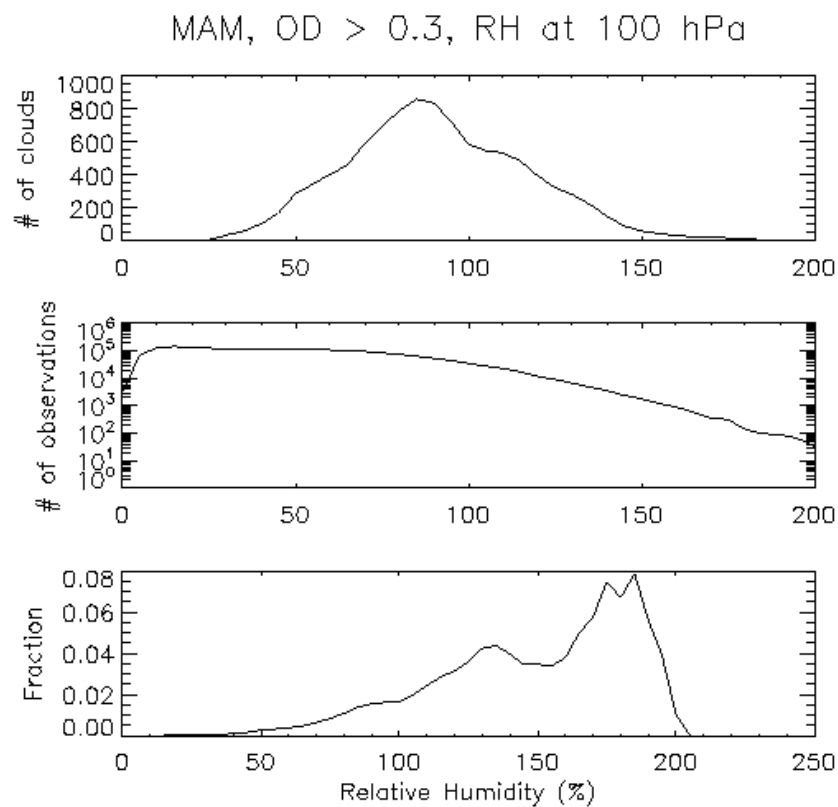
Figure 25: a) Number of thick clouds, b) number of observations, and c) cloud fraction as a function of RHI at 100-hPa for MAM. Bin size of 5% RHI is used.
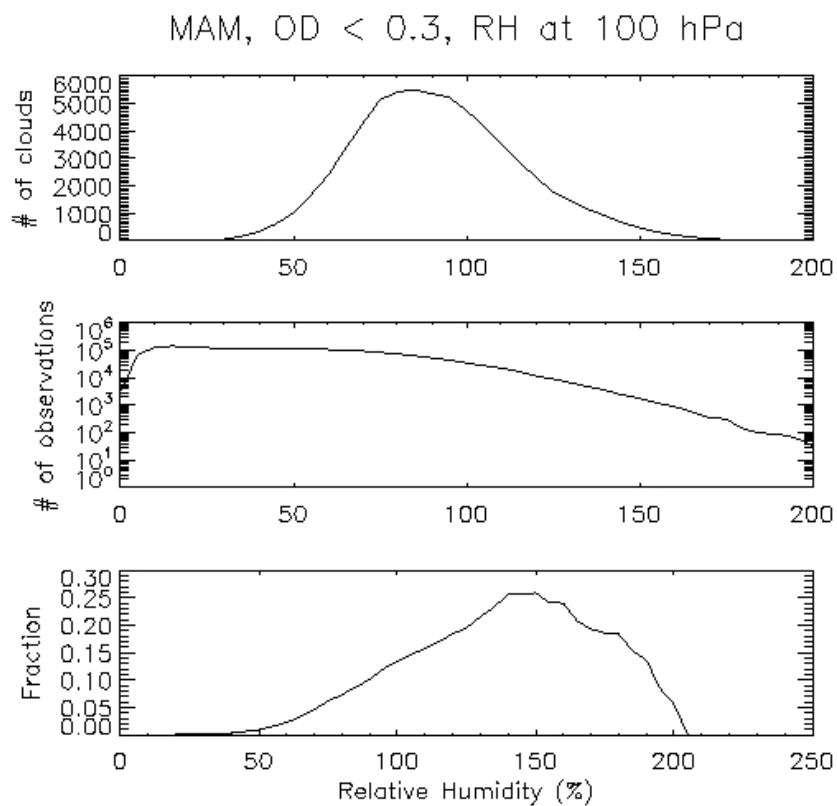
Figure 26: a) Number of thin clouds, b) number of observations, and c) cloud fraction as a function of RHI at 100-hPa for MAM. Bin size of 5% RHI is used.
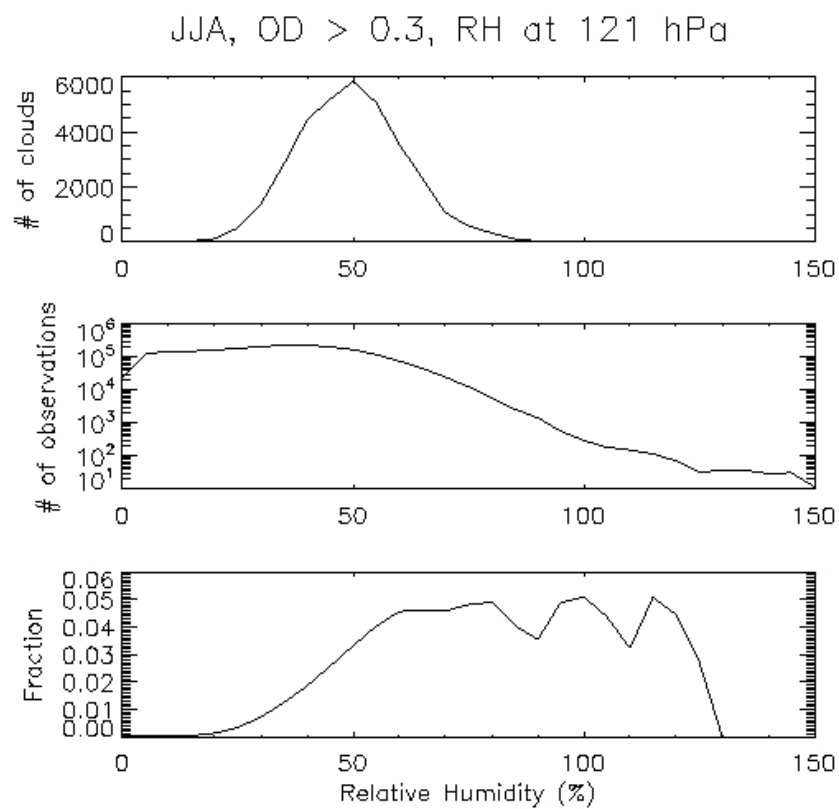
Figure 27: a) Number of thick clouds, b) number of observations, and c) cloud fraction as a function of RHI at 121-hPa for JJA. Bin size of 5% RHI is used.
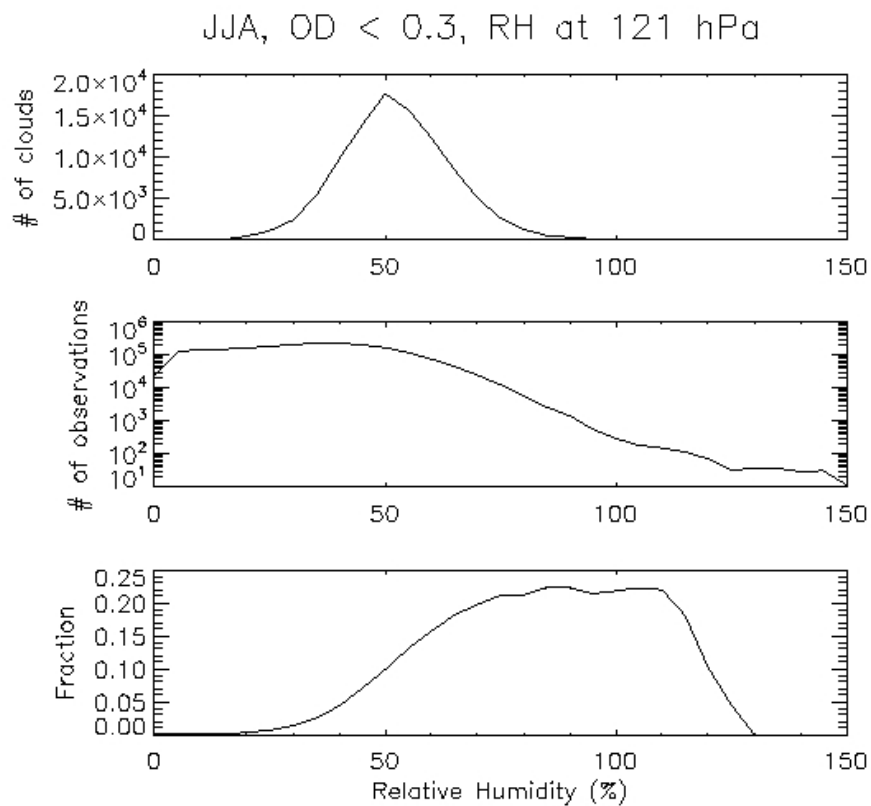
Figure 28: a) Number of thin clouds, b) number of observations, and c) cloud fraction as a function of RHI at 121-hPa for JJA. Bin size of 5% RHI is used.
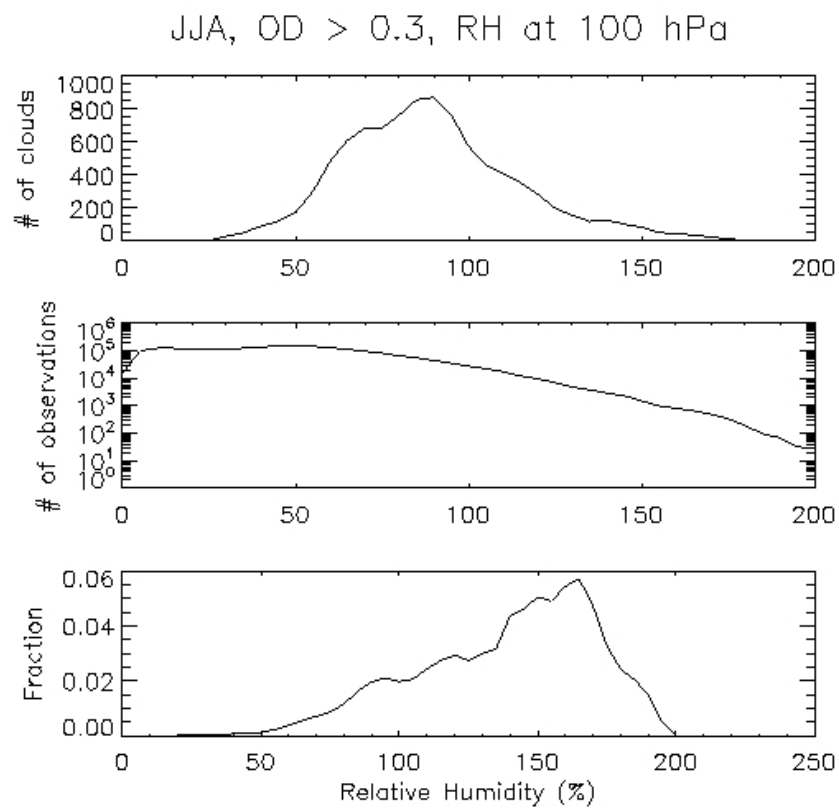
Figure 29: a) Number of thick clouds, b) number of observations, and c) cloud fraction as a function of RHI at 100-hPa for JJA. Bin size of 5% RHI is used.
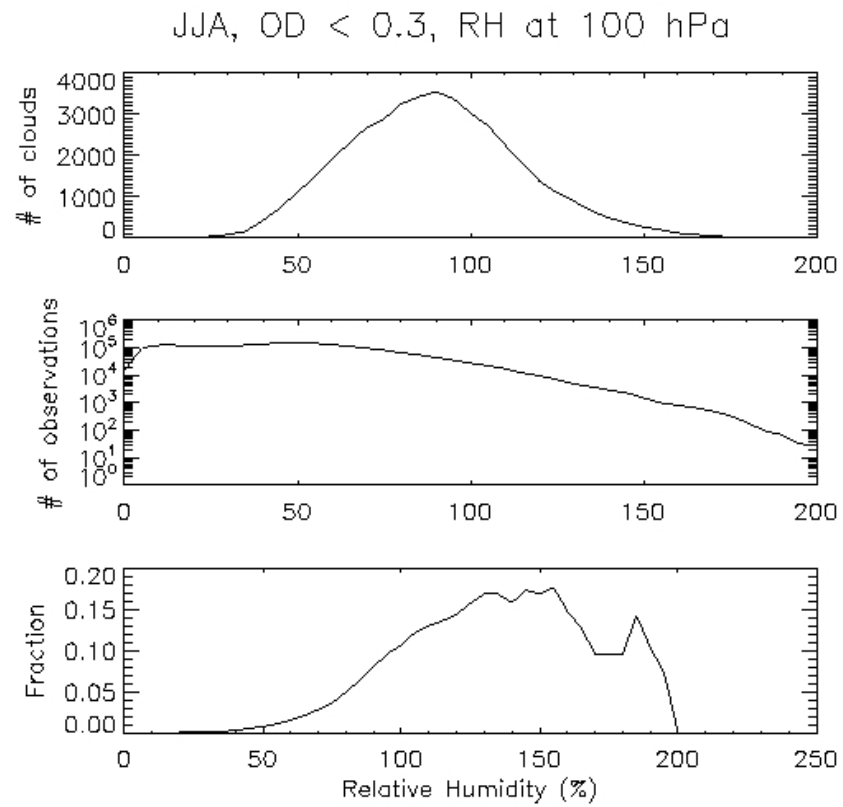
Figure 30: a) Number of thin clouds, b) number of observations, and c) cloud fraction as a function of RHI at 100-hPa for JJA. Bin size of 5% RHI is used.
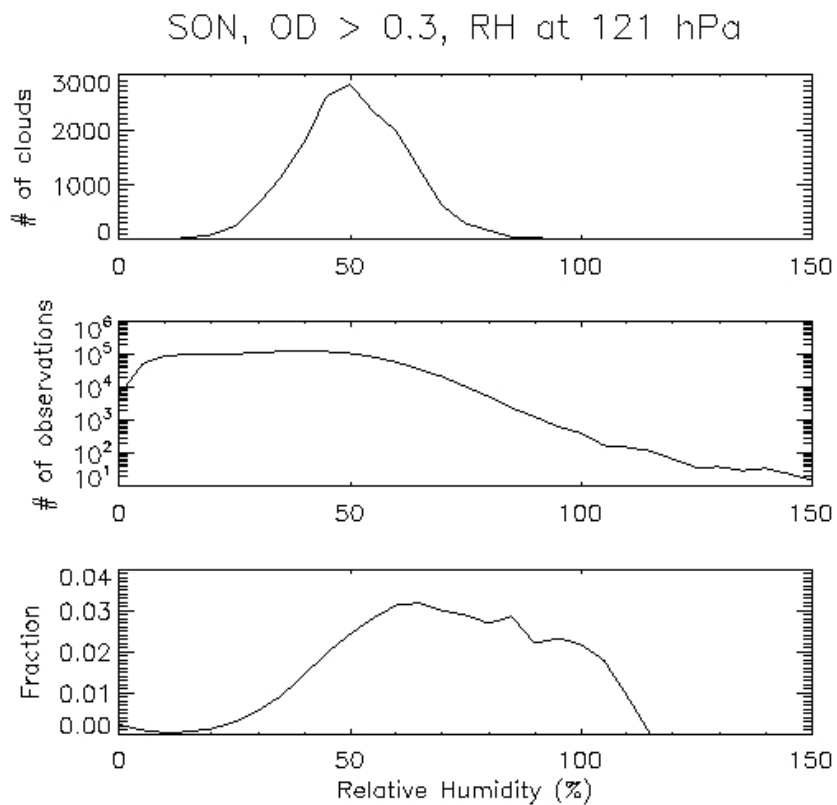
Figure 31: a) Number of thick clouds, b) number of observations, and c) cloud fraction as a function of RHI at 121-hPa for SON. Bin size of 5% RHI is used.
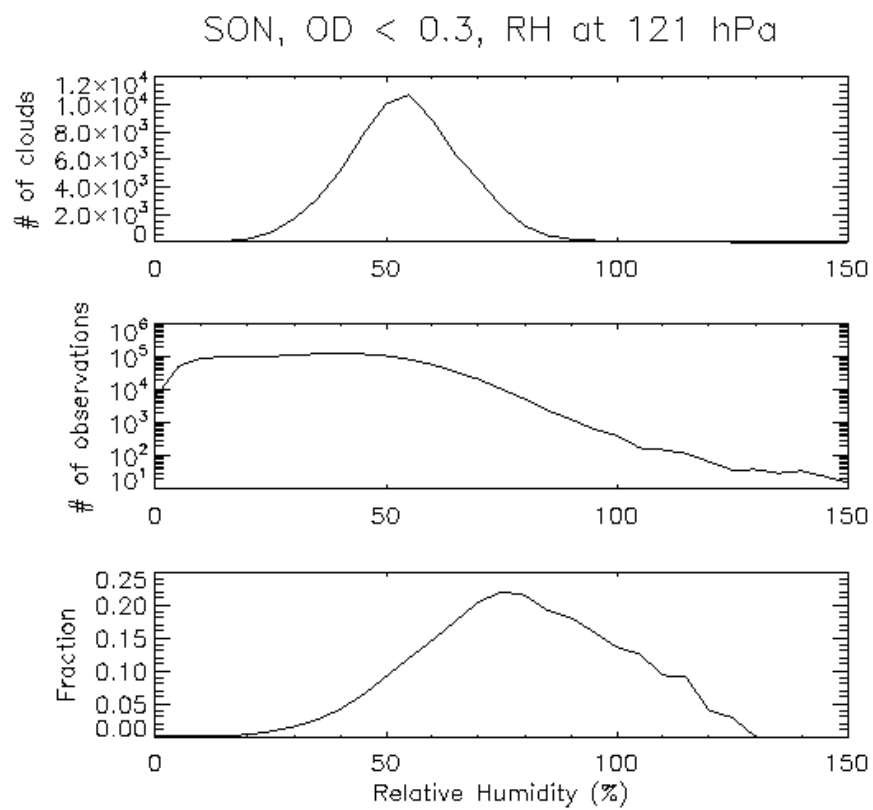
Figure 32: a) Number of thin clouds, b) number of observations, and c) cloud fraction as a function of RHI at 121-hPa for SON. Bin size of 5% RHI is used.
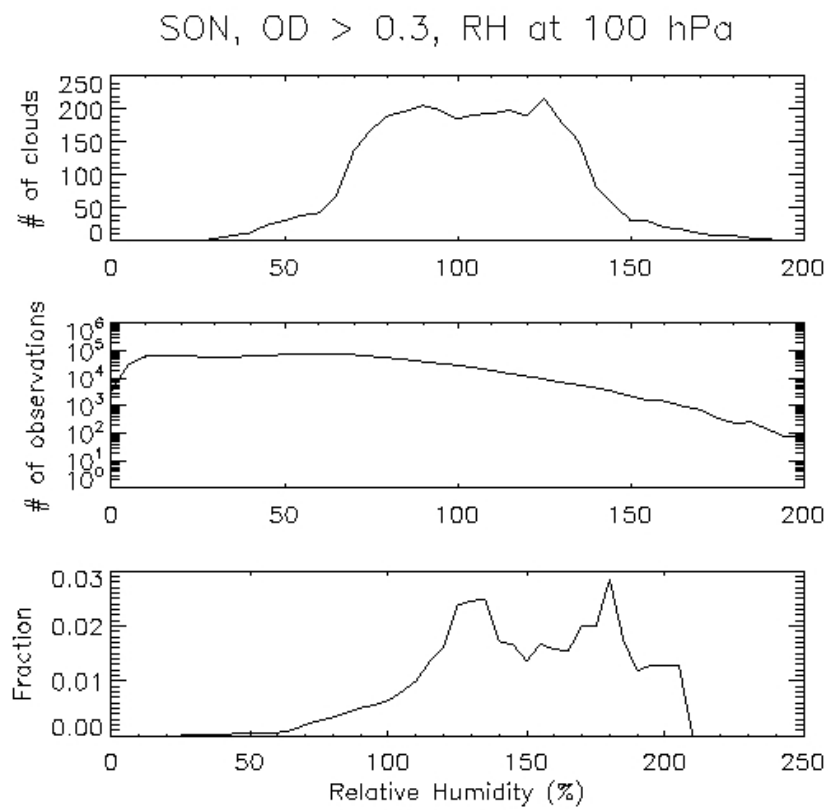
Figure 33: a) Number of thick clouds, b) number of observations, and c) cloud fraction as a function of RHI at 100-hPa for SON. Bin size of 5% RHI is used.

Figure 34: a) Number of thin clouds, b) number of observations, and c) cloud fraction as a function of RHI at 100-hPa for SON. Bin size of 5% RHI is used.
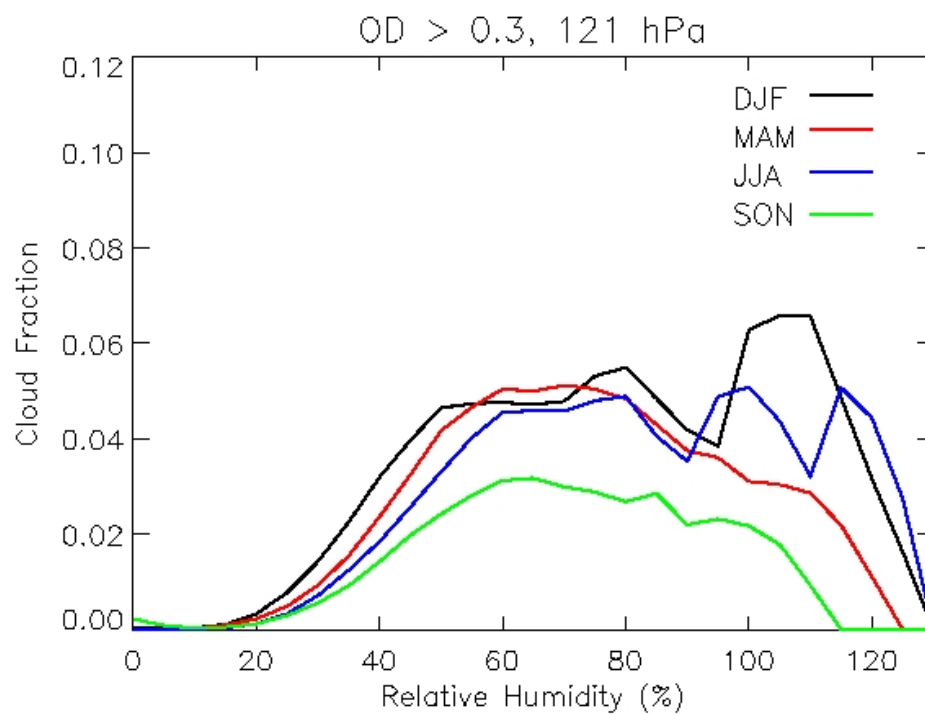
Figure 35: Thick cloud fraction as a function of relative humidity at 121-hPa for all seasons. Bin size of 5% RHI is used.
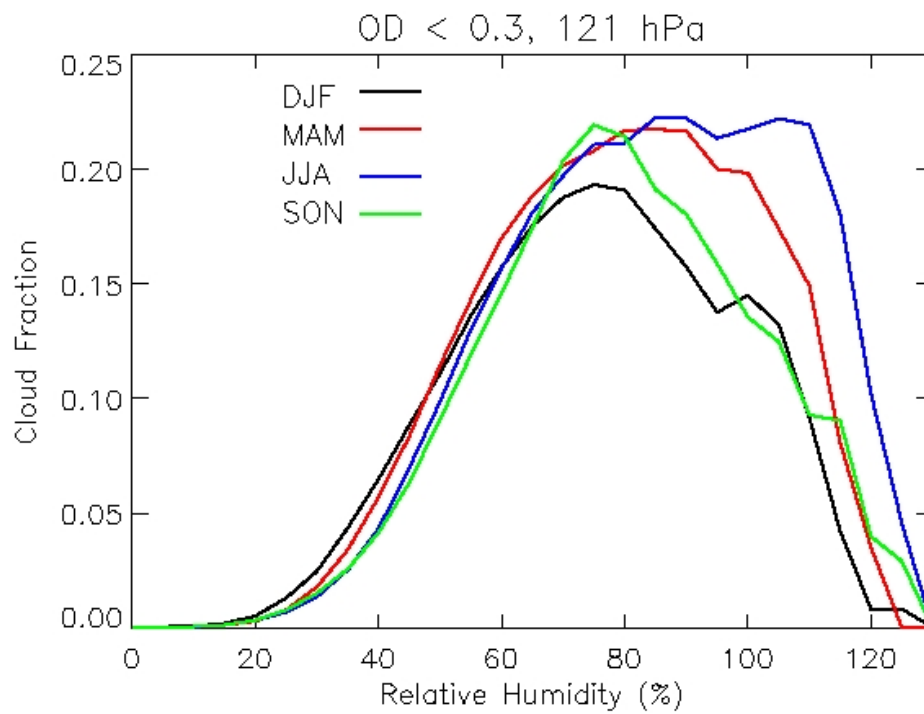
Figure 36: Thin cirrus fraction as a function of relative humidity at 121-hPa for all seasons. Bin size of 5% RHI is used.
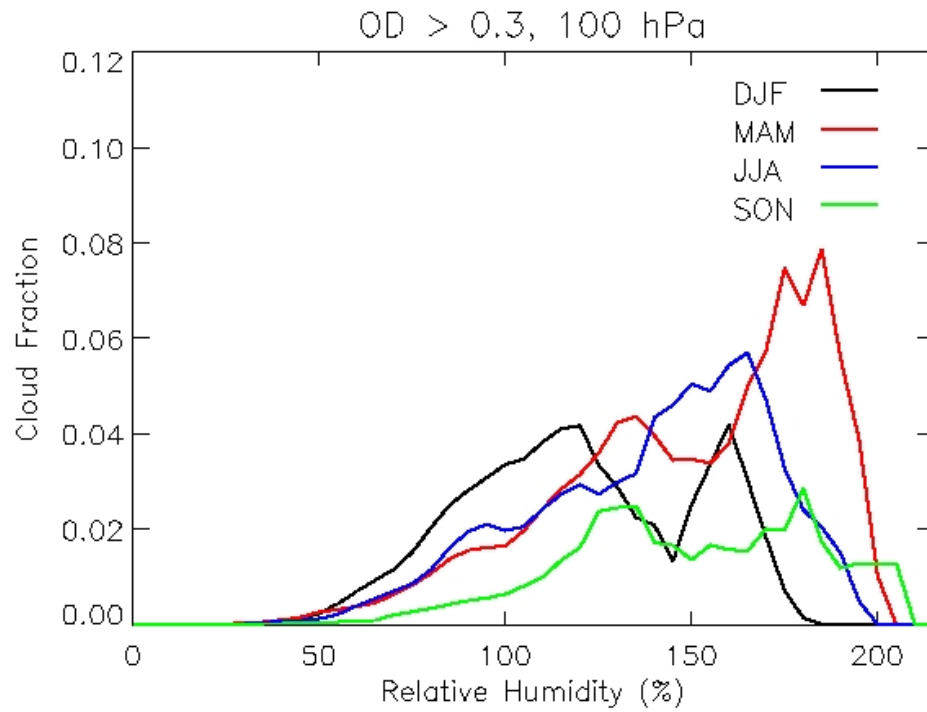
Figure 37: Thick cloud fraction as a function of relative humidity at 100-hPa for all seasons. Bin size of 5% RHI is used.
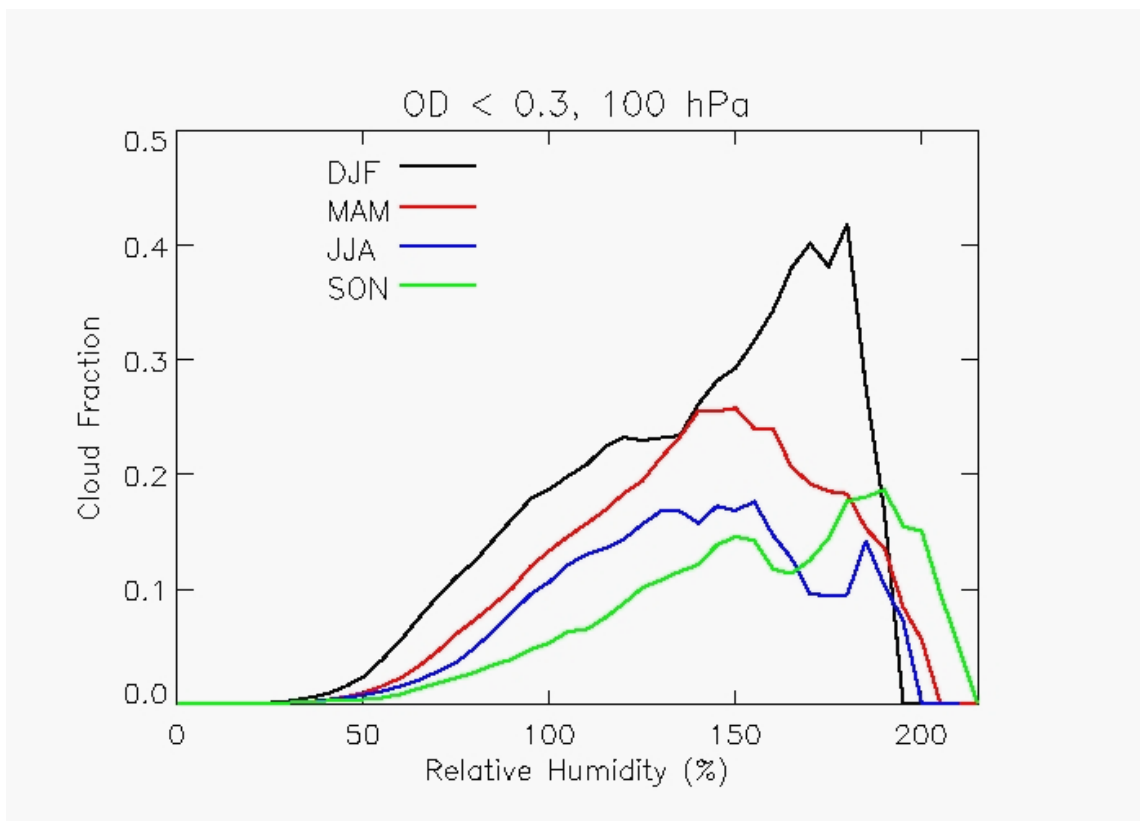
Figure 38: Thin cirrus fraction as a function of relative humidity at 100-hPa for all seasons. Bin size of 5% RHI is used.
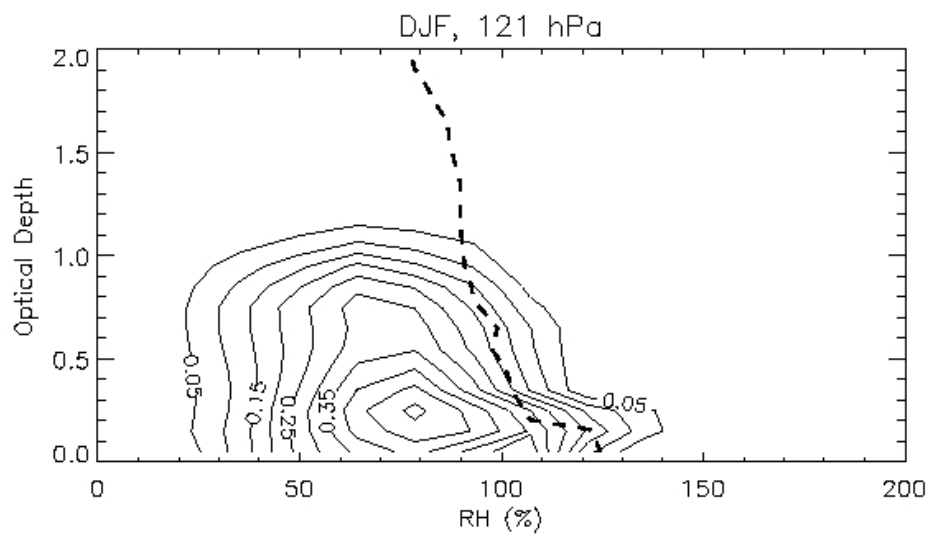
Figure 39: Cloud fraction as a function of RHI and optical depth for DJF at 121-hPa. Dashed line represents 50 total observations, solid lines represent cloud fraction. Bin size of 0.14 optical depth by 10% RHI is used.
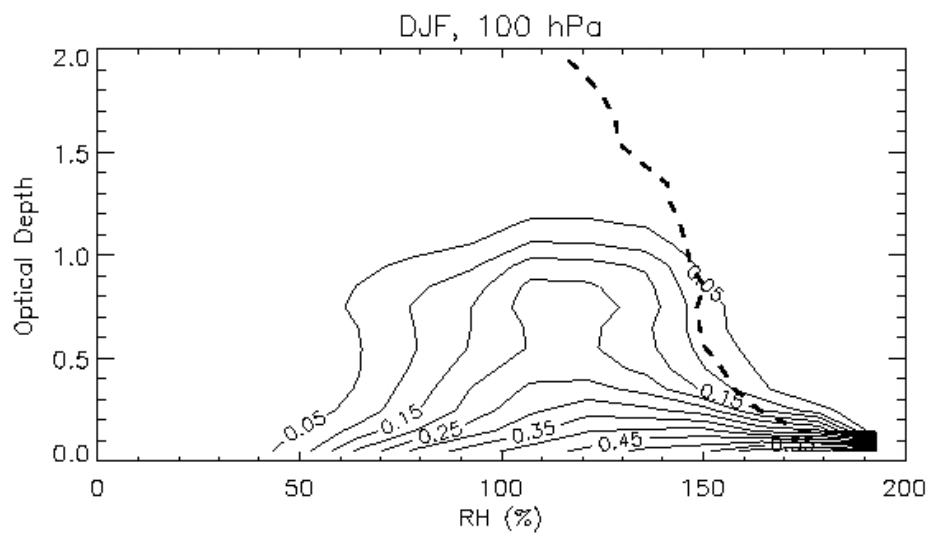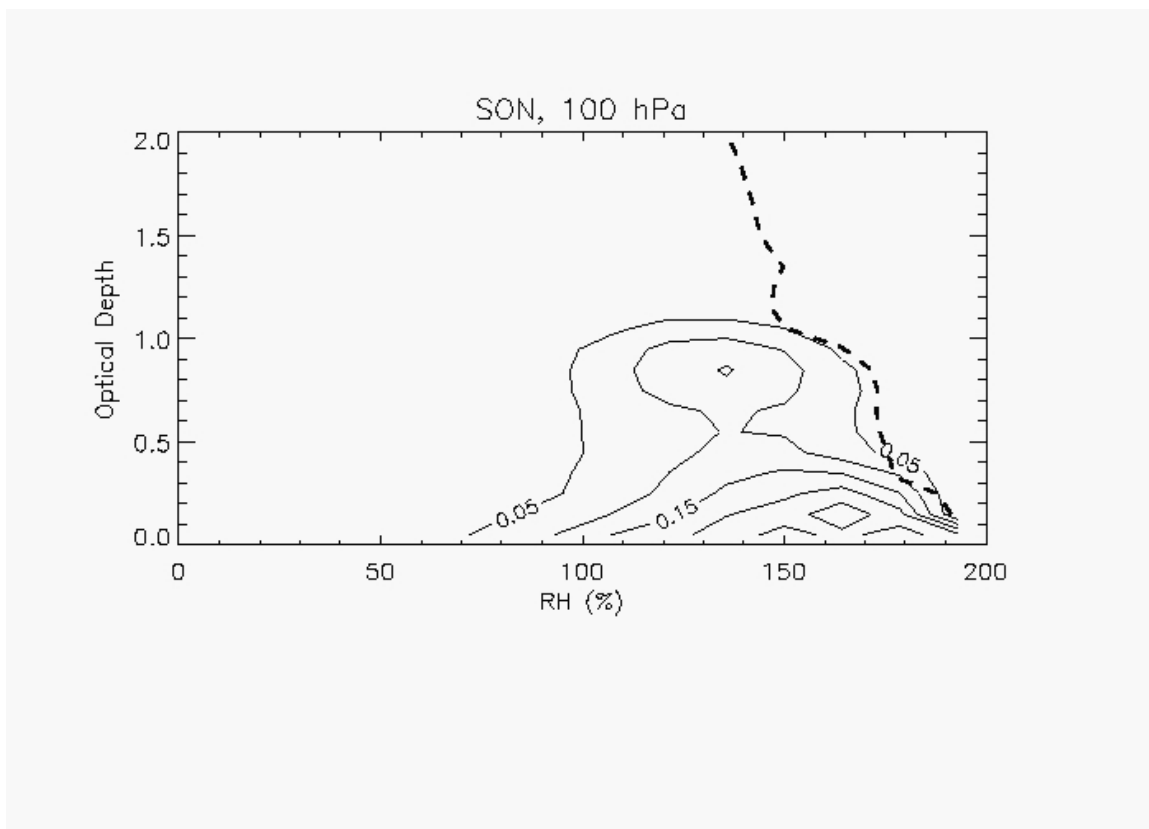
Figure 40: Cloud fraction as a function of RHI and optical depth for DJF at 100-hPa. Dashed line represents 50 total observations, solid lines represent cloud fraction. Bin size of 0.14 optical depth by 10% RHI is used.
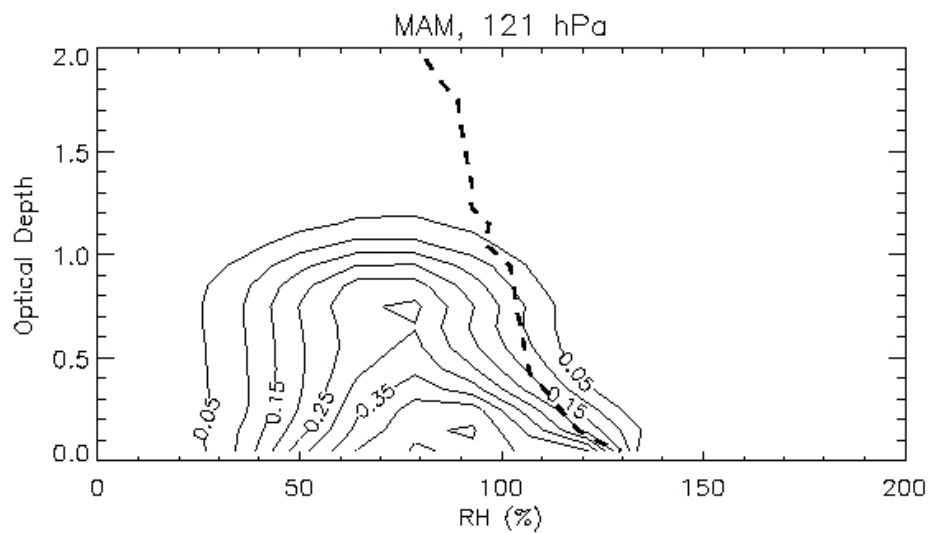
Figure 41: Cloud fraction as a function of RHI and optical depth for MAM at 121-hPa. Dashed line represents 50 total observations, solid lines represent cloud fraction. Bin size of 0.14 optical depth by 10% RHI is used.
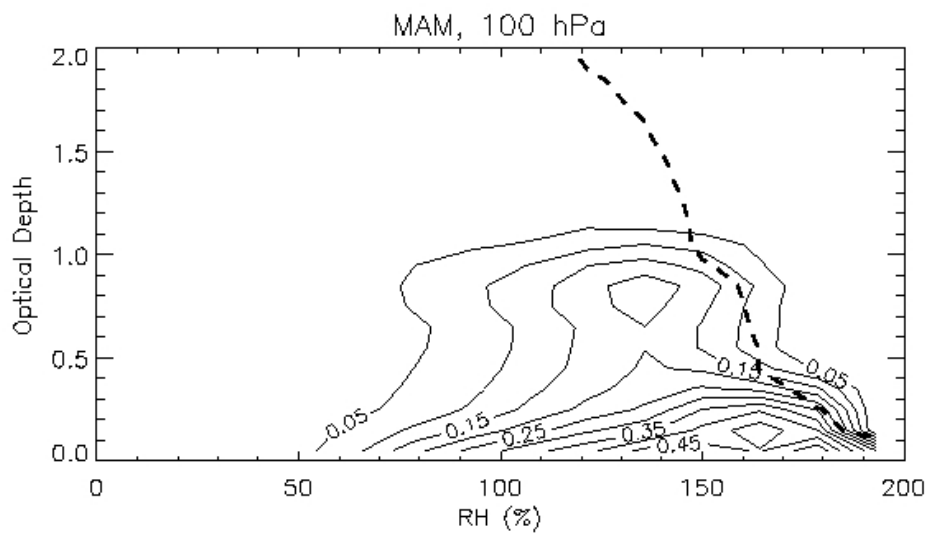
Figure 42: Cloud fraction as a function of RHI and optical depth for MAM at 100-hPa. Dashed line represents 50 total observations, solid lines represent cloud fraction. Bin size of 0.14 optical depth by 10% RHI is used.
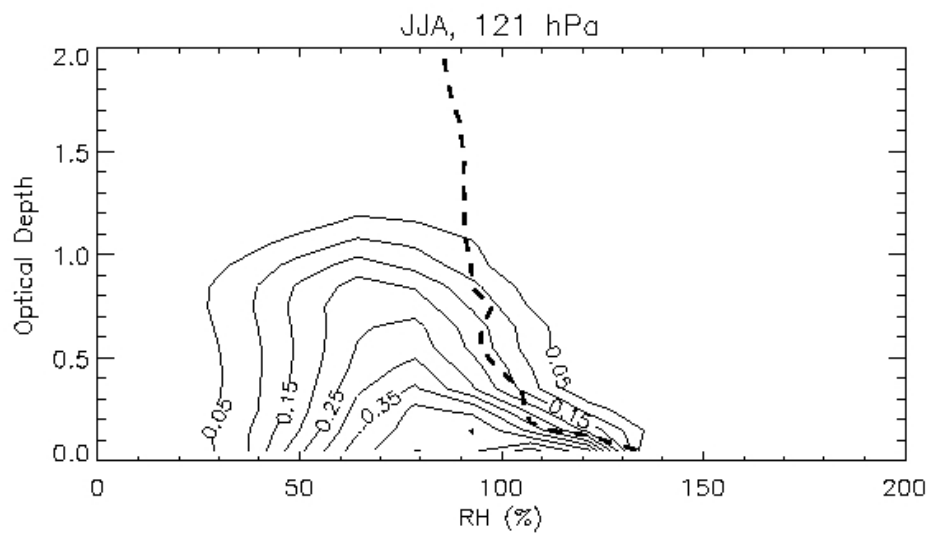
Figure 43: Cloud fraction as a function of RHI and optical depth for JJA at 121-hPa. Dashed line represents 50 total observations, solid lines represent cloud fraction. Bin size of 0.14 optical depth by 10% RHI is used.
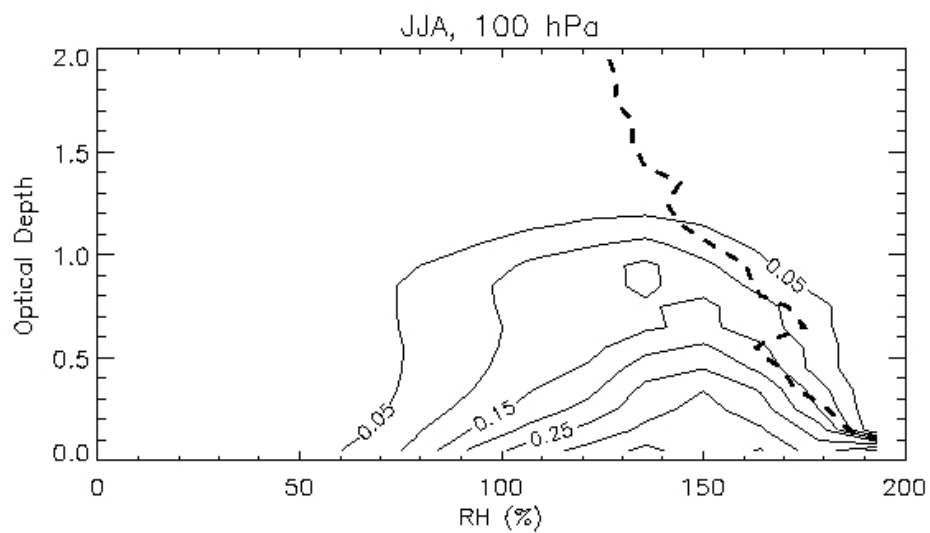
Figure 44: Cloud fraction as a function of RHI and optical depth for JJA at 100-hPa. Dashed line represents 50 total observations, solid lines represent cloud fraction. Bin size of 0.14 optical depth by 10% RHI is used.
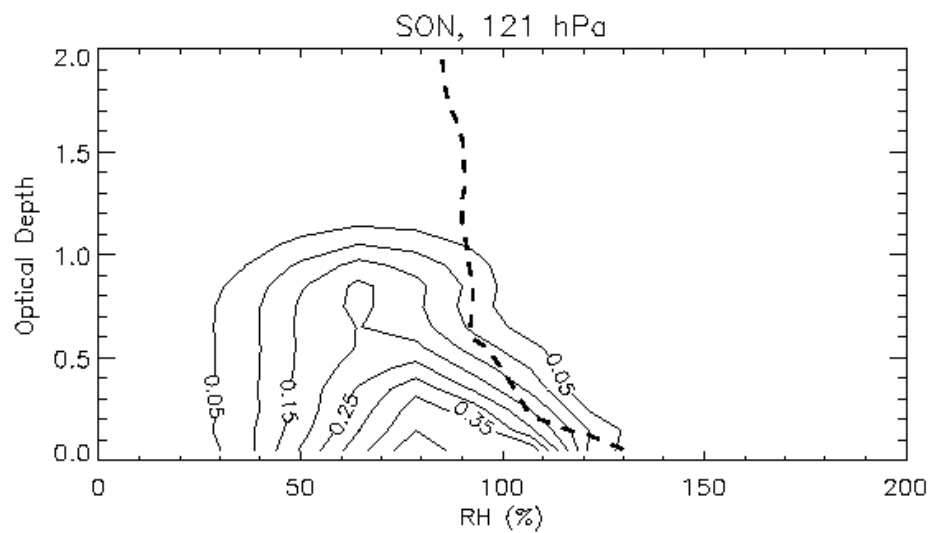
Figure 45: Cloud fraction as a function of RHI and optical depth for SON at 121-hPa. Dashed line represents 50 total observations, solid lines represent cloud fraction. Bin size of 0.14 optical depth by 10% RHI is used.

Figure 46: Cloud fraction as a function of RHI and optical depth for SON at 100-hPa. Dashed line represents 50 total observations, solid lines represent cloud fraction. Bin size of 0.14 optical depth by 10% RHI is used.
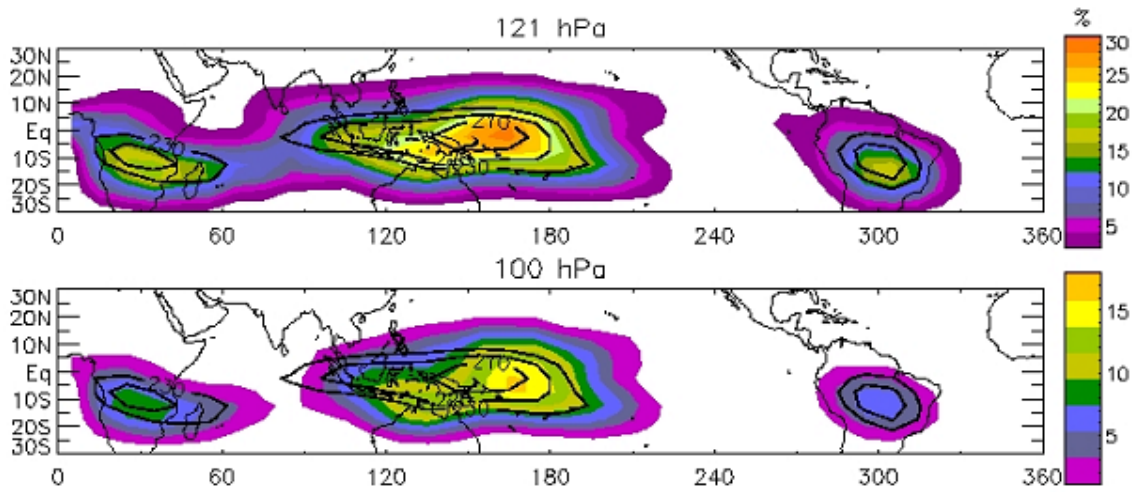
Figure 47: DJF thick frequencies in colored contours at a) 121-hPa and b) 100-hPa with OLR values of less than 230 W-m^{-2} in black contours.
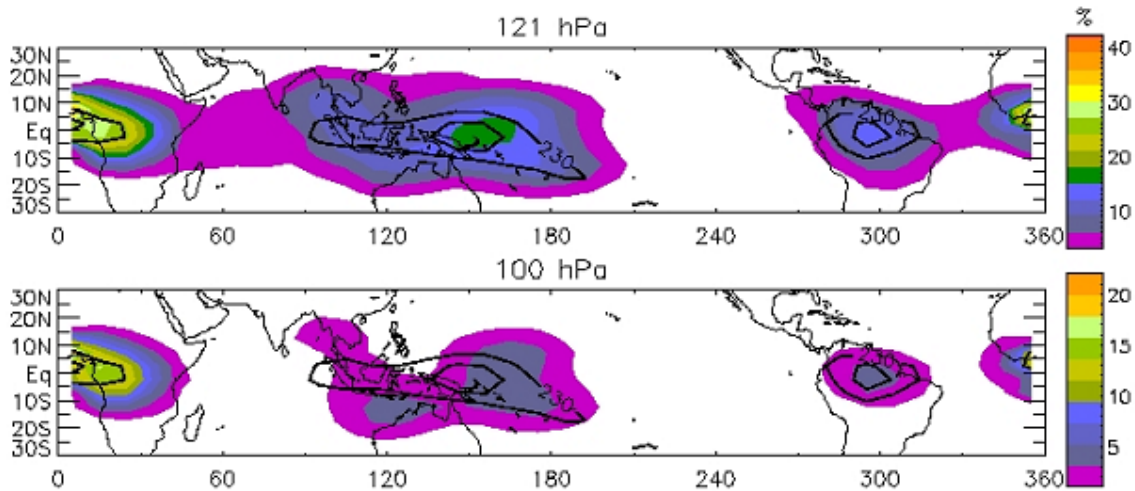
Figure 48: MAM thick cloud frequencies in colored contours at a) 121-hPa and b) 100-hPa with OLR values of less than 230 W-m^{-2} in black contours.
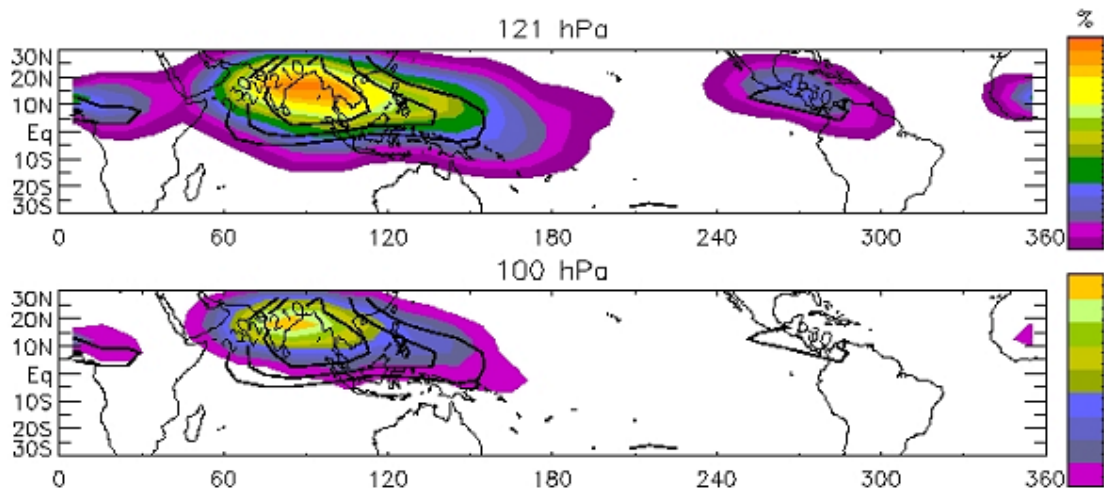
Figure 49: JJA thick cloud frequencies in colored contours at a) 121-hPa and b) 100-hPa with OLR values of less than 230 W-m^{-2} in black contours.
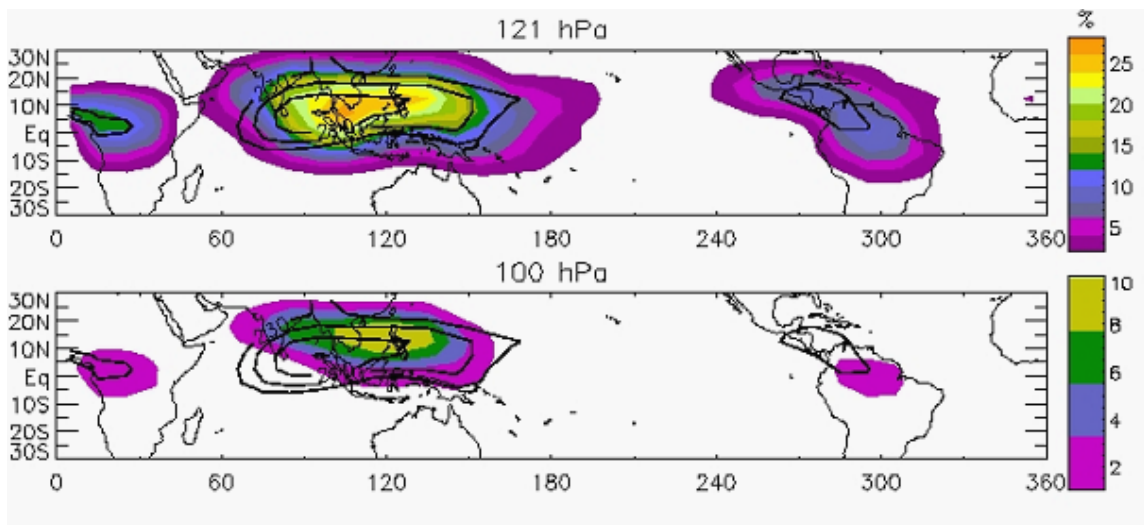
Figure 50: SON thick cloud frequencies in colored contours at a) 121-hPa and b) 100-hPa with OLR values of less than 230 W-m^{-2} in black contours.
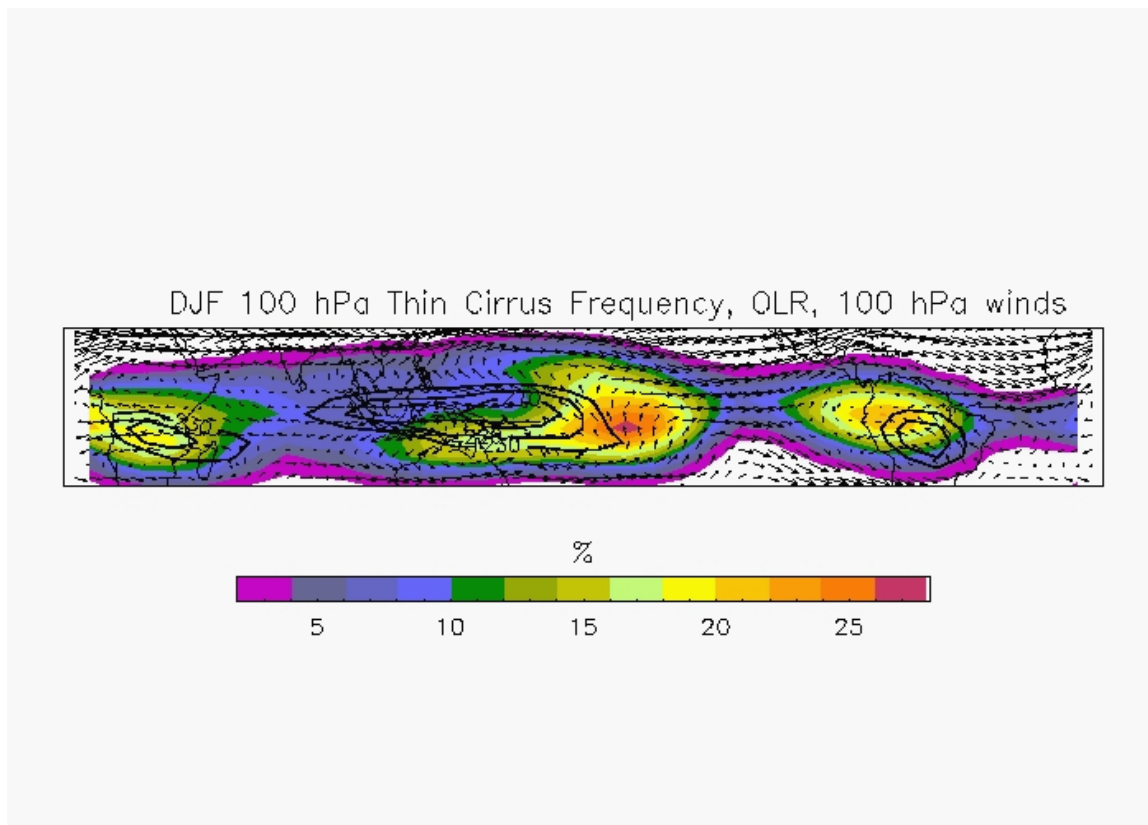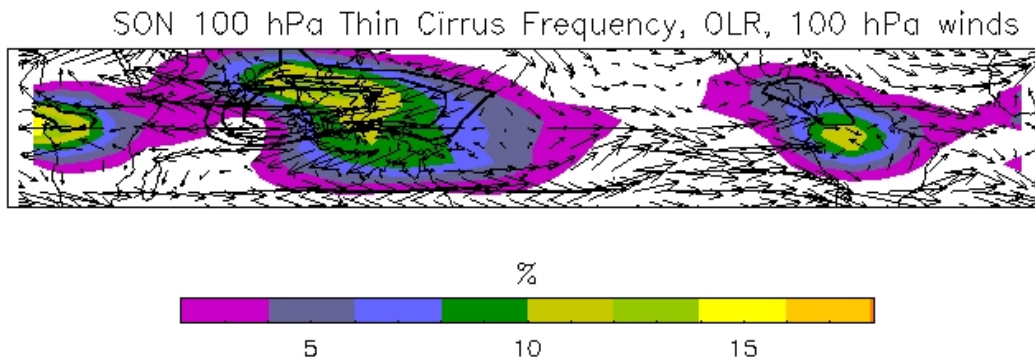
Figure 51: DJF 100-hPa thin cirrus frequencies in colored contours and OLR values less than 230 W-m^{-2} in black contours. NCEP reanalysis data plotted as vectors.
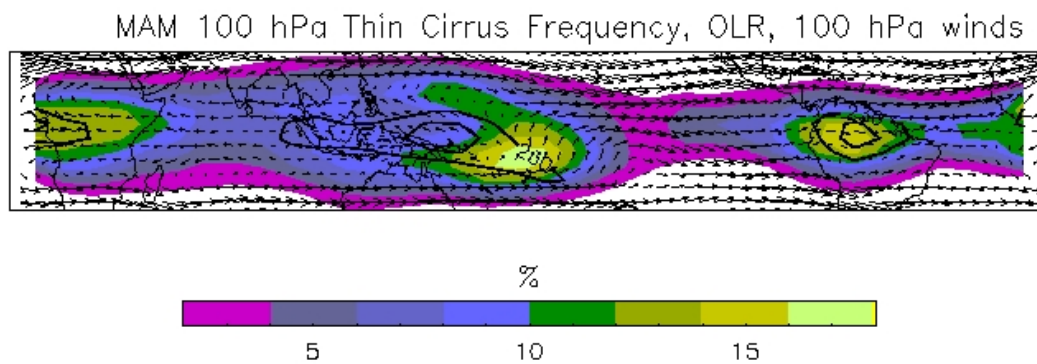
Figure 52: MAM 100-hPa thin cirrus frequencies in colored contours and OLR values less than 230 W-m^{-2} in black contours. NCEP reanalysis data plotted as vectors.
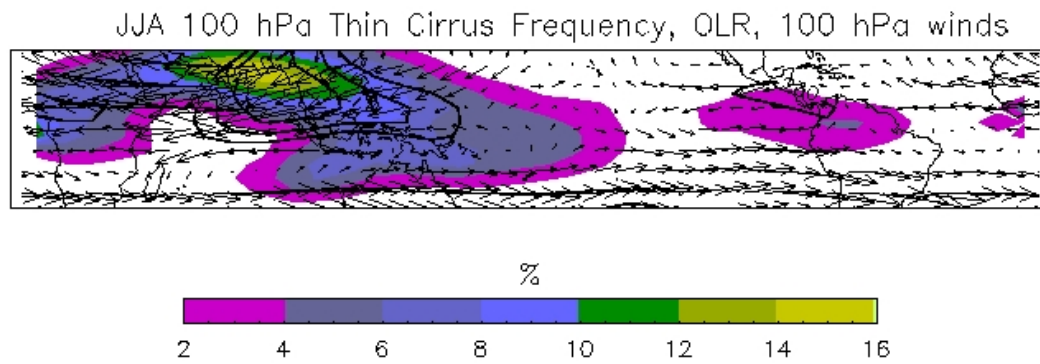
Figure 53: JJA 100-hPa thin cirrus frequencies in colored contours and OLR values less than 230 W-m^{-2} in black contours. NCEP reanalysis data plotted as vectors.

Figure 54: SON 100-hPa thin cirrus frequencies in colored contours and OLR values less than 230 W-m^{-2} in black contours. NCEP reanalysis data plotted as vectors.
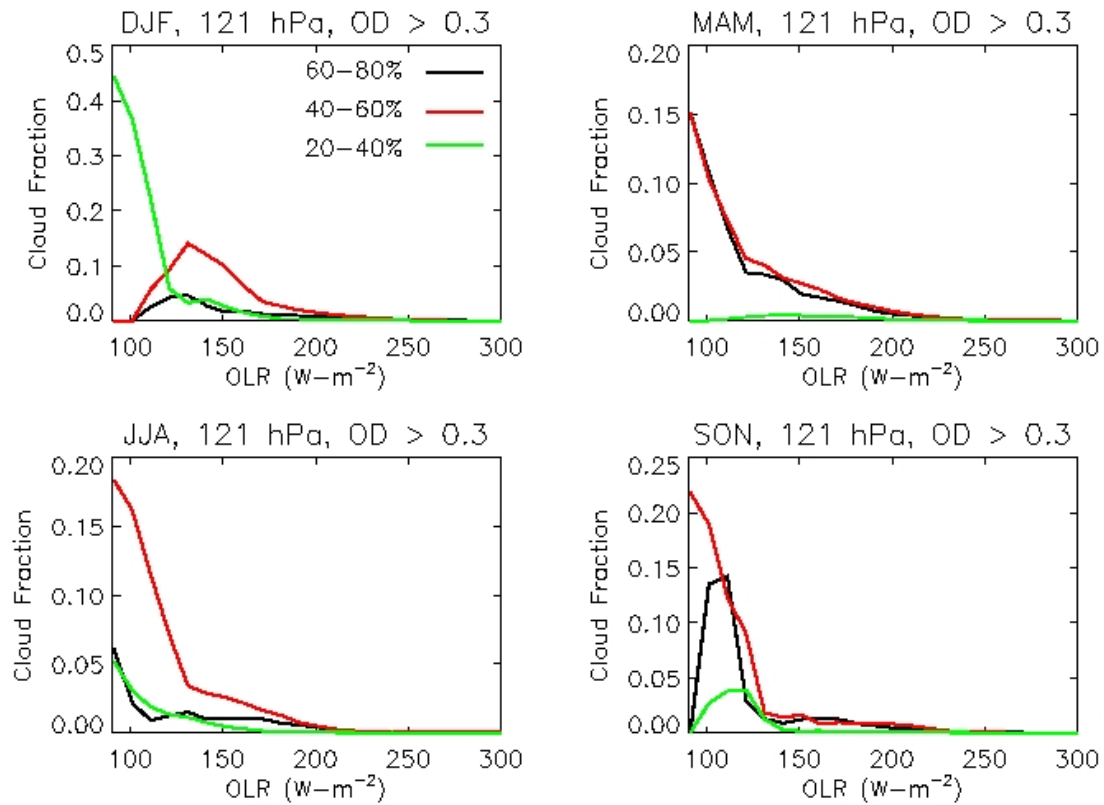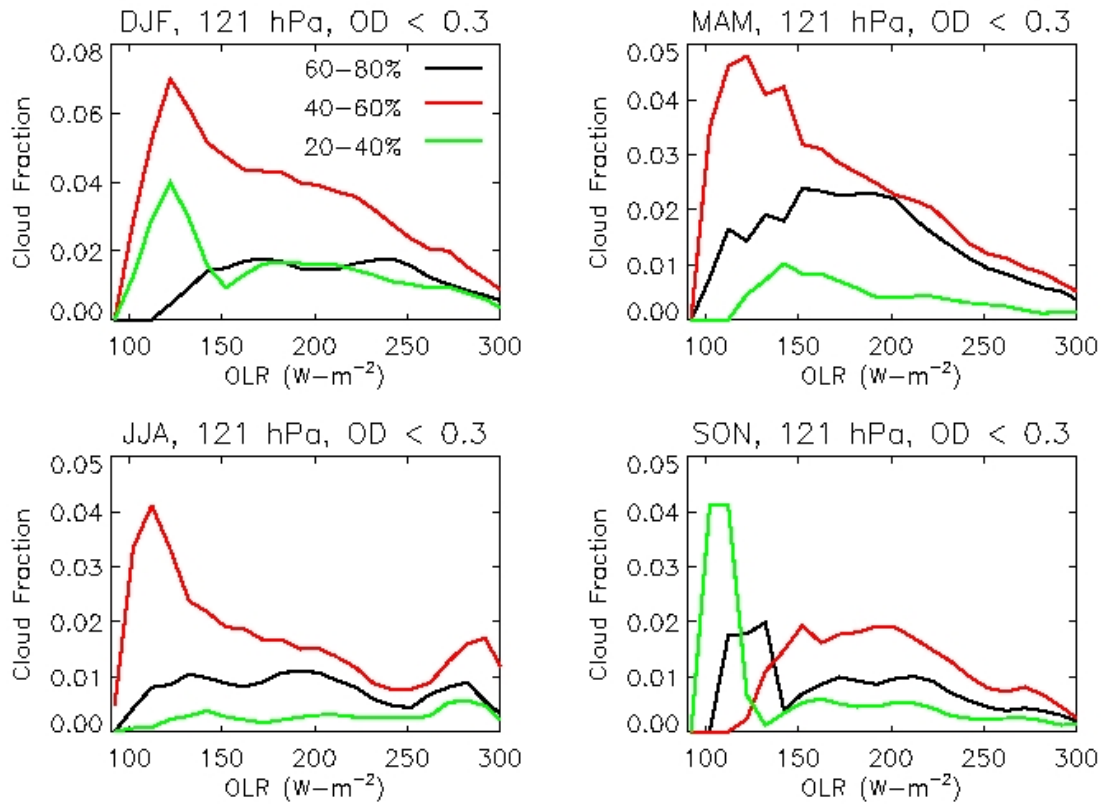
Figure 55: Thick cloud fraction as a function of OLR for RHI at 121-hPa for values between 20-40%, 40-60%, and 60-80% for a) DJF, b) MAM, c) JJA, and d) SON at 121 hPa. Bin size of 10 W-m^{-2} is used.
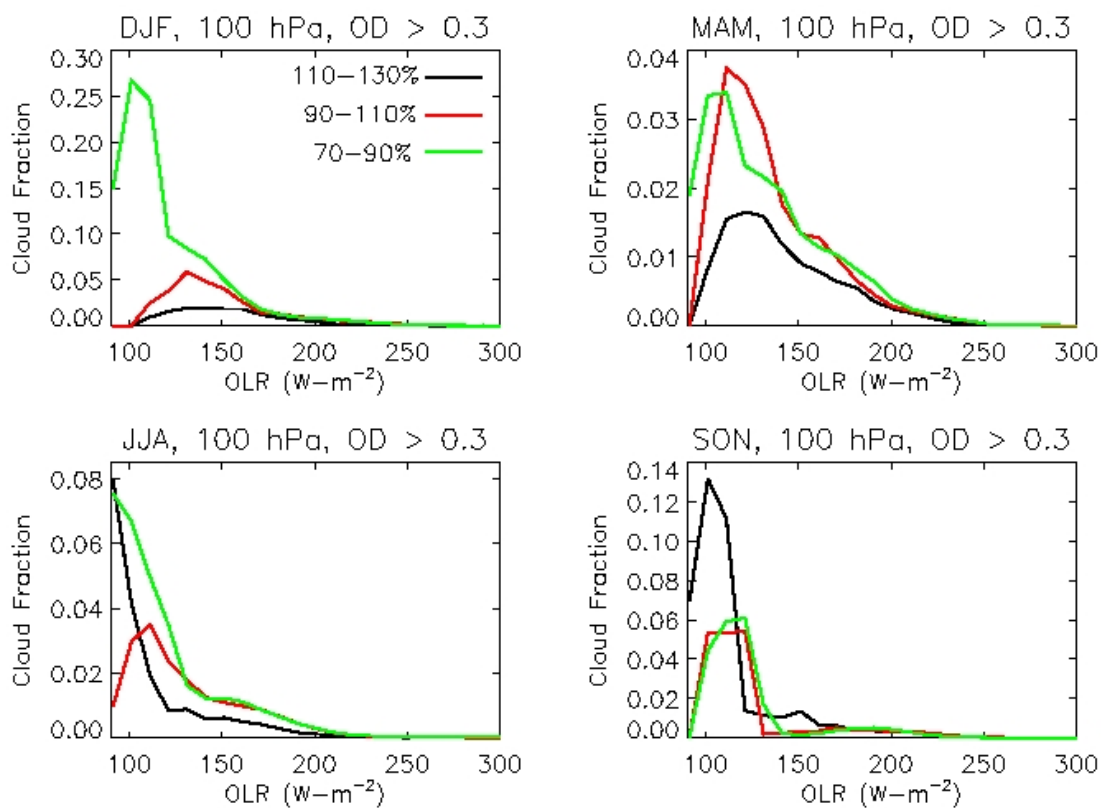
Figure 56: Thin cirrus cloud fraction as a function of OLR for RHI at 121-hPa for values between 20-40%, 40-60%, and 60-80% for a) DJF, b) MAM, c) JJA, and d) SON at 121-hPa. Bin size of 10 W-m^{-2} is used.

Figure 57: Thick cloud fraction as a function of OLR for RHI at 100-hPa for values between 70-90%, 90-110%, and 110-130% for a) DJF, b) MAM, c) JJA, and d) SON at 100-hPa. Bin size of 10 W-m^{-2} is used.
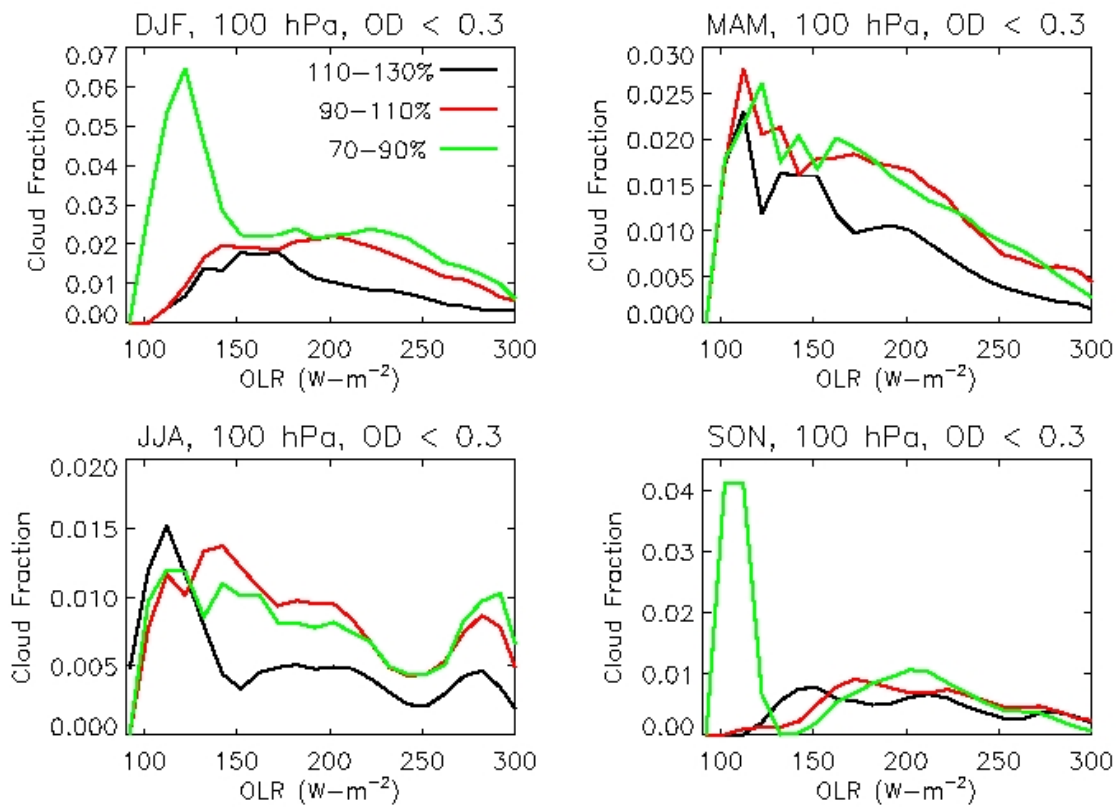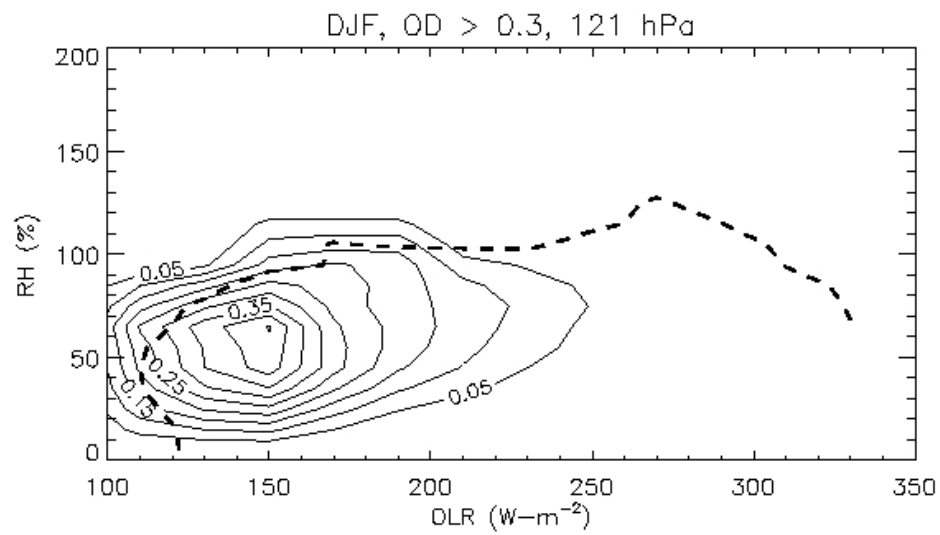
Figure 58: Thin cirrus fraction as a function of OLR for RHI at 100-hPa for values between 70-90%, 90-110%, and 110-130% for a) DJF, b) MAM, c) JJA, and d) SON at 100-hPa. Bin size of 10 W-m^{-2} is used.

Figure 59: Thick cloud fraction as a function of RHI and OLR for DJF at 121-hPa. Dashed line denotes 50 observations. Bin size of 10% RHI by 20 W-m^{-2} is used.
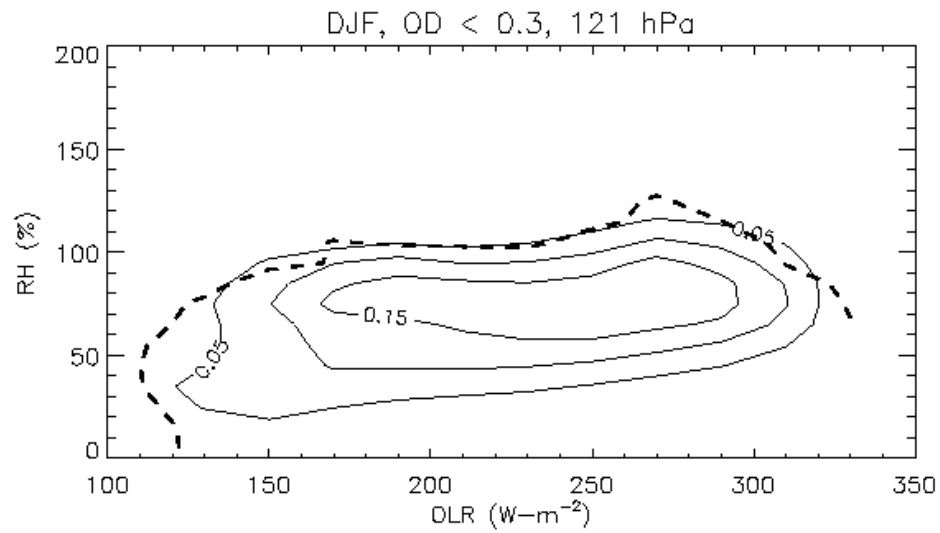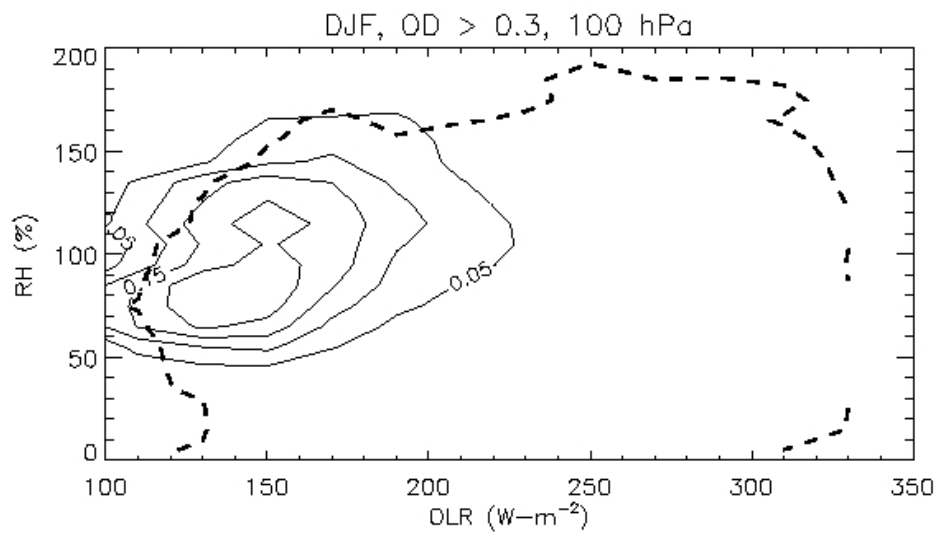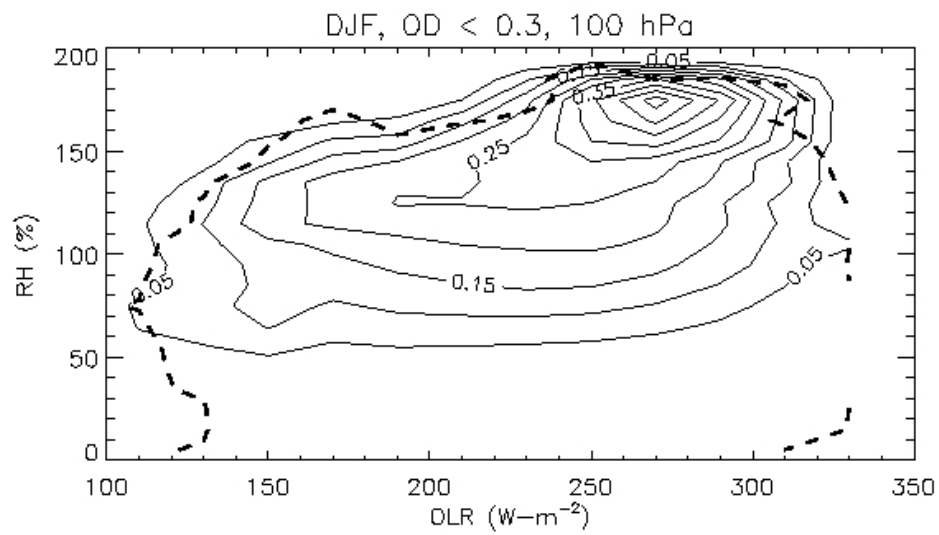
Figure 60: Thin cirrus fraction as a function of RHI and OLR for DJF at 121-hPa. Dashed line denotes 50 observations. Bin size of 10% RHI by 20 W-m^{-2} is used.

Figure 61: Thick cloud fraction as a function of RHI and OLR for DJF at 100-hPa. Dashed line denotes 50 observations. Bin size of 10% RHI by 20 W-m^{-2} is used.

Figure 62: Thin cirrus fraction as a function of RHI and OLR for DJF at 100-hPa. Dashed line denotes 50 observations. Bin size of 10% RHI by 20 W-m^{-2} is used.
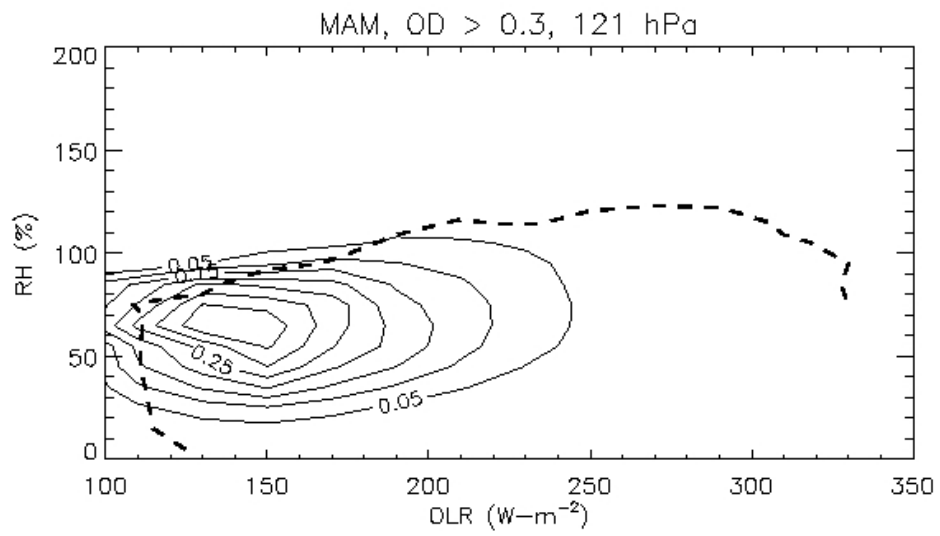
Figure 63: Thick cloud fraction as a function of RHI and OLR for MAM at 121-hPa. Dashed line denotes 50 observations. Bin size of 10% RHI by 20 W-m^{-2} is used.

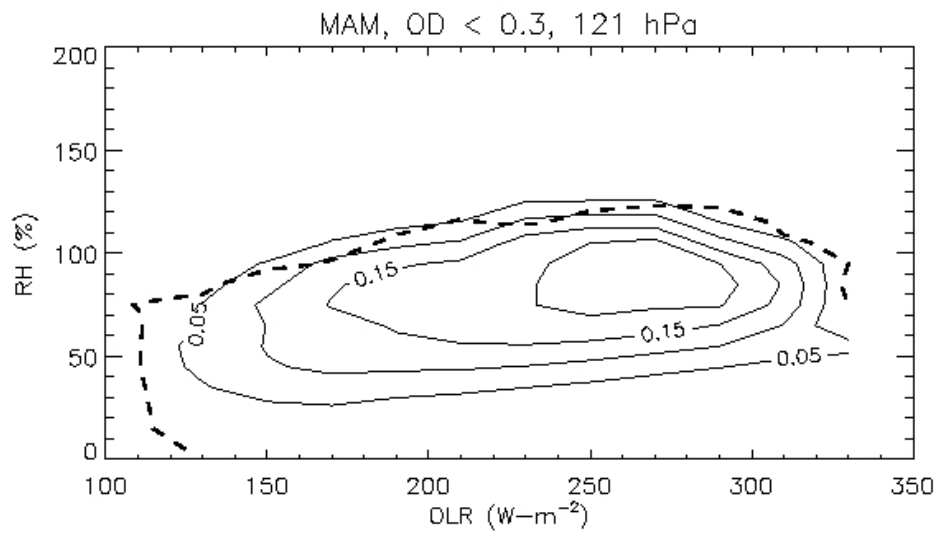**Figure 64:** Thin cirrus fraction as a function of RHI and OLR for MAM at 121-hPa. Dashed line denotes 50 observations. Bin size of 10% RHI by 20 W-m^{-2} is used.
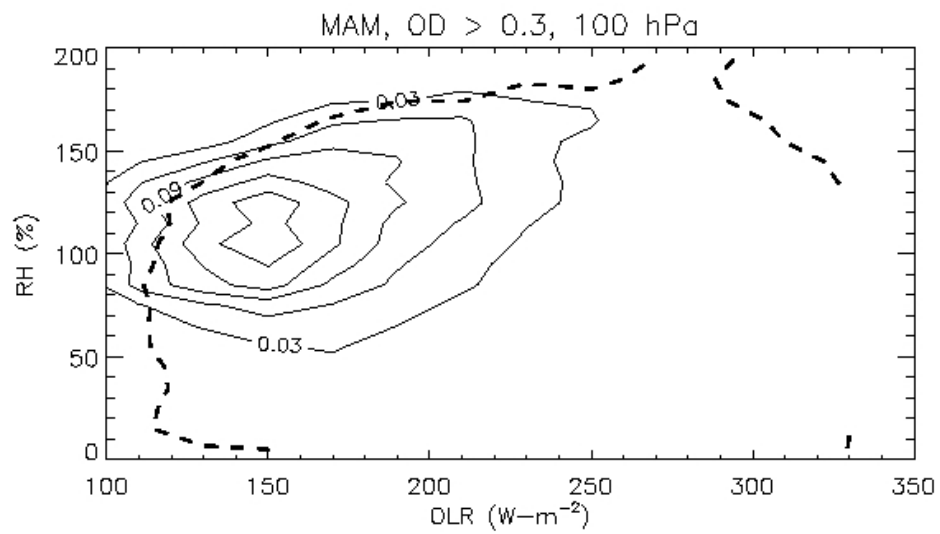
Figure 65: Thick cloud fraction as a function of RHI and OLR for MAM at 100-hPa. Dashed line denotes 50 observations. Bin size of 10% RHI by 20 W-m^{-2} is used.

Figure 66: Thin cirrus fraction as a function of RHI and OLR for MAM at 100-hPa. Dashed line denotes 50 observations. Bin size of 10% RHI by 20 W-m^{-2} is used.

Figure 67: Thick cloud fraction as a function of RHI and OLR for JJA at 121-hPa. Dashed line denotes 50 observations. Bin size of 10% RHI by 20 W-m^{-2} is used.
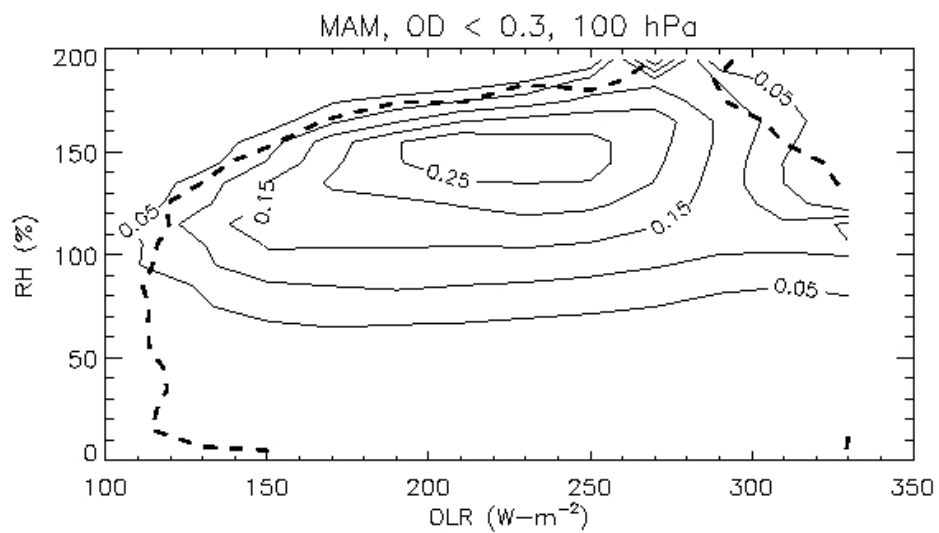
Figure 68: Thin cirrus fraction as a function of RHI and OLR for JJA at 121-hPa. Dashed line denotes 50 observations. Bin size of 10% RHI by 20 W-m^{-2} is used.

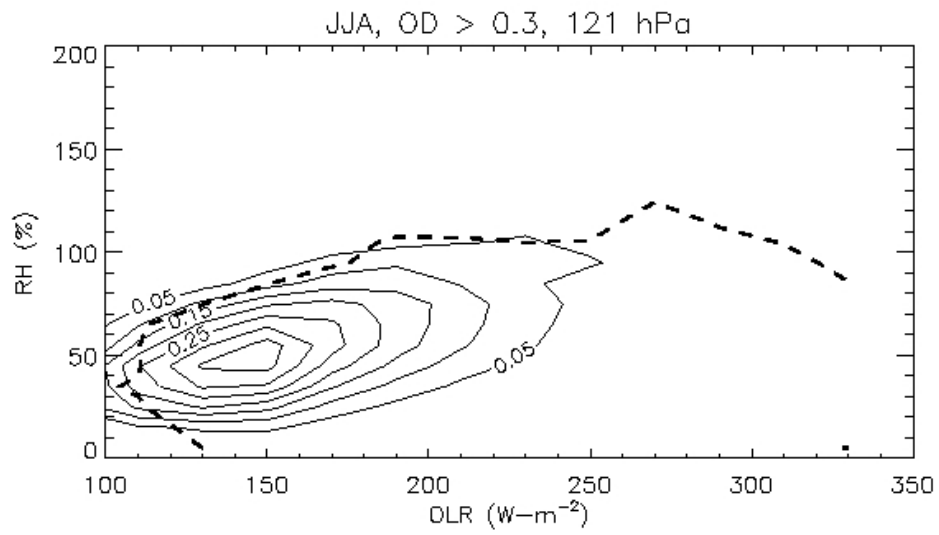**Figure 69:** Thick cloud fraction as a function of RHI and OLR for JJA at 100-hPa. Dashed line denotes 50 observations. Bin size of 10% RHI by 20 W-m^{-2} is used.
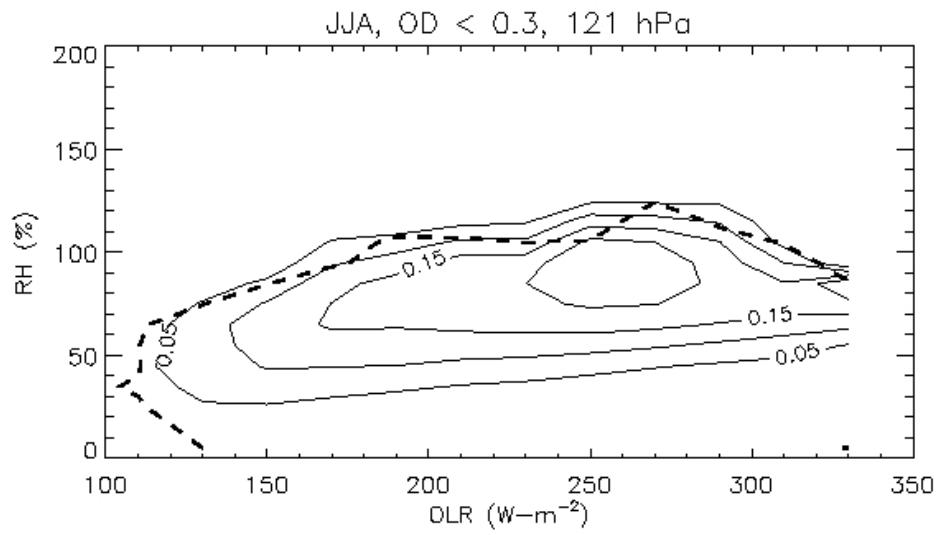
Figure 70: Thin cirrus fraction as a function of RHI and OLR for JJA at 100-hPa. Dashed line denotes 50 observations. Bin size of 10% RHI by 20 W-m^{-2} is used.
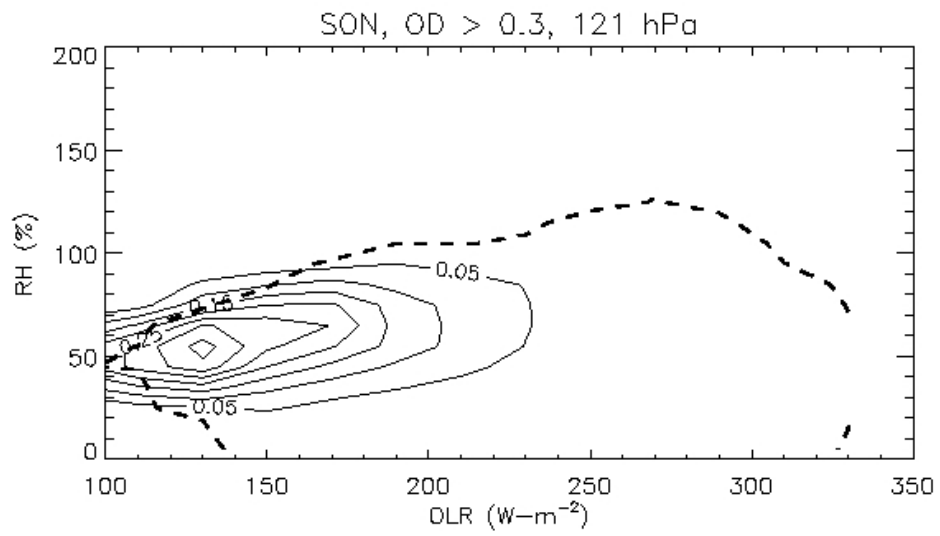
Figure 71: Thick cloud fraction as a function of RHI and OLR for SON at 121-hPa. Dashed line denotes 50 observations. Bin size of 10% RHI by 20 W-m^{-2} is used.

Figure 72: Thin cirrus fraction as a function of RHI and OLR for SON at 121-hPa. Dashed line denotes 50 observations. Bin size of 10% RHI by 20 W-m^{-2} is used.

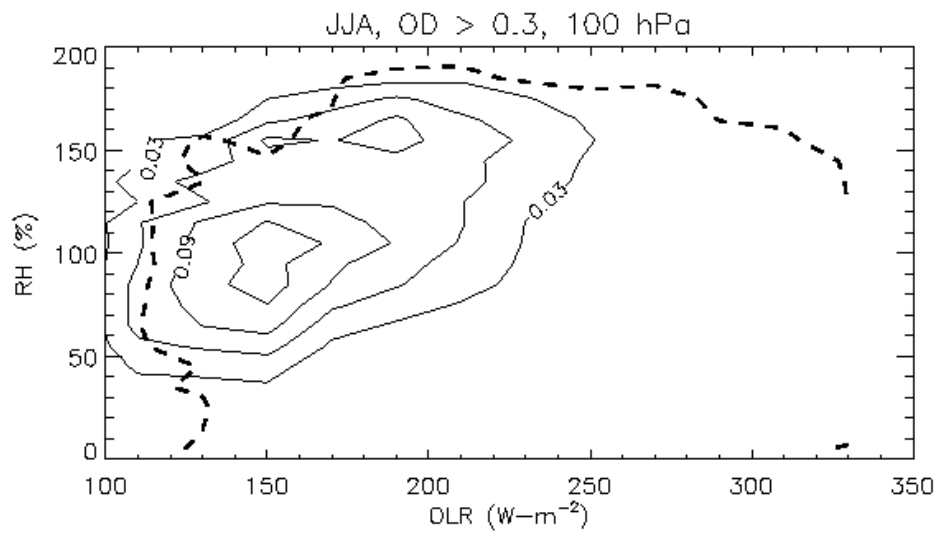**Figure 73:** Thick cloud fraction as a function of RHI and OLR for SON at 100-hPa. Dashed line denotes 50 observations. Bin size of 10% RHI by 20 W-m^{-2} is used.

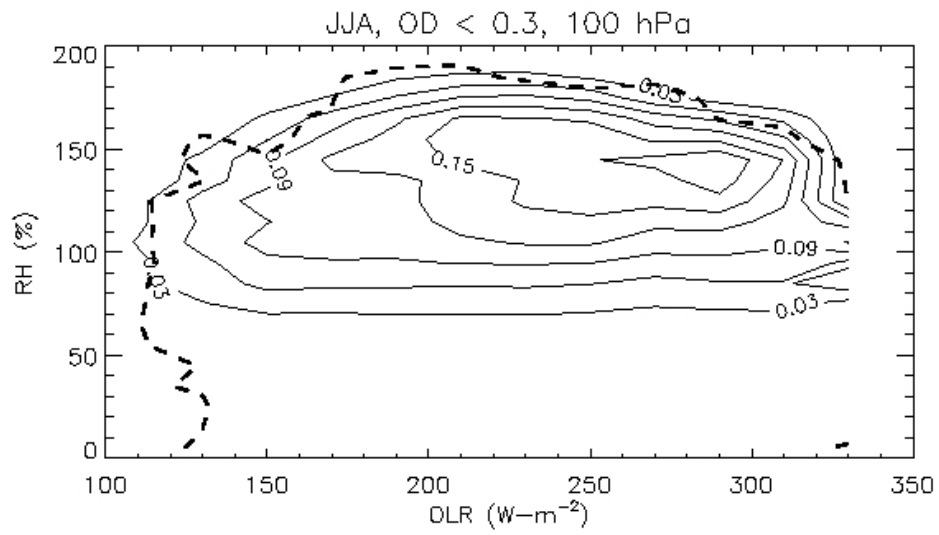**Figure 74:** Thin cirrus fraction as a function of RHI and OLR for SON at 100-hPa. Dashed line denotes 50 observations. Bin size of 10% RHI by 20 W-m^{-2} is used.
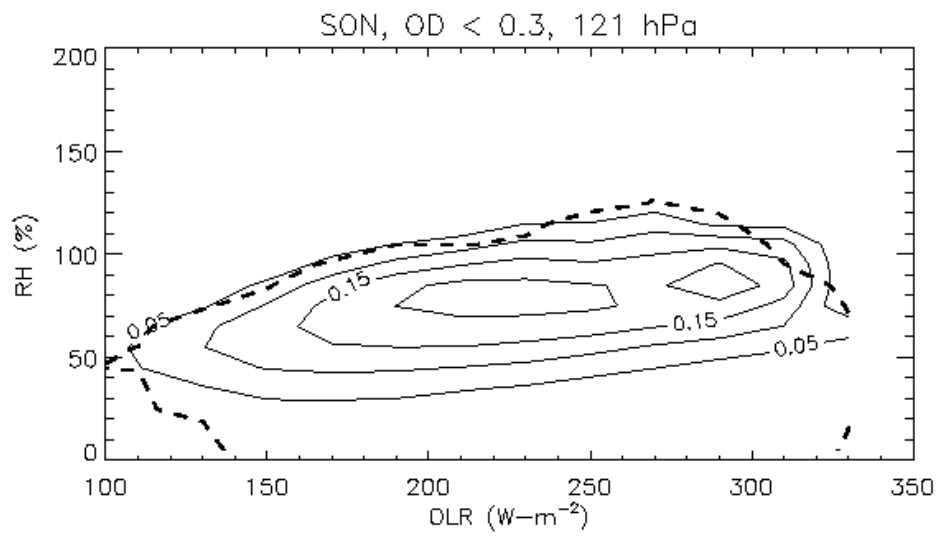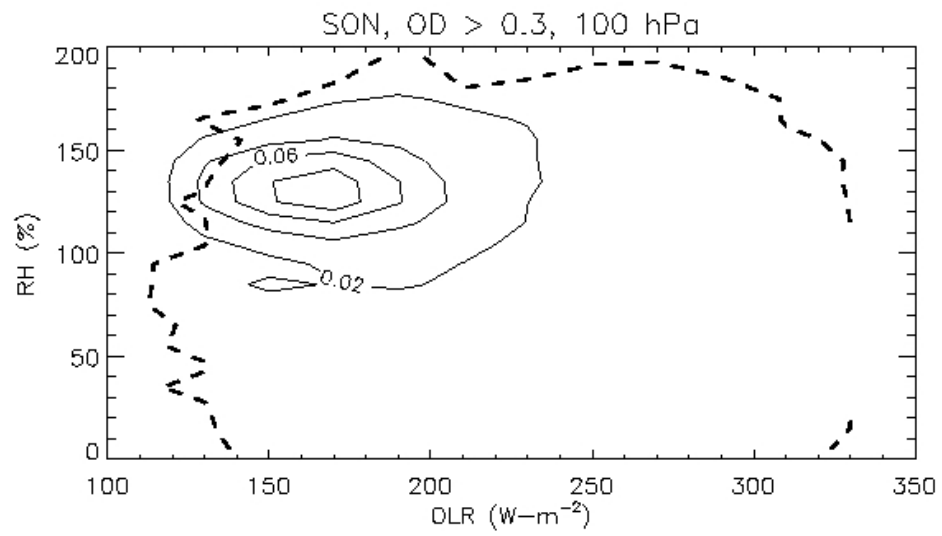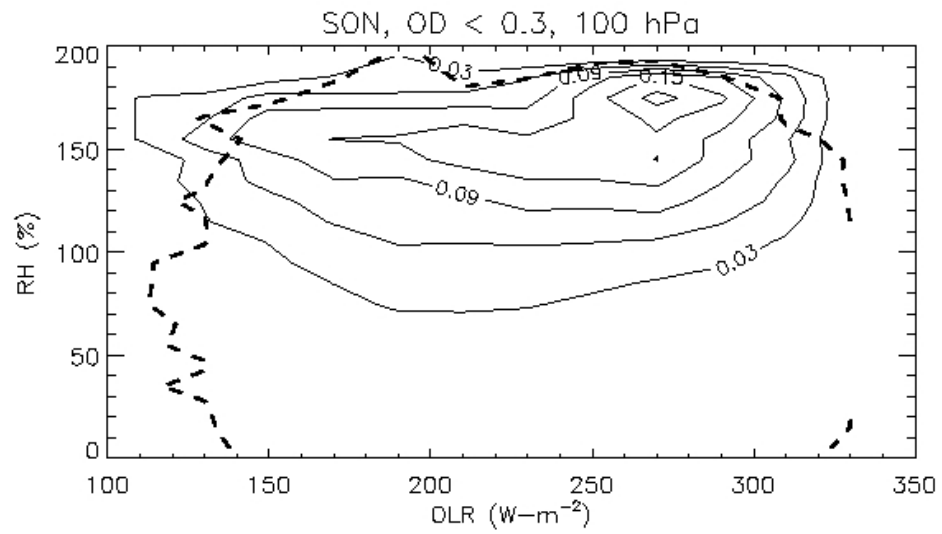
Table 1: Thin cirrus cloud-top occurrence integrated over pressure level ranges for DJF between 30°N and 30°S.

	All data	Day	Night
P ≤ 82 hPa	6.1	3.3	8.72
P ≤ 100 hPa	38.2	31.3	44.6
P ≤ 121 hPa	68.3	63.9	72.5
P ≤ 146 hPa	89.4	87.8	90.8

Table 2: Thin cirrus cloud-top occurrence integrated over pressure level ranges for MAM between 30°N and 30°S.

	All data	Day	Night
P ≤ 82 hPa	0.63	0.14	1.1
P ≤ 100 hPa	21.9	15.8	27.7
P ≤ 121 hPa	58.6	53.5	63.4
P ≤ 146 hPa	86.4	84.6	88.1

Table 3: Thin cirrus cloud-top occurrence integrated over pressure level ranges for JJA between 30°N and 30°S.

	All data	Day	Night
P ≤ 82 hPa	0.86	0.57	1.13
P ≤ 100 hPa	15.9	13.5	18.1
P ≤ 121 hPa	51.3	47.9	54.5
P ≤ 146 hPa	83.6	82.3	84.9

Table 4: Thin cirrus cloud-top occurrence integrated over pressure level ranges for SON between 30°N and 30°S.

	All data	Day	Night
P ≤ 82 hPa	0.26	0.045	0.45
P ≤ 100 hPa	13.3	8.5	17.7
P ≤ 121 hPa	52.4	46.6	57.6
P ≤ 146 hPa	85.3	83.3	87.1

Table 5: Thin cirrus cloud-top occurrence integrated over pressure level ranges for the entire study period between 30°N and 30°S.

	All data	Day	Night
P ≤ 82 hPa	2	1	2.9
P ≤ 100 hPa	22.8	17.7	27.5
P ≤ 121 hPa	57.9	53.3	62.2
P ≤ 146 hPa	86.2	84.5	87.7

Table 6: Thin cloud-top occurrence integrated over geometric altitude ranges, expressed as a fraction of total GLAS observations [*Dessler et al.*, 2006b]

	All data	Morning	Evening
z > 16.5 km	5.7	1.4	10.1
z > 14.5 km	25.6	12.6	38.9
z > 10 km	49.9	31.2	68.8
10 > z > 4 km	6.4	4.6	8

VITA

Biography

Allison L. Cardona was born in San Diego, CA in 1984. In 1987, she moved with her family to Levittown, PA. Her father was in the Navy and, as a result, her family was relocated to both Roosevelt Roads, Puerto Rico and Long Island, New York from 1994-1996. She and her family finally returned to Levittown, PA in early 1996. She graduated from Harry S Truman High School in 2002 and began her undergraduate career at Millersville University, graduating magna cum laude in 2006. She began work on her master's degree at Texas A&M University that fall. Her permanent address is 5 Rolling Lane, Levittown, PA 19055.

Educational Background

B.S., Meteorology, Millersville University, May 2006

M.S., Atmospheric Sciences, Texas A&M University, August 2008